AD-A158 044 DIFFERENTIAL SCATTERING CROSS SECTION AND TOTAL EXTINCTION MEASUREMENTS O.. (U) AIR FORCE INST OF TECH WRIGHT-PATTERSON AFB OH J M DORMAN 1985 1/2

UNCLASSIFIED AFIT/CI/NR-85-69T F/G 7/4 NL

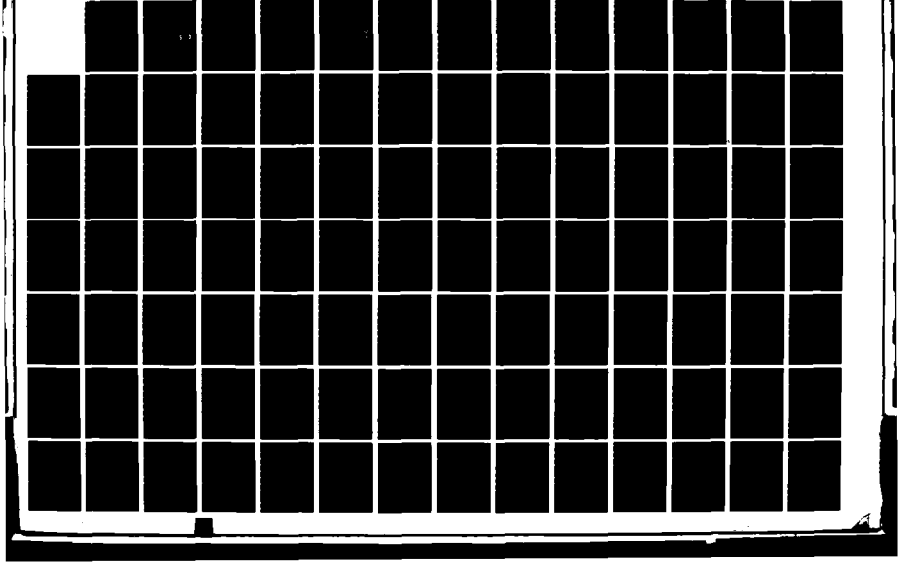

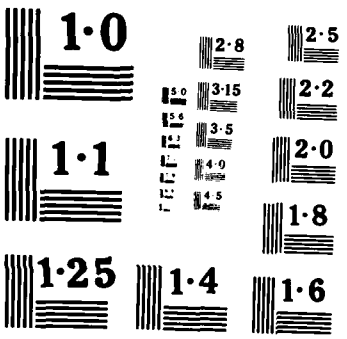

NATIONAL BUREAU OF STANDARDS
MICROCOPY RESOLUTION TEST CHART

AD-A158 044

(When Data Entered)

ITATION PAGE	READ INSTRUCTIONS BEFORE COMPLETING FORM
AFIT/CI/NR 85-69T	2. GOVT ACCESSION NO. / 3. RECIPIENT'S CATALOG NUMBER
4. TITLE (and Subtitle) Differential Scattering Cross Section and Total Extinction Measurements on $(CH)_n$ Spheres in 632.8 nm Laser Light	5. TYPE OF REPORT & PERIOD COVERED THESIS/DISSERTATION / 6. PERFORMING ORG. REPORT NUMBER
7. AUTHOR(s) James M. Dorman	8. CONTRACT OR GRANT NUMBER(s)
9. PERFORMING ORGANIZATION NAME AND ADDRESS AFIT STUDENT AT: University of California Davis	10. PROGRAM ELEMENT, PROJECT, TASK AREA & WORK UNIT NUMBERS
11. CONTROLLING OFFICE NAME AND ADDRESS AFIT/NR WPAFB OH 45433	12. REPORT DATE 1985 / 13. NUMBER OF PAGES 100
14. MONITORING AGENCY NAME & ADDRESS(if different from Controlling Office)	15. SECURITY CLASS. (of this report) UNCLASS / 15a. DECLASSIFICATION/DOWNGRADING SCHEDULE

16. DISTRIBUTION STATEMENT (of this Report)

APPROVED FOR PUBLIC RELEASE; DISTRIBUTION UNLIMITED

DTIC ELECTE S AUG 19 1985 D B

17. DISTRIBUTION STATEMENT (of the abstract entered in Block 20, if different from Report)

18. SUPPLEMENTARY NOTES

APPROVED FOR PUBLIC RELEASE: IAW AFR 190-1

Lynn Wolaver
LYNN E. WOLAVER
Dean for Research and
Professional Development
5 AUG 1985 AFIT, Wright-Patterson AFB OH

19. KEY WORDS (Continue on reverse side if necessary and identify by block number)

20. ABSTRACT (Continue on reverse side if necessary and identify by block number)

ATTACHED

DD FORM 1 JAN 73 1473 EDITION OF 1 NOV 65 IS OBSOLETE UNCLASS

SECURITY CLASSIFICATION OF THIS PAGE (When Data Entered)

DTIC FILE COPY

Thesis for M.A. in Physics
University of California, Davis

TITLE: Differential Scattering Cross Section and Total Extinction Measurements on $(CH)_n$ Spheres in 632.8 nm Laser Light

AUTHOR: CAPTAIN James M. Dorman, USAF

YEAR COMPLETED: 1985

ABSTRACT: A new laboratory system for aerosol research is discussed from the aspects of design, construction and preliminary testing. The system is subdivided into two cooperating subsystems known as the Optical System (OS) and the Aerosol Circulation/Sampling System (ACSS). Measurement of the extinction, scattering and absorption cross sections of an aerosol is the object of the Optical System. Aerosol production, containment, and sampling are the tasks of the ACSS. Mie scattering theory for monodisperse aerosols is discussed as it applies to the cross section measurements. Preliminary measurements on Polystyrene microspheres (1.0 μm in diameter) are presented. These measurements strongly indicate that the spheres are actually 0.85 μm in diameter. Problem areas in both the hardware and experimental procedure are presented as a precursor to full scale testing and calibration. Number of pages: 100

KEY REFERENCES: (1) Bohren, C.T. and Huffman, D.R. Absorption and Scattering of Light by Small Particles. New York: Wiley-Interscience, 1983.

(2) Hinds, W.C. Aerosol Technology. New York: Wiley-Interscience, 1982.

(3) Hecht, E. and Zajac, A. Optics. Reading, Mass: Addison-Wesley, 1975.

AFIT RESEARCH ASSESSMENT

The purpose of this questionnaire is to ascertain the value and/or contribution of research accomplished by students or faculty of the Air Force Institute of Technology (AU). It would be greatly appreciated if you would complete the following questionnaire and return it to:

AFIT/NR
Wright-Patterson AFB OH 45433

RESEARCH TITLE: Differential Scattering Cross Section and Total Extinction Measurements on $(CH)_n$ Spheres in 632.8 nm Laser Light

AUTHOR: James M. Dorman

RESEARCH ASSESSMENT QUESTIONS:

1. Did this research contribute to a current Air Force project?

( ) a. YES ( ) b. NO

2. Do you believe this research topic is significant enough that it would have been researched (or contracted) by your organization or another agency if AFIT had not?

( ) a. YES ( ) b. NO

3. The benefits of AFIT research can often be expressed by the equivalent value that your agency achieved/received by virtue of AFIT performing the research. Can you estimate what this research would have cost if it had been accomplished under contract or if it had been done in-house in terms of manpower and/or dollars?

( ) a. MAN-YEARS _____ ( ) b. $_____

4. Often it is not possible to attach equivalent dollar values to research, although the results of the research may, in fact, be important. Whether or not you were able to establish an equivalent value for this research (3. above), what is your estimate of its significance?

( ) a. HIGHLY SIGNIFICANT ( ) b. SIGNIFICANT ( ) c. SLIGHTLY SIGNIFICANT ( ) d. OF NO SIGNIFICANCE

5. AFIT welcomes any further comments you may have on the above questions, or any additional details concerning the current application, future potential, or other value of this research. Please use the bottom part of this questionnaire for your statement(s).

NAME GRADE POSITION

ORGANIZATION LOCATION

STATEMENT(s):

FOLD DOWN ON OUTSIDE - SEAL WITH TAPE

AFIT/NR
WRIGHT-PATTERSON AFB OH 45433

OFFICIAL BUSINESS
PENALTY FOR PRIVATE USE. $300

NO POSTAGE
NECESSARY
IF MAILED
IN THE
UNITED STATES

BUSINESS REPLY MAIL
FIRST CLASS PERMIT NO. 73236 WASHINGTON D.C.

POSTAGE WILL BE PAID BY ADDRESSEE

AFIT/ DAA
Wright-Patterson AFB OH 45433

FOLD IN

Differential Scattering Cross Section and Total Extinction Measurements on $(CH)_n$ Spheres in 632.8 nm Laser Light

By

CAPTAIN JAMES M. DORMAN, USAF
B.S. (Louisiana State University, Baton Rouge) 1977

THESIS

Submitted in partial satisfaction of the requirements for the degree of

MASTER OF ARTS

in

Physics

in the

GRADUATE DIVISION

of the

UNIVERSITY OF CALIFORNIA

DAVIS

Approved: ..... Chairman

.....

.....

Committee in Charge

Deposited in the University Library.....
Date Librarian

TABLE OF CONTENTS

TABLE OF CONTENTS

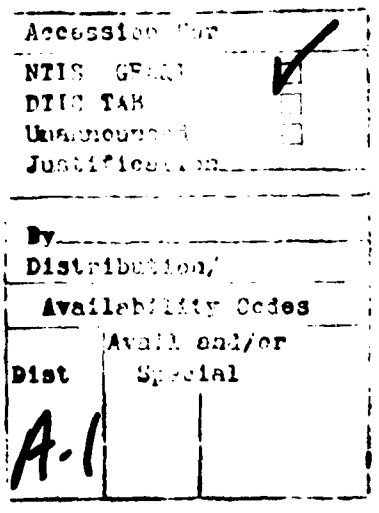

ABSTRACT

A new laboratory system for aerosol research is discussed from the aspects of design, construction and preliminary testing. The system is subdivided into two cooperating subsystems known as the Optical System (OS) and the Aerosol Circulation/Sampling System (ACSS). Measurement of the extinction, scattering and absorption cross sections of an aerosol is the object of the Optical System. Aerosol production, containment, and sampling are the tasks of the ACSS. Mie scattering theory for monodisperse aerosols is discussed as it applies to the cross section measurements. Preliminary measurements on Polystyrene microspheres (1.0 μm in diameter) are presented. These measurements strongly indicate that the spheres are actually 0.85 μm in diameter. Problem areas in both the hardware and experimental procedure are presented as a precursor to full scale testing and calibration. Number of pages: 100

ACKNOWLEDGEMENTS

Many feelings of gratitude are in my heart and mind for a number of individuals whose labors have culminated in this thesis. Special recognition and praise goes to my wife Susanne, whose love, encouragement and confidence have seen me through many difficult days. I also wish to extend a special thanks to Rich Axelbaum, M.S. whose physical insight and research experience were the cornerstone of this project. Dr. Tom Cahill, the master mind behind this entire project is extended my thanks for his financial and technical support, through his offices in the Physics Department and as director of Crocker Nuclear Laboratory (CNL). I wish to also applaud the technical assistance of the CNL Air Quality Group, especially that of Chuck Brock. Further thanks go to Jamie Vesenka and John Heijtmanek for many dedicated hours of technical support, number crunching and good humor. Also, I wish to say thank you to Dan Shadoan for tremendous support in computer programming and plotting. I further acknowledge the offices of the Air Force Institute of Technology for outstanding financial and administrative services during the long duration of this work. Many thanks also to Madelin for her superb work in production of this manuscript.

INTRODUCTION

Over the last ten years a number of systematic and exhaustive studies has been made of visibility and atmospheric particulates in the western United States. Studies of particulates have characterized them in terms of size and mass distributions as well as elemental analysis via laboratory techniques such as PIXE (Particle Induced X-ray Emission, for elements sodium through Uranium) and FAST (Forward Alpha Scattering Technique, for lighter elements). The Air Quality Group at U.C. Davis has been heavily involved in these studies through its establishment and operation of the Western Fine Particle Network (WFPN), under the auspices of the National Park Service. (Cahill, et. al., 1981) Visibility studies have involved quantitative investigations of atmospheric extinction of light by the measurement of the relative contrast between land mass formations and the adjacent sky. (Malm, 1981) For the so called, "fine particle regime", (particulates of diameter <2.5 μm) there have been observed inconsistencies between values of extinction measured and the values that are predicted from Mie scattering theory. The size of such deviations is large, being about one order of magnitude in some cases. For example, studies of smokes in the Grand Canyon area in June have shown that although fine particles are present in the atmosphere, the extinction associated with the particulates is effectively zero. (Malm, 1984) As another example, atmospheric studies in the eastern United States have shown a direct correlation between the presence of sulphur (usually in the form of sulfates, SO_x) in fine mass particulates and the degradation of visibility in the air. There exists though, a large body of evidence

that such a direct correlation does not apply in the arid western United States. (Ashbaugh, et. al. 1981)

The size, mass, and chemical analyses from programs such as WFPN are not enough to resolve these differences among observations and between observations and Mie theory. Visibility modeling requires a knowledge of the complex refractive index of the particulates involved in the model. Heretofore, the conventional wisdom has been to apply the refractive index of bulk materials to the particulates. This practice has been driven by necessity, for with the exception of water alone, few if any in-situ measurements of the refractive index of natural particulates has been made. To fill such a gap in experimental data is the long term goal of an apparatus whose initial design, construction, and testing are presented in this work. At the outset, the constraints on the apparatus were two-fold: 1) It must be able to measure the optical properties of an aerosol, but without having so much aerosol present as to be unrealistic in nature. 2) The system should have a large enough volume so that aerosol samples could be extracted simultaneous with the optical measurements. To the knowledge of the Air Quality Group, the system here presented, is a pioneering work in the field of aerosol physics. A detailed description of this system, as well as a preliminary test using an aerosol of known composition now follows.

THEORY

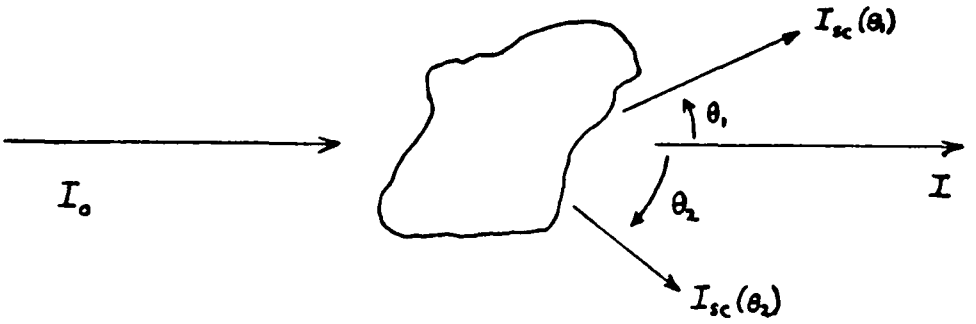

Fig 1

Consider a ray of light of intensity I_0, that encounters and traverses a material medium. This ray will experience scattering, absorption, and extinction while traversing the medium. Part of the ray's electromagnetic energy is changed into other forms of energy, e.g., heat. This loss of energy from the beam is called absorption. Scattering may be defined as the re-direction or redistribution of light energy from the incident direction of the beam. In this sense, it can be shown that the laws of reflection, refraction, and diffraction are manifestations of the process of scattering (Bohren & Huffman, 1983, p. 4). In a more exact way then, we define scattering to be the sum total of reflection, refraction, diffraction, and re-emission after absorption (Hecht & Zajac, 1975, p. 240). In general, the scattered light emanates out in all directions from the scattering center; these directions being defined by some angular measure. We define a scattering plane by the incident direction of the ray and the line from the scattering center to the observer. The angle between the incident direction and the observer is called the scattering angle θ. As a point of terminology the incident direction is denoted as the $\theta = 0$ degree, or forward direction. Scattering angles between 0 and 90 degrees are

1.4

BEAM PROFILER

1. LASER
2. CHOPPER
3. WAVE PLATE / MOUNT
4. SPATIAL FILTER
5. COLLIMATING LENS
6. ATTENUATOR
7. LASER POWER METER HEAD
8. BEAM SPLITTER / ENTRANCE WINDOW
9. OPTICAL BENCH
10. STONE BLOCK PEDESTALS

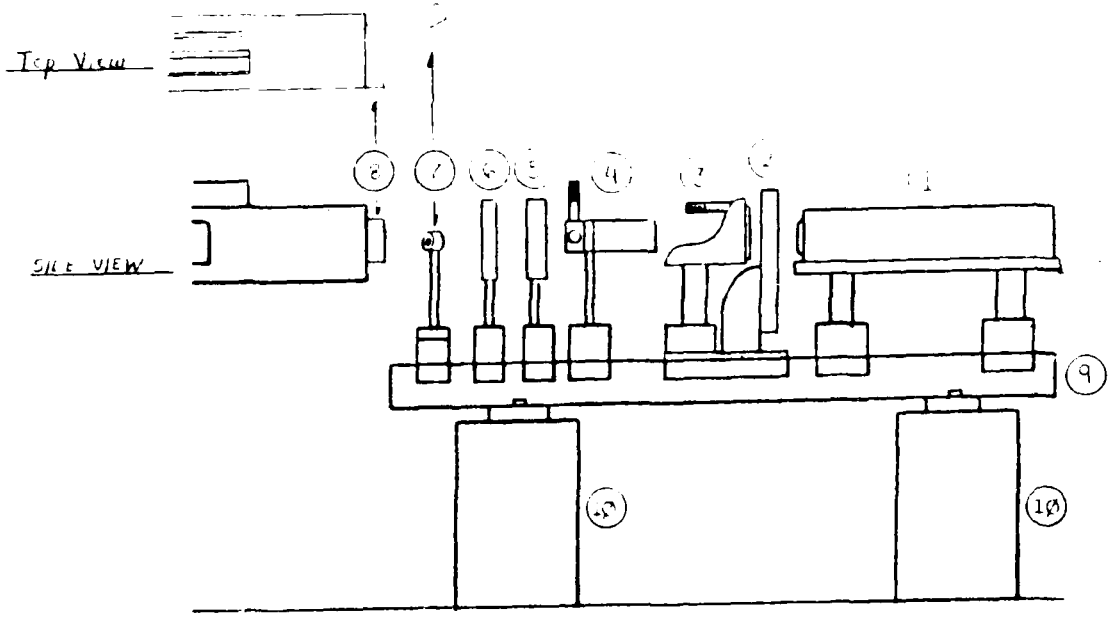

Fig. 3. What follows is a description of both systems and the associated electronics, as well as a study of the geometrical optics of the apparatus.

BEAM PRODUCTION SYSTEM

The Beam Production System (BPS) produces a collimated laser beam of known size and intensity and whose polarization is completely determined. See Fig. 4. As you can see the BPS is mounted on a rigid steel optical bench that rests on two small stone-block pedestals. These pedestals have the same qualities of rigidity and vibration insulation as the two pedestals supporting the chamber. The height of the blocks and bench was chosen so that the components on the bench could easily match the height of the centerline of the chamber. The optical bench is aligned parallel to the long axis of the chamber since the main laser beam will be fired along this axis. Because the bench is long and narrow, side to side stability needed improvement in order to accommodate the large amount of equipment to be mounted on it. We therefore machined and mounted two cross bar feet at the forward and aft ends of the bench. Each foot incorporates two adjusting screws with locking nuts to provide both lateral and longitudinal leveling. We thus have a rigid, adjustable and vibration insulated base upon which the other BPS components are mounted.

The most important component of the BPS is the laser. Our laser is a Spectra-Physics, Model 120, Helium-Neon type, with a maximum measured output of 6 mW. Being a Helium-Neon laser, the beam is quasi-monochromatic with a peak wavelength of 632.8 nm. Thus the beam exhibits a bright red color to the naked eye. The laser is linearly polarized with

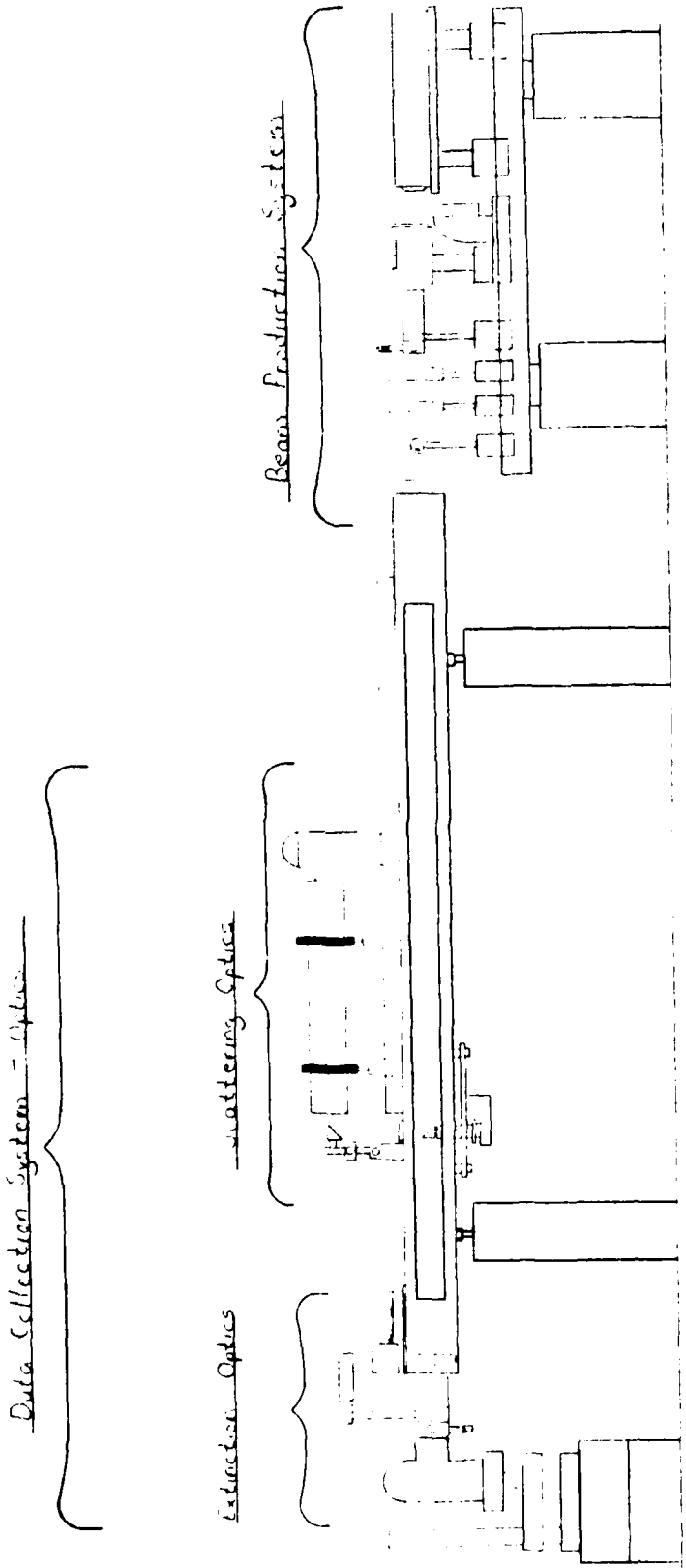

OPTICAL SYSTEM

Fig 3

be rigid enough so that any reasonable bump or jolt would not move the system out of alignment. Also, the mounts should provide enough damping so that the OS would be isolated from environmental dynamics. Such dynamics are the inherent vibrations in a building which arise from air conditioning systems, blowers, pumps, elevators, machine tools, and so on. In more direct terms we could say that the mounting requirements were: (1) If we bump it, it must come back to alignment, and (2) we don't want it to slowly vibrate out of alignment over a long period of time (days or weeks) from vibrations in the building. The stone-block pedestals we built meet both of these requirements. Each pedestal is a stack of six stone blocks with the lowest three being wider than the others for improved stability. The sheer weight of the blocks provided some rigidity, but because the mating faces were not completely flat, a significant amount of wobble had to be eliminated. This was accomplished by inserting a set of four O-rings between the floor and the first block as well as between the rest of the blocks in each pedestal. Each O-ring measures about 2.5 cm in diameter with a thickness of 2.5 mm. The proof is in the results; the alignment has remained true even after over three months of experimental activity in and around the device.

OPTICAL SYSTEM

The Optical System (OS) has two specific purposes. First it produces a laser beam with known characteristics and second it measures how the beam is extinguished and scattered by the aerosol in question. The first purpose is the job of the Beam Production System (BPS) and the second purpose is realized by the Data Collection System (DCS). See

chamber and mounts will provide a foundation that will help in understanding the entire apparatus.

The chamber is, "where it all happens," so to speak. An aerosol circulates through it while the laser beam is fired down the length of the chamber. Thus the interior of the chamber is where the aerosol extinguishes and scatters the beam. The interior surface of the chamber is coated with an optically absorbing black paint that improves the accuracy of measuring both the extinguished beam and scattered light from the aerosol. On the front face of the chamber is a slot measuring 2.4 m by 5 cm. The purpose of the slot is to provide access to the interior of the chamber when work is done on the internal optics, especially during the alignment of the OS. A faceplate covers the slot and seals the chamber during a measurement run. It is made of ultra high molecular weight polyethelene plastic whose inside facing surface is painted with the same optically black paint as the interior chamber walls. In addition to these properties, the chamber also acts as a rigid mounting surface for all of the scattering optics, as well as other parts of the OS. As a further aid to optical alignment the chamber is equipped with four adjustable feet (with locking nuts) by which it rests upon the mounting pedestals.

For many optical systems that are delicately aligned, the mounting must have qualities of rigidity and vibration insulation. For example, in interferometry the difference of a fraction of a wavelength can be crucial in the measurement of the refractive index of a material. In our device, though, such small differences in phase are not crucial since we measure only light intensities (which contain no phase information). Thus the requirements on our mounting blocks were two-fold. They must

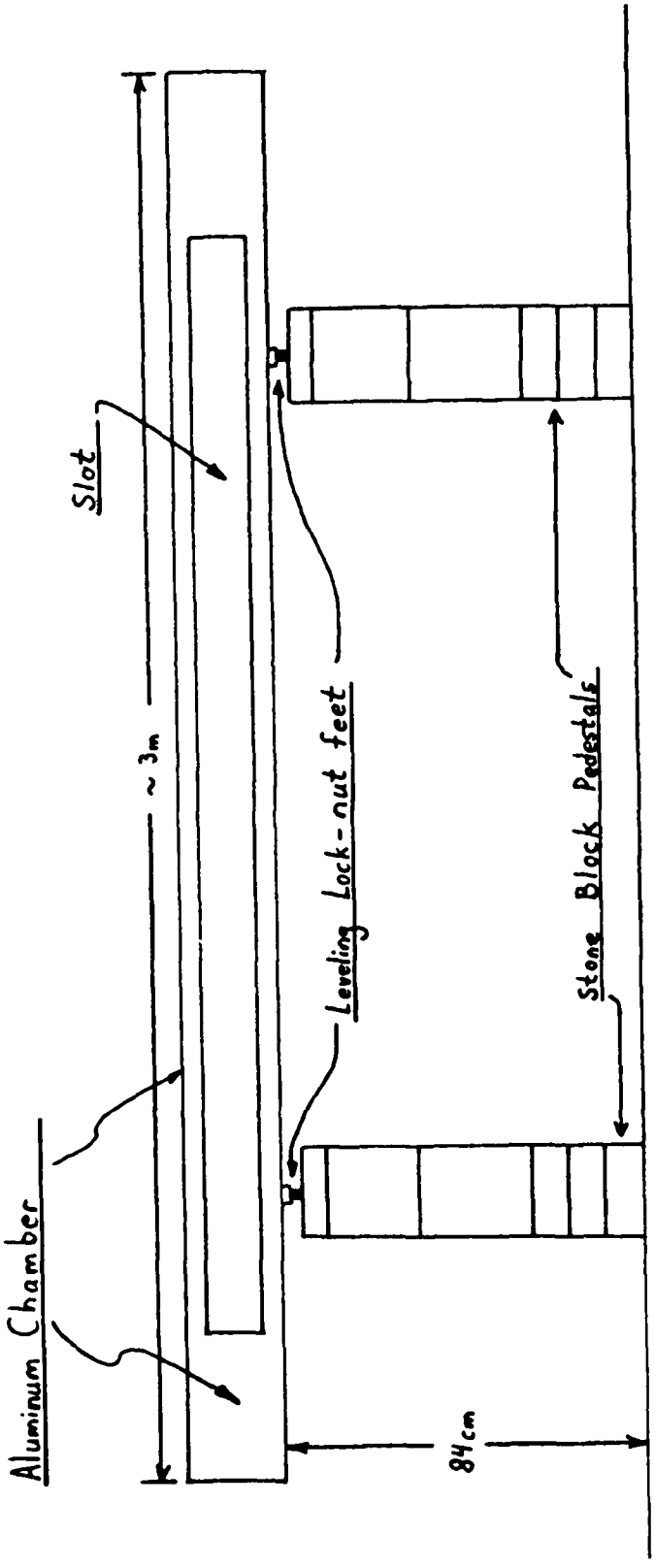

CHAMBER AND MOUNTING BLOCKS

Fig 2

APPARATUS

Approximately one year of research and development has culminated in a novel prototype system for investigating both the optical and physical characteristics of particulate aerosols. The optical properties include the extinction, absorption and scattering cross sections as well as the real and imaginary parts of the refractive index. Physical characteristics are the elemental composition as well as the size and mass distributions of a given aerosol. To investigate these properties the apparatus we have developed incorporates two cooperating subsystems. These are the Optical System (OS) and the Aerosol Circulation/Sampling System (ACSS). As its name suggests, the OS involves the optics and electronics of producing, directing and measuring the laser light which is used to probe the aerosol. Similarly, the ACSS consists of the hardware needed to keep the particles suspended and mixed in a closed and controlled environment. It also provides two methods by which samples of the aerosol may be extracted for mass, size and elemental analysis.

CHAMBER AND MOUNTING BLOCKS

The heart of the apparatus is a large aluminum chamber that measures about three meters long and having a square cross section 10 cm by 10 cm. The walls have a thickness of 6 mm. This chamber is mounted on two stone block pedestals weighing 250 pounds each, with the base of the chamber resting about 84 cm above floor level. See Fig. 2. Since the chamber and its mounts are a fundamental part of both the OS and ACSS, it will be mentioned often in the detailed discussions of these systems. Therefore, a discussion of the general characteristics of the

By knowing the differential scattering cross sections for a full spectrum of angles (0 through 180), it is possible to numerically integrate that data to get the total scattering cross section, i.e.,

$$\sigma_{sc} = \int_{4\pi} \sigma_{sc}(\theta) d\Omega \tag{16}$$

Finally, the total extinction cross section is given by,

$$\sigma_{ex} = \frac{4\pi}{k^2} \mathrm{Re}\{S(0)\} \tag{17}$$

where $S(0) = S_1(0) = S_2(0)$. (Bohren & Huffman, 1983, p. 112) The bottom line is that the reading of the scattering detector is directly related to the quantities $|S_1(\theta)|^2$ and $|S_2(\theta)|^2$. In this way measured quantities may be compared to theoretical values to determine the effectiveness of the apparatus.

d is the diameter of the sphere and λ is the wavelength of the incident light. The arguments π_n and τ_n are angular dependent functions whose behavior dictate the angular distributions of the scattered energy. (Bohren & Huffman, 1983, pp. 96, 97, 101) As mentioned before, the series in Eqns. 13A and 13B are also truncated after n_c terms. For the case of dielectric spheres, the following relations hold: if the incident light is 100% polarized perpendicular to the scattering plane, then the scattered light is also 100% polarized perpendicular to the scattering plane. The intensity distribution of the scattered light is given by,

$$I_1(\theta) = \frac{I_{01}|S_1(\theta)|^2}{k^2r^2} \qquad (14A)$$

k is the wave number of the incident light and r is the radial distance from the scattering center to the observer. Similarly, incident light 100% polarized parallel to the scattering plane results in scattered light 100% polarized parallel to the scattering plane. Its intensity distribution is given by,

$$I_2(\theta) = \frac{I_{02}|S_2(\theta)|^2}{k^2r^2} \qquad (14B)$$

(Bohren & Huffman, 1983, p. 113). The differential scattering cross sections are related to the Amplitude Scattering functions via the following relations:

$$\sigma_{sc(1)}(\theta) = \frac{|S_1(\theta)|^2}{k^2} \qquad (15A)$$

$$\sigma_{sc(2)}(\theta) = \frac{|S_2(\theta)|^2}{k^2} \qquad (15B)$$

where the $\vec{N}_{enm}$ and $\vec{N}_{onm}$ are related to the respective $\vec{M}$ functions via Eq. 6B. The resultant expansion of the incident plane wave in terms of these spherical harmonics is

$$\vec{E} = E_o \sum_{n=1}^{\infty} i^n \left(\frac{2n+1}{n(n+1)}\right)\{\vec{M}^{(1)}_{o1n} - i\vec{N}^{(1)}_{e1n}\} \qquad (11)$$

where the superscript (1) indicates that the radial portion of the function is given by the spherical Bessel function, jn(kr). A similar expression for the $\vec{H}$ field is obtained by taking Curl ($\vec{E}$). (Bohren & Huffman, 1983, pp. 83-93) In the far field region at some distance, r, from the scattering center, the series can be truncated after some value of the summation index, n_c, resulting in negligible error. Also, if $kr >> (n_c)^2$, where k is the wave number of the incident light, then the terms in the series may be replaced by their asymptotic expressions in this far field region. Such manipulations result in the following expressions for the scattered field, whether perpendicular or parallel to the scattering plane: (Bohren & Huffman, 1983, p. 112)

$$\begin{bmatrix} E_{\parallel s} \\ E_{\perp s} \end{bmatrix} = \frac{e^{ik(r-z)}}{-ikr} \begin{bmatrix} s_2 & 0 \\ 0 & s_1 \end{bmatrix} \begin{bmatrix} E_{\parallel i} \\ E_{\perp i} \end{bmatrix} \qquad (12)$$

where

$$s_1(\theta) = \sum_n \left(\frac{2n+1}{n(n+1)}\right)(a_n\pi_n + b_n\tau_n) \qquad (13A)$$

$$s_2(\theta) = \sum_n \left(\frac{2n+1}{n(n+1)}\right)(a_n\tau_n + b_n\pi_n) \qquad (13B)$$

These last two equations are called the Amplitude Scattering Functions for light scattered perpendicular and parallel to the scattering plane. The arguments a_n and b_n are functions of the complex refractive index and $\alpha = (\pi)d/\lambda$, the so-called Mie number for the particle in question.

solving a scalar wave equation rather than these in vector form. To do so he constructed two vector functions $\vec{M}$ and $\vec{N}$ where,

$$\vec{M} = \vec{\nabla}\times\{\vec{c}\ \psi\} \tag{6A}$$

$$\vec{N} = \frac{1}{k}\{\vec{\nabla}\times\vec{M}\} \tag{6B}$$

$\vec{C}$ is some constant vector and ψ is an unknown scalar function. It turns out that $\vec{M}$ and $\vec{N}$ have all the required properties of the electromagnetic field. They satisfy the vector wave equations and Maxwell's equations, but of more practical importance, $\vec{M}$ and $\vec{N}$ may be determined by knowing the scalar ψ. This is because $\vec{M}$ and ψ are related by

$$\nabla^2\vec{M} + k^2\vec{M} = \vec{\nabla}\times\{\vec{c}[\nabla^2\psi + k^2\psi]\} \tag{7}$$

Clearly $\vec{M}$ satisfies the vector wave equation if and only if ψ satisfies the scalar wave equation

$$\nabla^2\psi + k^2\psi = \phi \tag{8}$$

This equation is most easily solved in spherical polar coordinates using the method of separation of variables. Thus ψ becomes a three subscripted even or odd function of r, θ, and ϕ:

$$\psi_{enm} = \cos(m\phi)P_n^m(\cos\theta)Z_n(kr) \tag{9A}$$

$$\psi_{onm} = \sin(m\phi)P_n^m(\cos\theta)Z_n(kr) \tag{9B}$$

Here the P_n^m are the associated Legendre polynomials and the Zn(kr) are one of the spherical Bessel functions j_n, y_n, $h_n^{(1)}$, or $h_n^{(2)}$. These solutions for ψ constitute the generating functions for the vector spherical harmonics, $\vec{M}$ and $\vec{N}$ according to the following relations:

$$\vec{M}_{emn} = \vec{\nabla}\times[\vec{r}\ \psi_{emn}] \tag{10A}$$

$$\vec{M}_{onm} = \vec{\nabla}\times[\vec{r}\ \psi_{onm}] \tag{10B}$$

Geometrical Optics. Rayleigh scattering is the domain in which the particles are very small compared to the wavelength of the light that illuminates them. In this regime the fields of the scattered light are approximated as those of an oscillating electric dipole at the scattering center. The other extreme is where particles are very large compared to the wavelength of the illuminating light. For this case, Geometrical Optics provides an excellent approximation for describing the extinction and scattered light distribution. What about the intermediate region in which the size of the particles is comparable to the wavelength of the illuminating light? In this regime there exists no useful approximation to calculate the relevant parameters of the extinction, scattering, and absorption problem. In the early 1900's Gustav Mie rigorously applied Maxwell's equations to the problem of scattering of electromagnetic radiation from a homogeneous dielectric sphere. It is this theory that our apparatus exploits for the purpose of aerosol research. We will now survey those portions of Mie Theory that apply to the aerosol that will be used to test the merits of our system.

Consider applying Maxwells equations to the problem of an electromagnetic wave traversing a homogeneous dielectric sphere. Normally one would be faced with the prospect of solving the vector wave equations in the fields $\vec{E}$ and $\vec{H}$, namely

$$\nabla^2\vec{E} + k^2\vec{E} = \phi \qquad (5A)$$

$$\nabla^2\vec{H} + k^2\vec{H} = \phi \qquad (5B)$$

not to mention the boundary conditions at $r = 0$ (sphere center), $r = R$ (sphere surface), and infinity. Being a good physicist, Mie preferred

The Bouguer-Lambert Law applies equally well to continuous media and discontinuous media like suspensions of small particles in the air. In this latter case the law takes the form,

$$I(x) = I(0)\ \exp\{-x[N(\sigma_{sc} + \sigma_{ab})]\} \qquad (4A)$$

or

$$I(x) = I(0)\ \exp\{-x[N(\sigma_{ex})]\} \qquad (4B)$$

σ_{ex}, σ_{sc}, and σ_{ab} are the total cross sections for extinction, scattering, and absorption, respectively, for the particles in question. N is the number of particles per unit volume in the suspension. Note that $\sigma_{ex} = \sigma_{sc} + \sigma_{ab}$. Equations 4A and 4B are valid in a particular range of number densities; this range being referred to as the single scattering regime. Single scattering means that each ray of light that is scattered, has been scattered from one and only one particle before it is observed. The idea is that N particles scatter N times as much light and absorb N times as much light as does one particle. Thus for example, the extinction coefficient for N particles is N times the extinction coefficient for one particle. (Van de Hulst, 1981, p. 5) If N gets too large this simple rule does not apply. This is the domain of multiple scattering in which light is scattered from more than one particle before it is observed. A rigorous treatment of multiple scattering is under the guise of radiative transfer, which is beyond the scope of this work. We treat only single scattering in this study. As a rule of thumb, the single scattering domain is obtained if the total extinction ratio, $I/I_o > 90.4\%$. (Van de Hulst, 1981, p. 6)

The interaction of light with small particles falls into three broad categories. They are Rayleigh scattering, Mie scattering, and

referred to as forward scattering angles, whereas backward scattering angles run from $\theta>90$ to 180 degrees. Absorption and scattering remove energy from the beam so that the ray emerging from the medium at the forward direction has an intensity $I < I_o$. In general, this attenuation of light is directly proportional to the path lengtn through the extinguishing medium. More succinctly we can write,

$$I = I_o e^{-Ax} \tag{1}$$

I_o and I are the incident and subsequent intensity of the light. "A" is named the extinction coefficient and x is the length through the material, in the direction of propagation. Notice that the minus sign preceding "A" indicates that the incident intensity decreases as the path length, x, increases. This exponential decay law is known as the Bouguer-Lambert Law. (Jenkins & White, 1976, pp. 230-231) Closer scrutiny of the extinction coefficient shows that it is the sum of two terms; one due to absorption and one due to scattering, i.e.,

$$A_{ex}(\lambda) = A_{ab}(\lambda) + A_{sc}(\lambda) \tag{2}$$

Note that in general, "A" is a function of the wavelength of the incident light, λ. So Eq. 1 takes the form,

$$I(x) = I(0)\ \exp\{-x[A_{ab}(\lambda) + A_{sc}(\lambda)]\} \tag{3}$$

Thus we see that absorption and scattering are constituent processes of phenomenon of extinction. Needless to say, the goal of much theory and experiment is to predict and/or measure A_{ex}, A_{sc}, and A_{ab}. Knowing these parameters, one can accomplish much in describing how light behaves as it traverses a material medium.

the direction of the electric field vector set at 20 degrees clockwise of verticle (when viewed facing the output aperture of the laser). Knowing the polarization of the beam is an important factor since the scattering is such a strong function of polarization. It also allows us to vary the polarization of the beam in a known way so that a variety of aerosol properties can be probed.

The power output of a laser is an important consideration to weigh when choosing one for a research project. This model is particularly well suited to our needs. It has the power needed to give us enough scattered light to measure, whereas its power is low enough so that stringent safety requirements do not have to be enforced during its use.

A full set of extinction and scattering measurements takes about 40 minutes. So it is important to know how the laser power behaves over such a period of time or even over several such periods. From a cold start, the power output of our laser is shown in Fig. 5. This spectrum covers a period of about 40 hours. Note that it takes about 15 hours for the power output to stabilize to an acceptable level. This plateau is the region best suited for data taking because the power does not fluctuate more than ±2% from the mean power output in this region. The plateau exists for about 16 hours, providing ample time to take measurements. Since each plateau data point is taken at half hour intervals, and since a set of measurements takes only a few minutes, it behooves us to scrutinize the power output over a shorter period of time as shown in Fig. 6. Here we have data points for each minute of a one hour period, from 24 to 25 hours on Fig. 5. The power output is flat, not varying more than ±0.9% from the mean. The main point of all this is that when we take measurements, the last thing we want to detect is variations in

Fig.5

SPECTRA PHYSICS He-Ne LASER MODEL 120S POWER OUTPUT

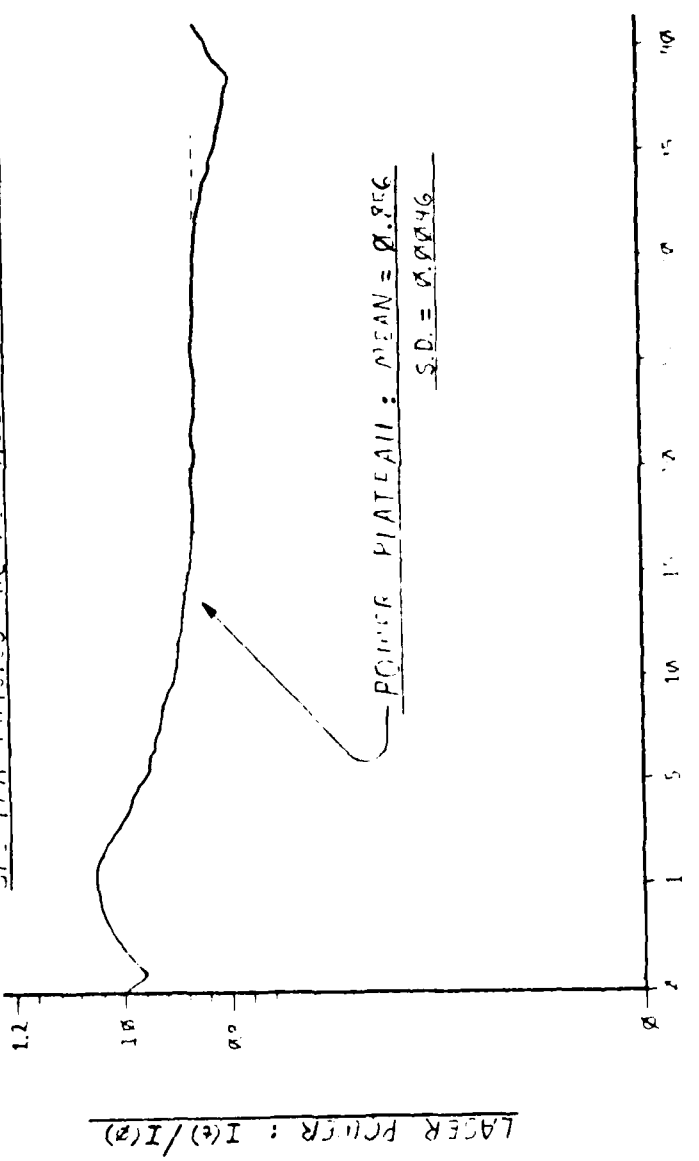

Fig 6

LASER POWER BETWEEN 24 HOURS AND 24 HOURS 53 MINUTES

MEAN : M = Ø.856 MAX DEVIATION ABOVE MEAN = + Ø.55% M

MAX DEVIATION BELOW MEAN = −Ø.86% M

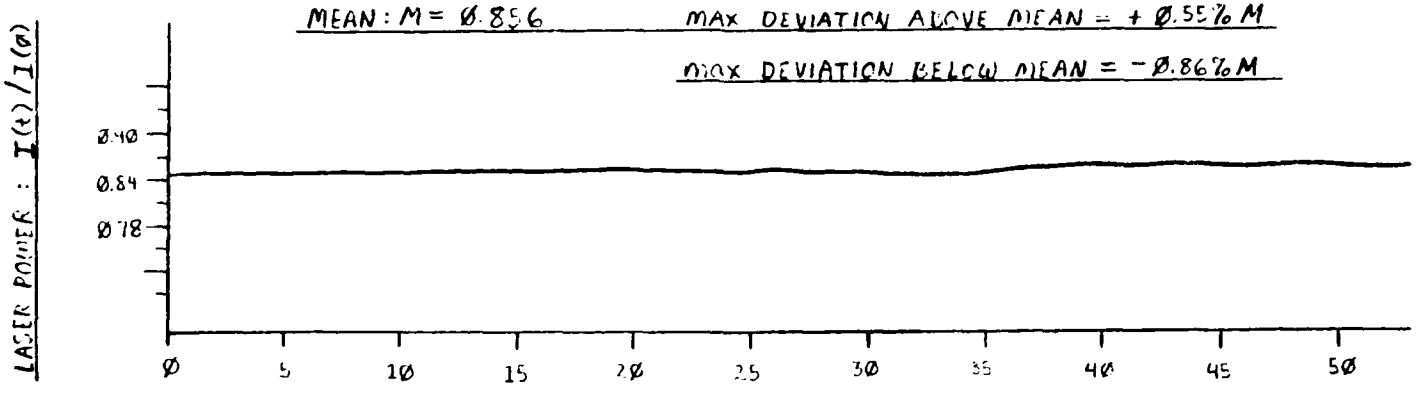

the power output of the laser. We want to be able to say that any structure in our data is due to aerosol characteristics and nothing else.

To improve the signal to noise (S/N) ratio of the photo detectors, the BPS includes an EG&G Model 125A light chopper. It's purpose is to chop (modulate) the laser beam and to simultaneously generate a square wave reference which is synchronous with the chopping rate. By using the proper detection electronics, the modulated laser signal can be selected out from among random signals and other noise that is modulated at other frequencies. For our experiment the chopper modulates the beam at 338 Hz.

The next component of the BPS is a ½-wave plate optical retarder. In a nutshell, the half wave plate is an optical component that is used to rotate the plane of polarization of the laser beam to any desired orientation without touching the laser at all (Melles Griot, 1982, pp. 270-274). This is an important capability because most scattering measurements are made for the two cases in which the incident beam is linearly polarized parallel and then perpendicular to the scattering plane. (Bohren & Huffman, 1983, pp. 112-114) The wave plate is a single crystal of quartz which is optically anisotropic. Specifically, the plate exhibits two different refractive indices along two orthogonal directions. One direction is called the optical axis. When viewed along this axis, the crystal is optically isotropic because this is the one direction in the crystal about which the atoms are arranged symmetrically. Because of the existence of this one unique direction, the crystal is called uniaxial. The direction of the other refractive index on the crystal is perpendicular to this optical axis. See Fig. 7.

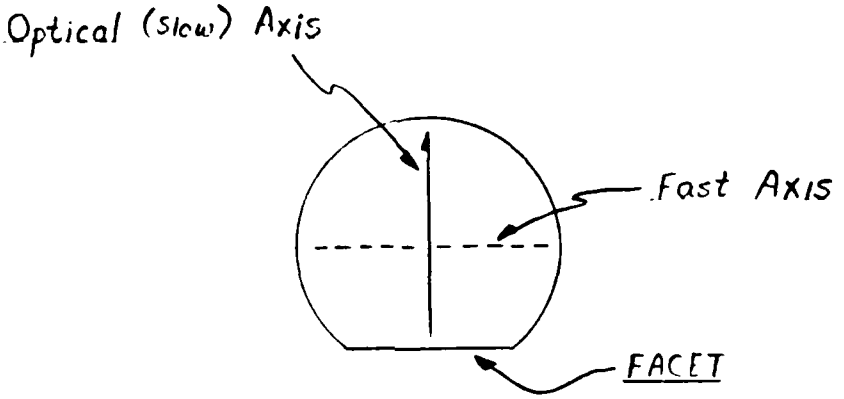

½ WAVE PLATE

Fig 7

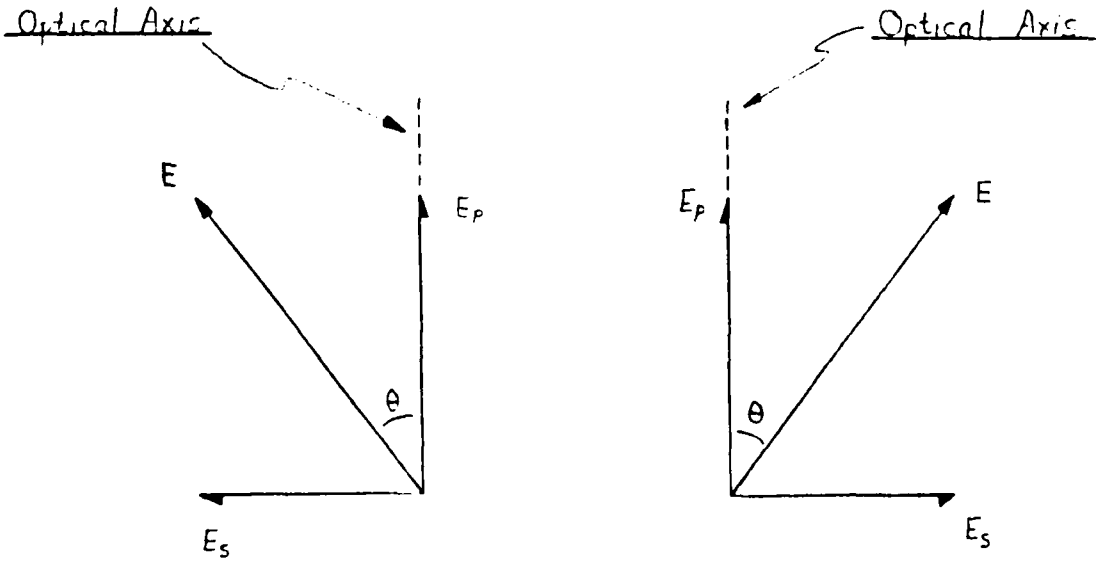

BEFORE RETARDATION AFTER RETARDATION

EFFECT OF ½ WAVE PLATE ON ELECTRIC VECTOR

Fig 8

Recall that since the laser beam is linearly polarized, the direction of its electric field vector lies along some fixed line. This electric vector can be resolved into components lying along the two preferred directions in the half wave plate. Call them E_p and E_s (p-parallel; s-senkrecht, the German for perpendicular; both directions relative to the optical axis). See Fig. 8.

Each component of E has its own phase velocity given by V = c/n, where c is the speed of light in vacuum and n is the refractive index along the given direction. Therefore, $Vp = c/n_p$ and $Vs = c/n_s$. In quartz, since it is a positive uniaxial crystal, the optical axis has the higher refractive index and thus the slower phase velocity. Thus it is called the "slow axis"; the other being called the, "fast axis". The net phase difference between the two components upon exiting the plate is a function of how thick the plate is. Evidently, for a net phase difference of $\lambda/2$, the requirement is that:

$$d(n_p - n_s) = (N + \tfrac{1}{2})\lambda \qquad (18)$$

where d is the thickness of the plate and N is some positive integer. Note again Fig. 8. The effect of the two components being $\lambda/2$ out of phase is that the E vector is, "reflected", about the optical axis of the half wave plate. Thus we have achieved a net rotation of the original plane of polarization through an angle of 2θ. By selectively setting the initial angle θ, we can put the plane of polarization of the laser anywhere we want it.

We have mounted the wave plate in a housing that has three degrees of freedom in adjustment. See Fig. 9. Axes 1 and 2 allow fine adjustment of the plate so that the beam is normally incident upon it.

Fig 9

½ - WAVE PLATE MOUNT

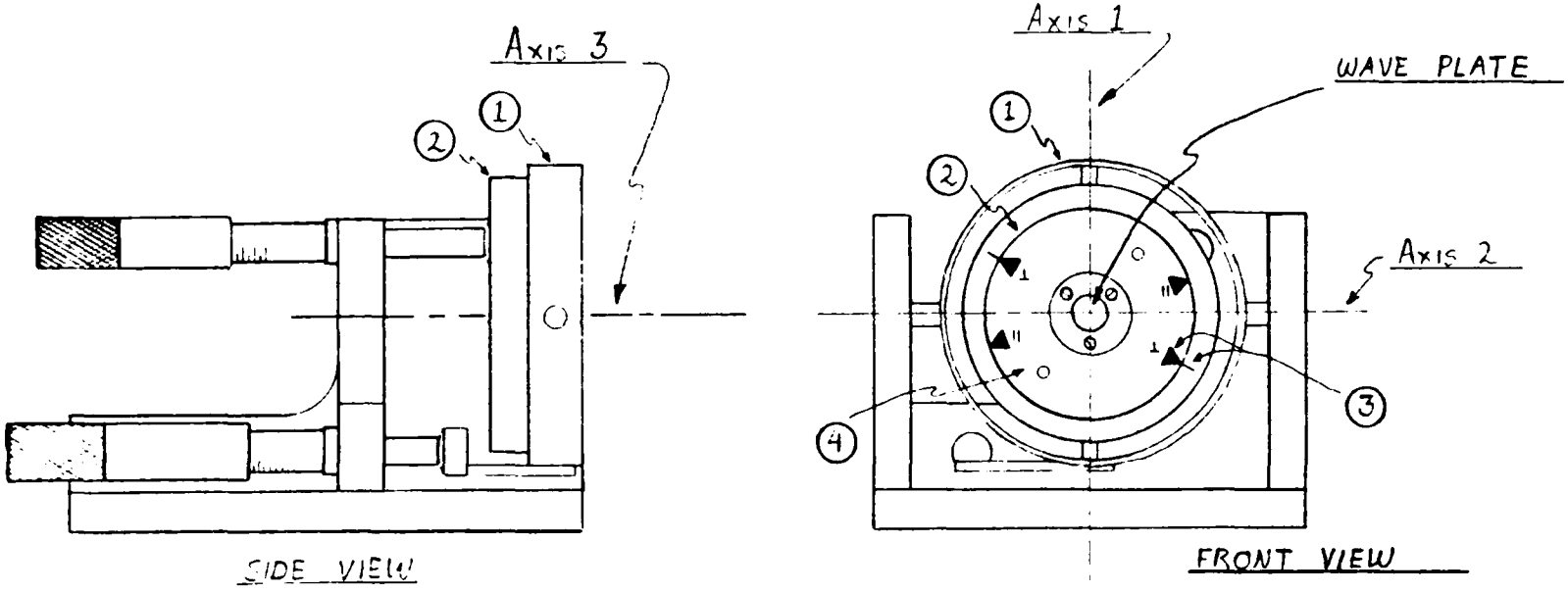

(1),(2) ALIGNMENT RINGS

(3) ALIGNMENT TICK MARKS: $\perp$ BEAM IS LINEARLY POLARIZED PERPENDICULAR TO SCATTERING PLANE
$\parallel$ BEAM IS LINEARLY POLARIZED PARALLEL TO SCATTERING PLANE

(4) ROTATING INNER PLATE – AS PLATE ROTATES THROUGH ANGLE θ, BEAM ROTATES THROUGH ANGLE 2θ

Normal incidence must be insured so that the entire beam is phase shifted by the same amount. Note the micrometers that affect these adjustments. Axis 3 allows the rotation of the optical axis of the plate so that the plane of polarization of the beam can be tuned to the desired angle.

The fourth element of the BPS is an Oriel model 1522 Spatial Filter Assembly. This device improves the spatial coherence of the beam by removing irregular intensity variations, interference fringes from dust on optical surfaces, as well as non-laser off axis light that might get into the beam line. Of particular nuisance is the glow of the plasma tube inside the laser, which propagates along the outer edge of the beam. (For He-Ne lasers it has a bluish hue to it.) We don't want to be detecting scattered light from these kinds of unwanted light sources. Ideally, we want the beam to have a smooth and uniform power distribution. The spatial filter produces such a uniform, near Gaussian energy distribution. The filter exploits the fact that off axis light and interference patterns propagate in directions other than that of the direct beam. By using a microscope objective, all of these sources are brought to the focal plane of the lens. The focal spot of the direct beam will not lie at the same point of the focal plane as the other unwanted signals. Thus, by placing a pinhole at the exact focus of the beam, it is possible to block out the unwanted light in favor of the pure beam alone. See Fig. 10. The resultant diverging (but now filtered) beam can be recollimated to almost any desired beam size.

To collimate the filtered beam, we use a bi-convex lens having a diameter of 38 mm and a focal length of 5 cm. From the previous figure it is clear that the smaller the focal length of the collimating lens,

Fig 10

SPATIAL FILTER & BEAM COLLIMATION

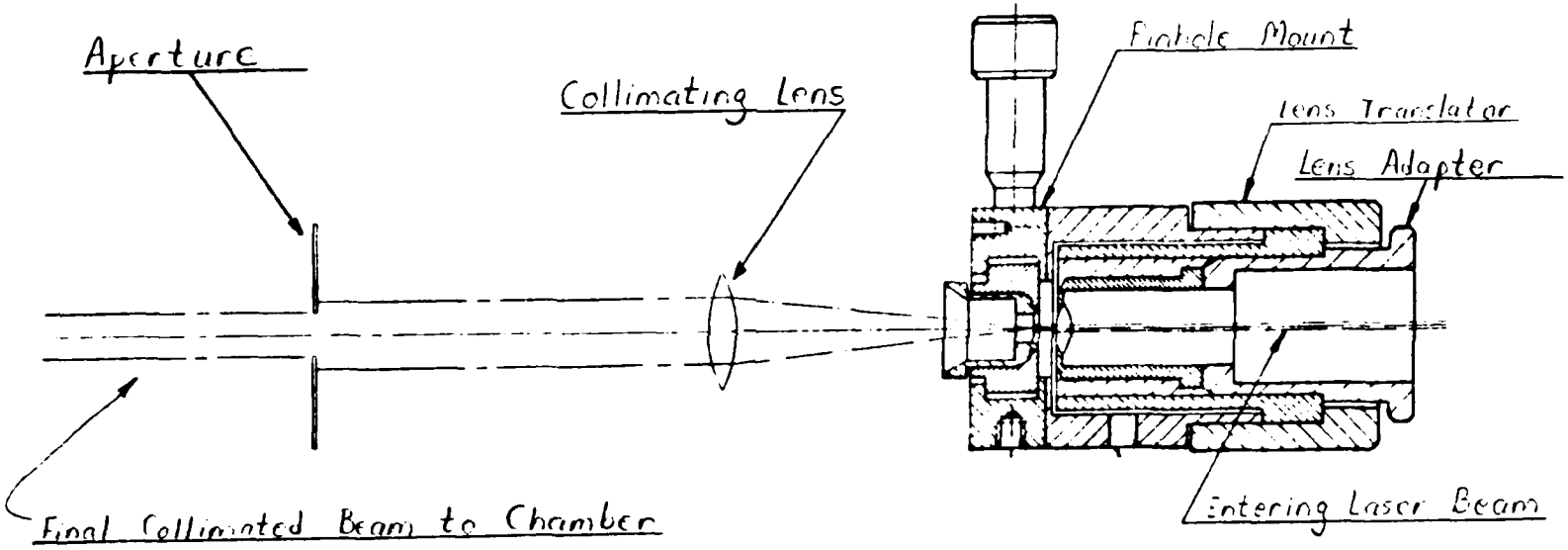

ORIEL MODEL 1522 SPATIAL FILTER

the smaller the beam divergence before collimation and therefore the smaller the collimated beam will be. Because of the limited amount of room on the BPS optical bench, the 5 cm focal length fits nicely, giving us a collimated beam with an 8.3 mm diameter. But the beam was still too large to make a clean pass through a window at the extinction end of the chamber. So we added after the collimating lens, an aperture to further stop down the beam size to 7.2 mm. The completed beam finally enters the chamber through a beam splitting window mounted at an angle on the end of the chamber. The angled mounting throws the reflected beam off axis where it is collected by a laser power meter photo diode. Thus we have, in addition to the desired beam, the capability to continuously monitor the power output of the laser.

DATA COLLECTION SYSTEM (DCS)

In addition to producing the desired input beam, we must also measure the extinction and scattering of the beam by the aerosol. This is the job of the Data Collection System (DCS). Here is where we put to work our understanding of geometrical optics, light detectors and electronic signal processing to exploit Mie theory in investigating the properties of an aerosol.

EXTINCTION OPTICS (EXOP)

The optics involved in measuring the extinction in the beam consists of a light trap assembly, and a spatial filter assembly followed by the extinction photomultiplier tube (EPMT). See Fig. 11. Early in the development of EXOP we had a clear window capping off the extinction end of the chamber, through which the beam passed before

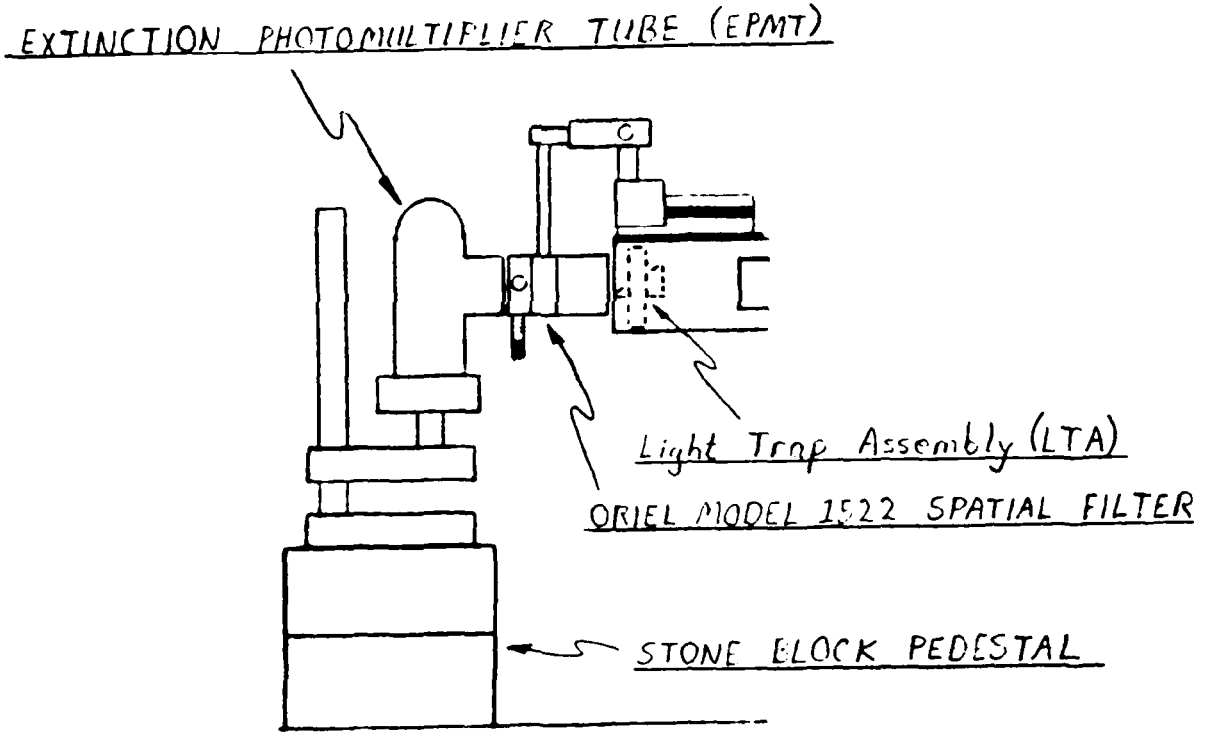

EXTINCTION OPTICS (EXOP)

Fig 11

entering the spatial filter assembly. With that arrangement though, we were plagued with excessive reflections off of the spatial filter back into the chamber. Such reflections were unacceptable because they interferred with back angle (90 to 180 degrees) measurement of scattering off of the beam. To eliminate this problem, we developed a Light Trap Assembly (LTA) as shown in Fig. 12. The LTA is constructed of one piece of clear plexiglass coated with our optically black paint. This piece serves to seal the extinction end of the chamber (so that no aerosol escapes) and also serves as a mount for the Light Trap (LT). The LT consists of two pieces of black plexiglass connected at an angle of 25 degrees. The top piece has a cutout which houses a 1.05% transmission Neutral Density Filter (NDF). 1.05% corresponds to an optical density D = 1.98 for λ = 632.8 nm at normal incidence. The NDF acts as the exit window for the beam at this end of the chamber and also performs an important function as part of the LT. Since the NDF makes a angle of 25 degrees with the forward direction of the laser beam, the beam, "sees" a path length of 4.97 mm through the NDF. The, "at normal incidence", thickness of the NDF is 2.1 mm. Thus, the actual optical density affecting the beam is (4.97/2.1)D = D' = 4.69. The transmission is related to optical density via, $T = 10^{-D}$. As a result, the actual transmission, T, experienced by the beam is 0.002%, or five orders of magnitude. (This sounds like a lot, and it is, but the transmitted beam is still quite visible to the naked eye.) Such a heavy attenuation keeps the direct beam from saturating or burning out the EPMT. In addition, it effectively blocks out any reflected light from the spatial filter from entering back into the chamber. For example, a light beam that goes through the NDF, strikes the spatial filter and is reflected

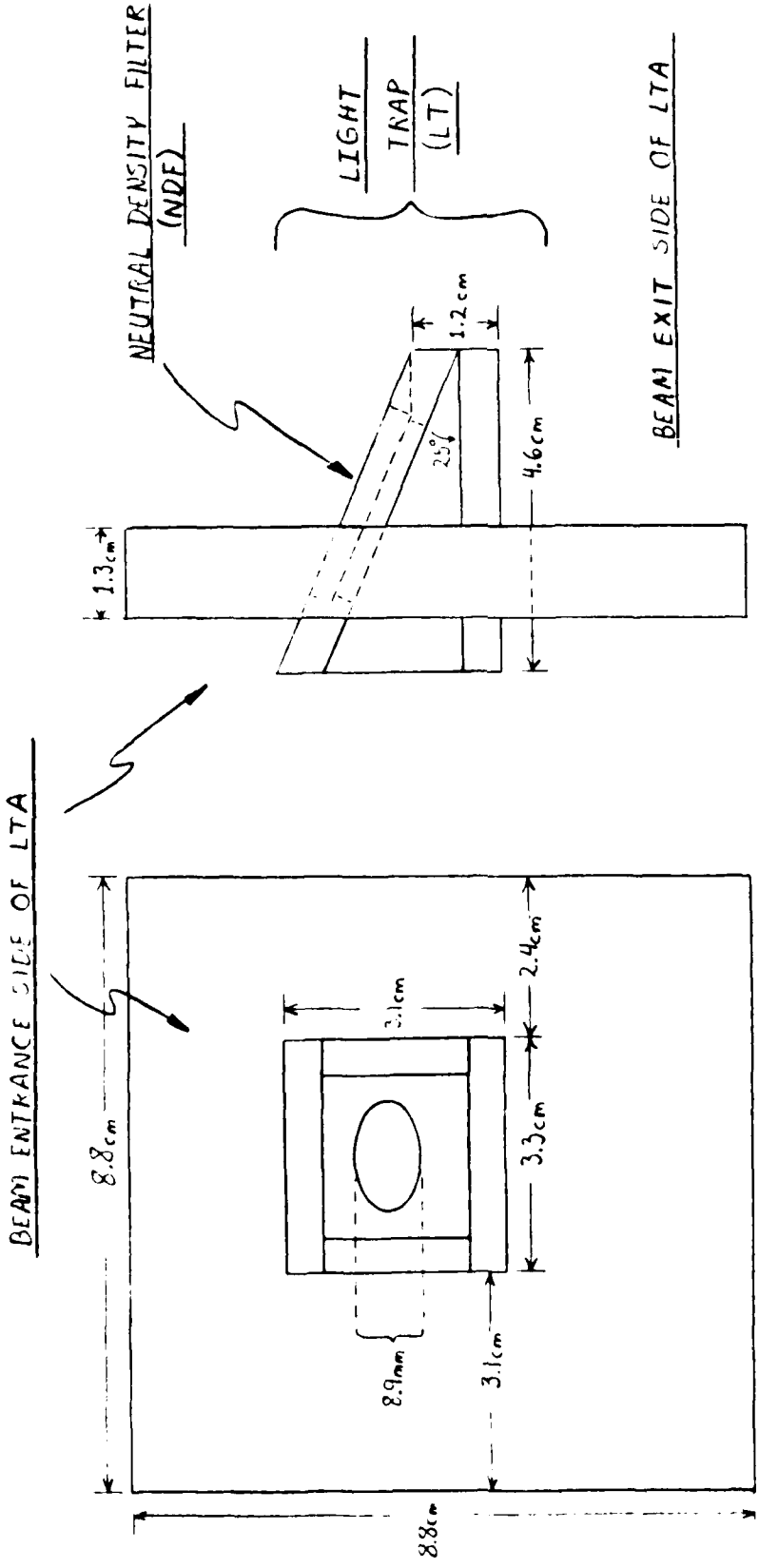

LIGHT TRAP ASSEMBLY / EXIT WINDOW (LTA)

Fig 12

back through the NDF into the chamber, experiences an attenuation by 10 orders of magnitude from the NDF alone, not to mention losses by reflection at the spatial filter.

To eliminate (or minimize) reflections from the LT back into the chamber we rely on the process of attenuation by multiple reflections. See Fig. 13. We consider only the case of the direct beam in this analysis since it is several orders of magnitude brighter than any scattered light entering the LT. So if we can effectively deal with the direct beam, the rest will be taken care of also. From Fig. 13 we note that the reflected part of the direct ray experiences a total of six reflections inside the LT before re-entering the chamber. Since the refractive indices of the plexiglass and the NDF are the same (1.5), we can treat all the reflections the same with respect to calculating how much light is reflected. Using the following laws and equations we can calculate how much light of the incident ray, I_0, gets back into the chamber. We consider each case of I_0; polarization parallel and then perpendicular to the scattering plane. Note that parallel to the scattering plane is perpendicular to the plane of incidence in the LT. Similarly, perpendicular to the scattering plane is parallel to the plane of incidence.

(i) $\theta_1 = \theta_1'$ Angle of incidence = Angle of reflection (19)

(ii) $n_1[\sin\theta_1] = n_2[\sin\theta_2]$ Snell's Law of refraction (θ_2 is an angle of refraction) (20)

NOTE: Angles θ_1, θ_1' and θ_2 are measured from the normal of the surface of incidence to the incidence ray.

following results for the important geometric quantities for data reduction.

(1) Distance from detector to center of FWHM segment as a function of θ:

$$R(\theta) = d_1 + L_1 + L_2 + D(\theta) \tag{24}$$

(2) FWHM beam segment viewed as a function of angle θ:

$$x(\theta) = \frac{A}{\sin\theta} + \frac{A}{2\sqrt{L^2+A^2}}\left[\frac{L_2+D(\theta)+E(\theta)}{\sin(\theta-\alpha)} + \frac{L_2+D(\theta)-E(\theta)}{\sin(\theta+\alpha)}\right] \tag{25}$$

(3) Uncertainty in angular measure at the detector as a function of θ:

$$\Delta\theta = \text{Arctan}\left[\frac{(U+P_1)\sin\theta}{2R(\theta)+(U+P_1)\cos\theta}\right] + \text{Arctan}\left[\frac{(U+P_2)\sin\theta}{2R(\theta)-(U+P_2)\cos\theta}\right] \tag{26}$$

This data is presented in tabular form in the appendix and graphical form in Fig. 19. Note that all three quantities are symmetric about 90 degrees. For example, the same values hold for both 80 and 100 degrees. Another point of interest is the flatness of the curve for $\Delta\theta$, as well as how small these values are. This behavior owes to the fact that $X(\theta)$ and $R(\theta)$ increase and decrease in concert with one another so that their ratio $\Delta\theta \sim X(\theta)/R(\theta)$ is approximately constant over the spectrum.

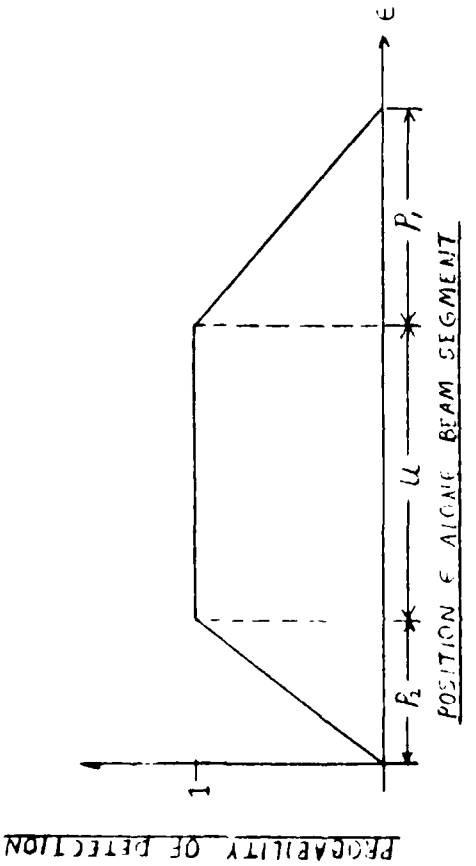

Fig 18A

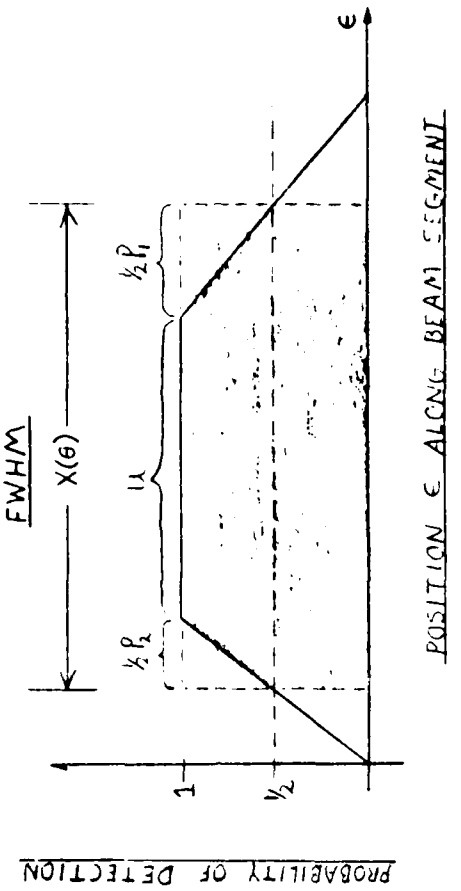

Fig 18B

at the detector. Rather, the two openings of the aperture tube, denoted by AA, are the limiting apertures for the system. By drawing in parallel and extreme rays at the points of tangency with these apertures we can determine the beam segment viewed by the detector. The result is a reverse umbra/penumbra type effect in which there is a bright central region which uniformly contributes to the detector signal along with dimmer peripheral regions whose contributions to detector signal diminish as the extremities are approached. This idea is displayed graphically in the next figure, Fig. 18A.

This figure depicts the full beam segment viewed by the detector. The probability that a photon emitted at ε, is received at the detector, is denoted by the trapezoidal behavior. All photons emitted in the central (umbra) will be received at the detector. In the penumbra regions though, the probability of detection falls off linearly from the edge of the umbra to the extreme edge of the penumbra. Note that the slopes of the two penumbra regions are in general not the same. (The only place they are the same is when the beam is viewed directly side on at θ = 90 degrees.) The easiest way to deal with this type of behavior is to assume that the entire detector signal comes from the full width of the beam segment at half the maximum detection probability. This idea is depicted in Fig. 18B. The area in the shaded region has the same area as that of the trapezoid.

The bottom line is this: We can calculate this FWHM segment of the beam and use it as though the entire detector signal is contributed to uniformly from all parts of the segment. Thus we can normalize all the detector signals to a unit volume of beam for the purpose of data comparisons. By applying the laws of plane trigonometry, we find the

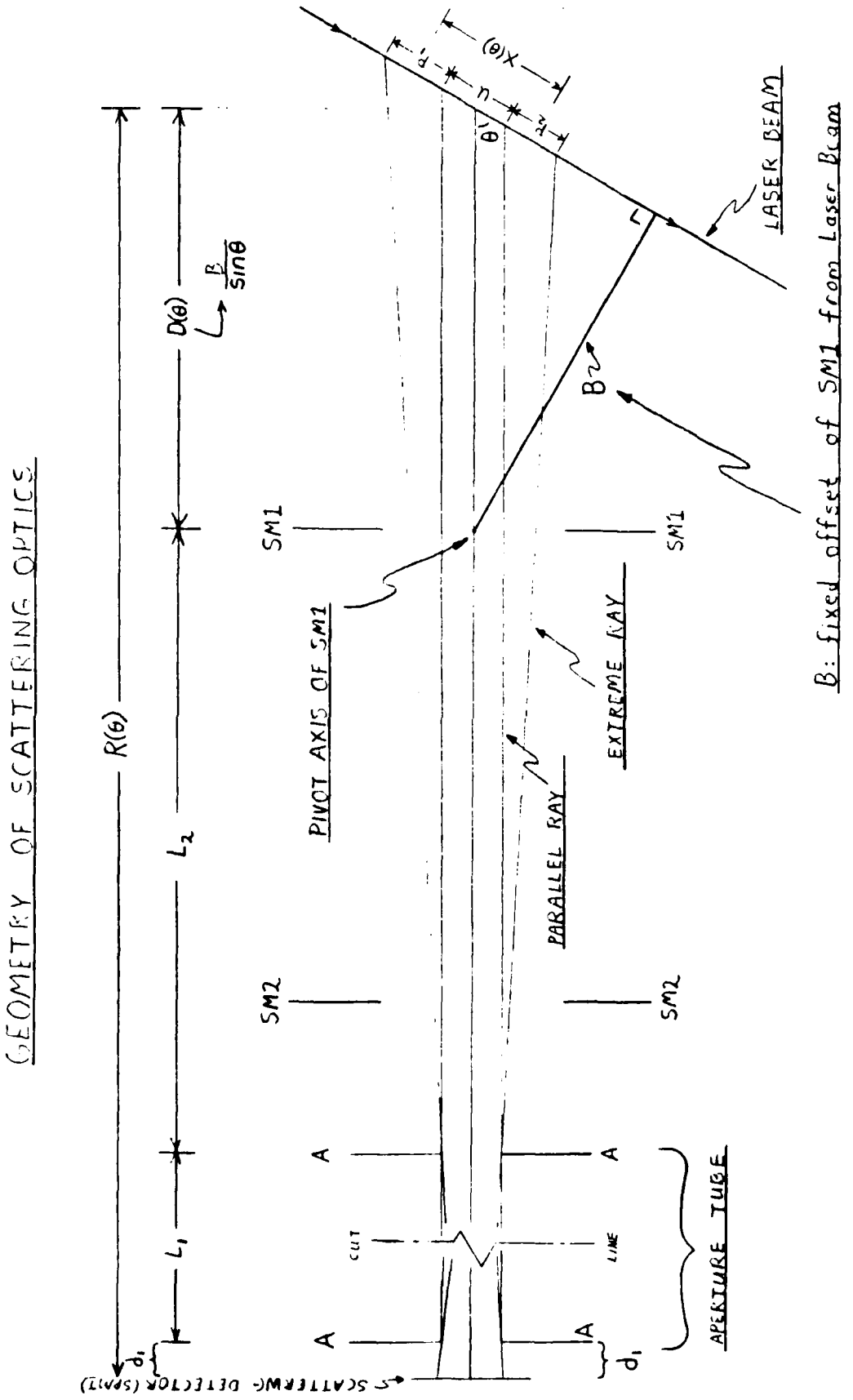
GEOMETRY OF SCATTERING OPTICS
R(θ)
L1
L2
D(θ)
B/sinθ
SM1
SM2
PIVOT AXIS OF SM1
PARALLEL RAY
EXTREME RAY
A
A
A
A
CUT
LINE
d1
d1
APERTURE TUBE
SCATTERING DETECTOR (SPOT)
LASER BEAM
B
θ'
X(θ)
h
B: fixed offset of SM1 from Laser Beam

Fig 17

Chart Recorder (SCR) #1 for the LPM reference, and by SCR #2 for the LIA scattering data.

GEOMETRY

For any detector system it is critical to data reduction, to know the detailed geometry of the system. The most important factors to know for scattering are:

(1) How far away is the detector from the scattering source?

(2) For a detector viewing a beam line as in our case, how much of the beam does the detector "see" at each angle where measurements are taken?

(3) Of that length of beam viewed by the detector, does it all contribute uniformly to the detector signal? If not, how does one account for the nonuniformity of the beam segment in terms of detector signal?

(4) What is the uncertainty in the angle viewed by the detector, i.e., since the detector views a finite beam segment at each angle, what does this convert to in terms of a $\Delta\theta$ about θ?

Our first step in answering these questions was to make a full scale drawing of the scattering optics to determine what the limiting apertures of the system are. A reduced version of this drawing is shown in Fig. 17. Although the optics do not lie in a straight line as shown, the geometry is just as if they did. Mirrors serve only to change the direction that a ray travels. Thus each mirror is treated like an aperture in this in-line layout. Note that the centroid of SM1 is the pivot point of the entire optical system, and therefore determines the primary scattering angle, θ. It turns out that SM1 and M2, the two scattering mirrors, have no effect on the size of the beam line viewed

Note from Fig. 16B how the image of the beam at SPMT rotates through 180 degrees, as SM1 scans from 0 to 180 degrees.

Thus, parts of the image of the beam would fall on different parts of the SPMT face having different sensitivities. We minimize this problem by the following technique. The glass surface of the SPMT has been, "bead blasted", to give the surface a diffusing quality (a frosted glass type effect). This diffusing surface tends to spread the beam out evenly over the photocathode, thus minimizing variations in sensitivity due to position.

A regulated bias for SPMT is provided by the same Fluke, high voltage source that powers the EPMT. Signal current from SPMT is amplified and measured by the EG&G Model 5101 Lock-In-Amplifier (LIA). Because of the low levels of light in the scattering regime, we employ the combination LIA and chopper to reduce the signal to noise (S/N ratio of the measurements. As mentioned before, the chopper modulates the beam in time at a rate of 338 pulses per second. The chopper also generates a square wave reference that is synchronous with the chopped signal. This reference signal is input to the LIA which uses it as a fingerprint of the kind of signal it will accept for measurement. In effect, the LIA searches for and locks onto only those signals from the SPMT that are modulated just like the chopper reference. Thus much unwanted noise is negated, allowing one to measure smaller signals than would normally be possible. As a further safeguard on the quality of our measurements, the EG&G LIA is also powered by a voltage regulated AC power supply, to minimize the effects of voltage fluctuations at wall outlets. Finally, hard copies of measured data are obtained via Strip

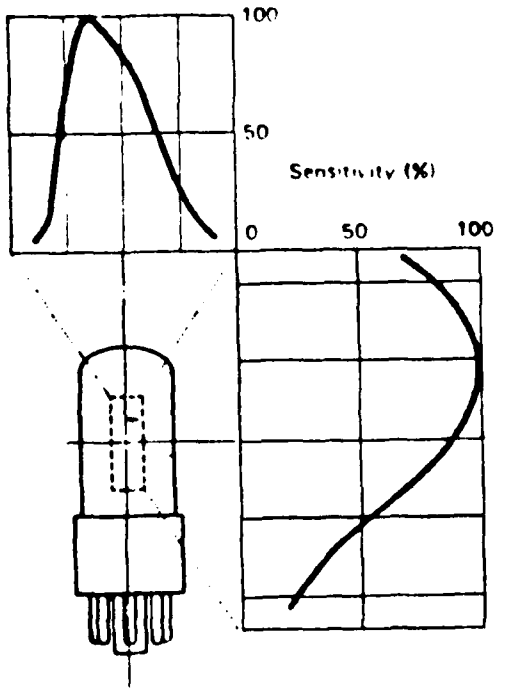

Fig 16 A

TYPICAL TUBE SENSITIVITY AS A FUNCTION OF POSITION

ROTATION OF BEAM IMAGE, VIEWED AT SPMT

Fig 16 B

with a 7 mm aperture at its center. The entire tube is painted flat black inside and out. The aperture tube serves three important functions:

(i) ALIGNMENT---By having the aperture tube aligned with BL2, it makes it easy to center the SPMT on BL2 by centering it on the final aperture.

(ii) RESOLUTION---The first aperture reduces the width of the beam image that is reflected from SM1 and SM2. By reducing the beam length viewed for scattering, we increase the angular resolution of the scattering measurements. The resolution we have is better than 1 degree.

(iii) STRAY LIGHT---Even though the scattered light is modulated by the chopper, there could be other signals in the room that are also modulated by the chopper. An example would be laser light reflected off of BPS components. The aperture tube's small apertures minimize the amount of room light entering the SPMT in favor of actual scattered signal from BL1. Furthermore, what room light does get into the first aperture is effectively attenuated by reflection from the black interior walls of the tube.

The final component of the SCTOP is the Scattering Photomultiplier Tube (SPMT). This device is a Hammamatsu R-928 side on type. It has excellent response in the red and is extremely sensitive to very low levels of light. The only problem with this tube (as with all side on types) is the variation in sensitivity over the face of the tube. Fig. 16A shows a typical map of tube sensitivity as a function of position.

Fig 15

SCATTERING MEASUREMENT / ELECTRONICS SCHEMATIC

① SCATTERING MIRROR # 1 (SM1)
② SCATTERING MIRROR # 2 (SM2)
③ APERTURE TUBE
④ SCATTERING PHOTOMULTIPLIER TUBE (SPMT)
⑤ OPTICAL BENCH
⑥ BEAM CHOPPER
⑦ LOCK IN AMPLIFIER
⑧ STRIP CHART RECORDER # 1

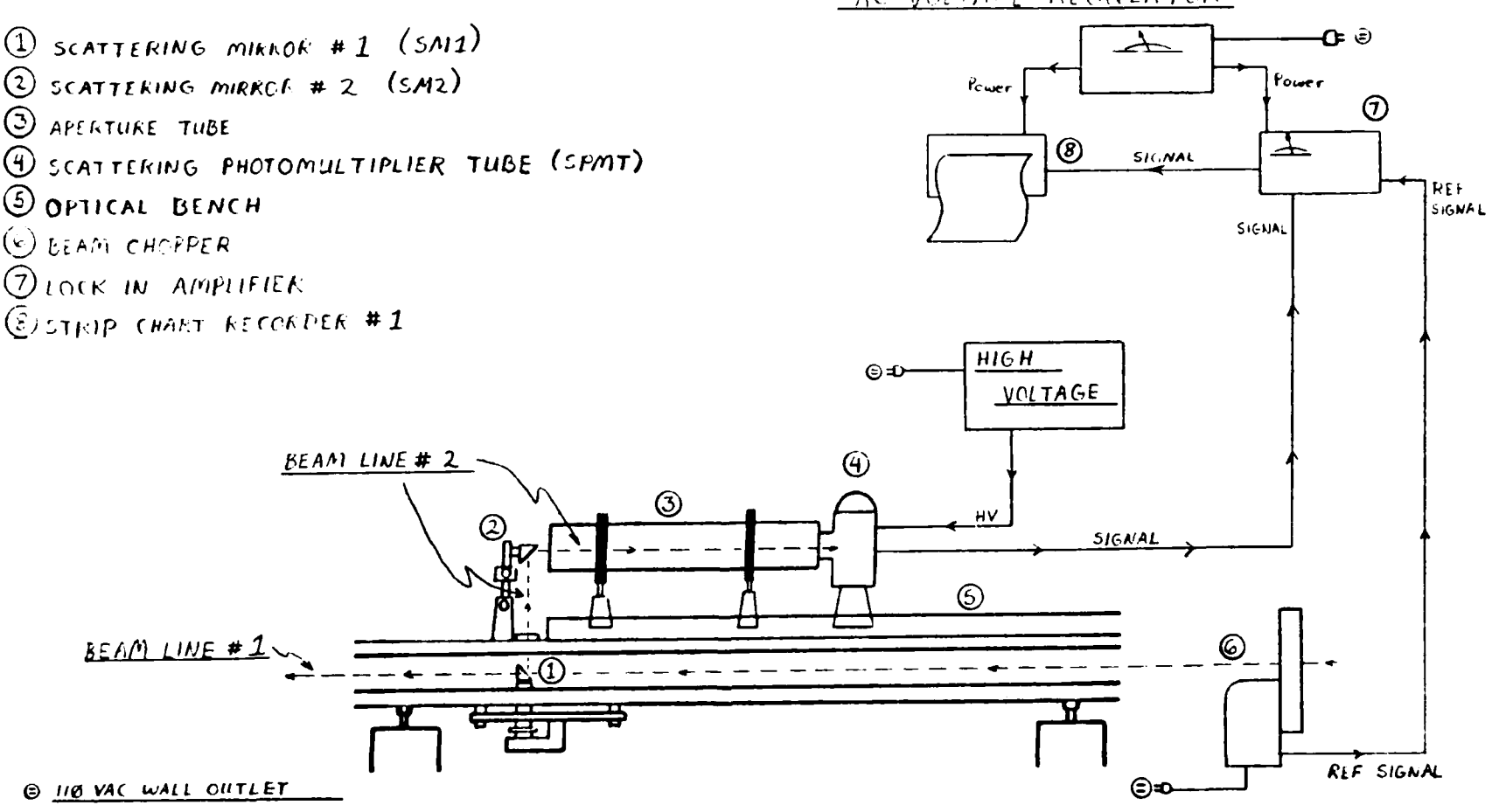

SCATTERING OPTICS (SCTOP)

To detect and measure light that is scattered out of the main beam, the DCS utilized two mirrors, an aperture tube and a photomultiplier. See Fig. 15. Scattering Mirror #1 (SM1) gives us the ability to scan the beam, from the side, from about 2 degrees at the forward direction to about 178 degrees to back angles. SM1 is located inside the chamber, 2.13 meters from the entry window (about 2/3 the way down the length of the chamber) and offset from beam centerline by 2.2 cm. It rests atop an aluminum post that is firmly attached to a base which allows it no side to side, or up and down movement. The base is mounted to the underside of the chamber by four adjustable bolts with locking nuts. The adjustable base is required for proper leveling and aligning of SM1. When correctly adjusted, SM1 is inclined at an angle of 45 degrees to the scattering plane. Measurement of the scattering angle is by a degree wheel which is mounted to the base of the mirror post just beneath the lower chamber wall. The image of the beam from SM1 is reflected straight up, out of the chamber through a small viewing port covered by optically flat glass. (We call the path that the scattering image traverses, Beam Line 2 (BL2)). This image is intercepted and re-directed another 90 degrees by Scattering Mirror #2 (SM2), which is located atop an adjustable mount directly above SM1. SM2 is identical to SM1 except for its mount and location. Both are front surface, aluminum mirrors. The mount for SM2 incorporates six different adjustments to facilitate exact alignment with SM1 and the other scattering optics. Upon reflection from SM2, the scattered light enters what we call the aperture tube. It consists of a cylindrical tube 87 cm long and 8.5 cm in diameter. At each end of the tube is a plastic plate

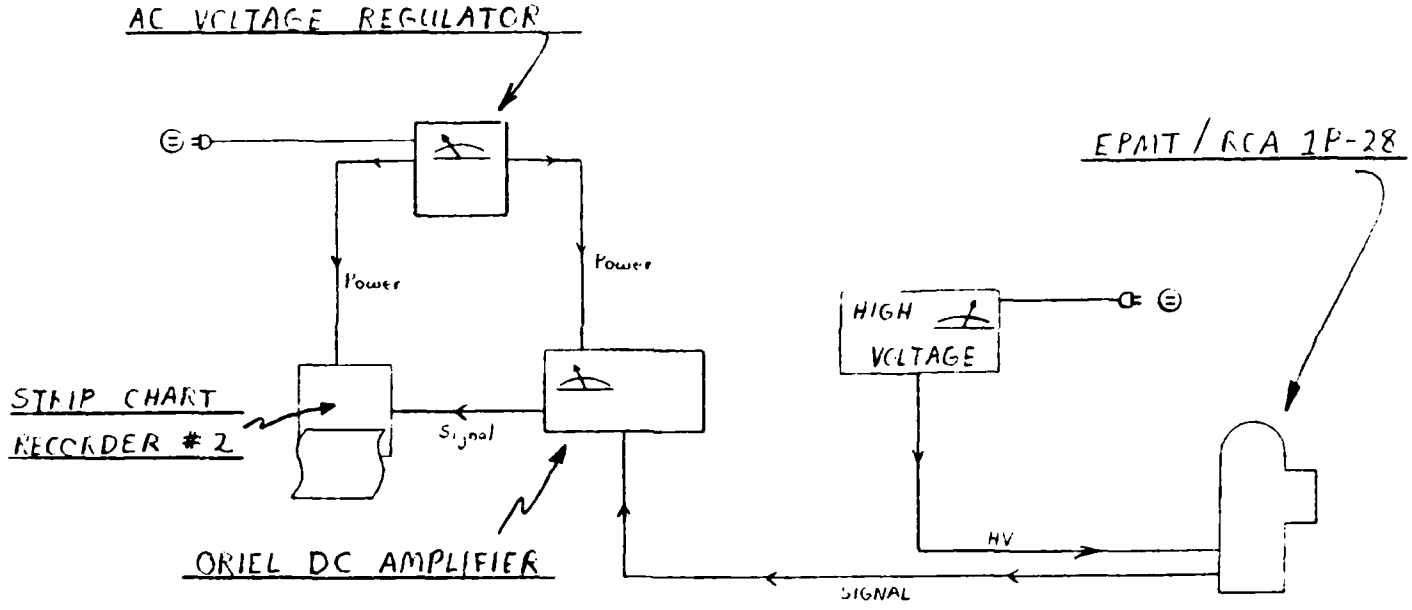

⊜ 110 VAC WALL OUTLET

EXTINCTION MEASUREMENT / ELECTRONICS SCHEMATIC

Fig 14

(iii) Fresnel coefficients of reflection for a source polarized parallel or perpendicular to the scattering plane.

$$r_p = \frac{n_2\cos\theta_1 - n_1\cos\theta_2}{n_2\cos\theta_1 + n_1\cos\theta_2} = \frac{(1.5)\cos\theta_1 - \cos\theta_2}{(1.5)\cos\theta_1 + \cos\theta_2} \qquad (21A)$$

$$r_s = \frac{n_1\cos\theta_1 - n_2\cos\theta_2}{n_1\cos\theta_1 + n_2\cos\theta_2} = \frac{\cos\theta_1 - (1.5)\cos\theta_2}{\cos\theta_1 + (1.5)\cos\theta_2} \qquad (21B)$$

(iv) R_s and R_p: Reflectances for oblique incidence at an interface.

$$R_p = [r_p]^2 \qquad (22A) \qquad\qquad R_s = [r_s]^2 \qquad (22B)$$

TABLE OF DATA

RFL#	θ_1	θ_2	r_s	r_p	R_s	R_p
1	65	37	-0.478	-0.115	0.2289	0.0132
2	40	25	-0.279	0.118	0.0779	0.0139
3	15	10	-0.209	0.191	0.0438	0.0364
4	10	6.65	-0.204	0.196	0.0417	0.0384
5	35	22.5	-0.257	0.142	0.0660	0.0201
6	60	35	-0.422	-0.044	0.1777	0.0019

TOTAL R_s = {product of the $(R_s)_i$; i = 1 through 6}. Similarly for R_p.

$$R_s = 3.8 \times 10^{-7} \qquad\qquad R_p = 9.8 \times 10^{-12}$$

Thus our light trap can attenuate reflections of the main beam by as much as 11 orders of magnitude. (Reitz, et. al., 1980, pp. 389-391) The result of this scheme is that the background signals measured in this region ($90<\theta<180$) are only a small percentage of the scattered signal.

With the problem of back reflected light taken care of, we move on to point out that the LTA is followed by a spatial filter assembly identical to the one described under the BPS. The purpose of this spatial filter is to eliminate all off axis scattered light from the main beam. Our goal is to measure only the attenuated main beam and nothing else. Unfortunately, it is impossible to filter out light that is scattered into the exact forward direction, since it is co-directional with the main beam. On the other hand, for particles about the size of the wavelength of the incident light, the mixing can be neglected, and we can assume that we are measuring only the attenuated beam (Van de Hulst, 1981, p. 388).

The final component of EXOP is the extinction photomultiplier tube (EPMT). Ours is an RCA 1P28 side on type. The response of the tube at a wavelength of 632.8 nm is about 4% of its peak efficiency at 330 nm. Nevertheless, even at this response level the tube effectively measures the attenuated beam. It is well suited to our needs, because for extinction we are only interested in a measurement of I/I_o; not in absolute intensities. A high voltage bias of 850 volts is applied to EPMT from a Fluke, regulated high voltage source. See Fig. 14. The output signal is amplified and measured on an ORIEL Model 7072, DC amplifier/readout. This device can detect as little as 10^{-12} amps of signal current. It employs a useful Ambient Suppress feature which allows us to cancel out as low as 10^{-12} amps of noise from the measured signal. Both digital and analog readouts are provided for signal readout. For a permanent record of the measurements, the readout of the ORIEL amplifier is recorded on Strip Chart Recorder #2, as shown in Fig. 14.

MULTIPLE REFLECTION EFFECT AT LIGHT TRAP

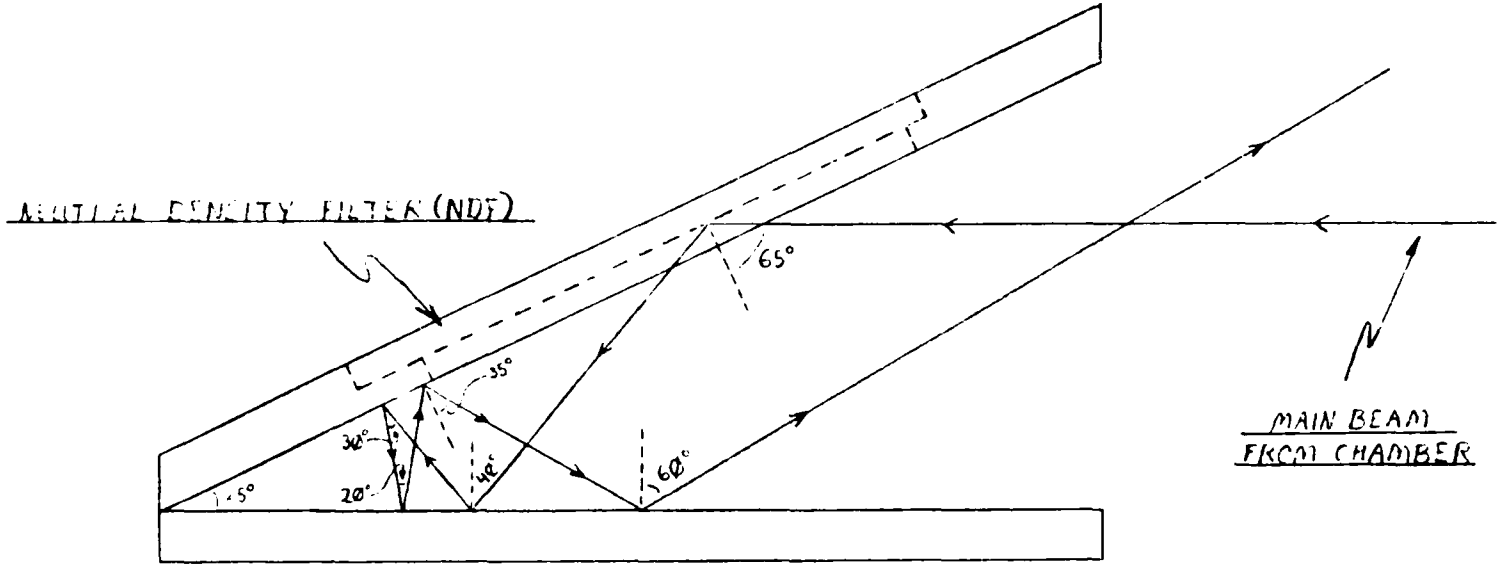

Fig 13

Fig 19

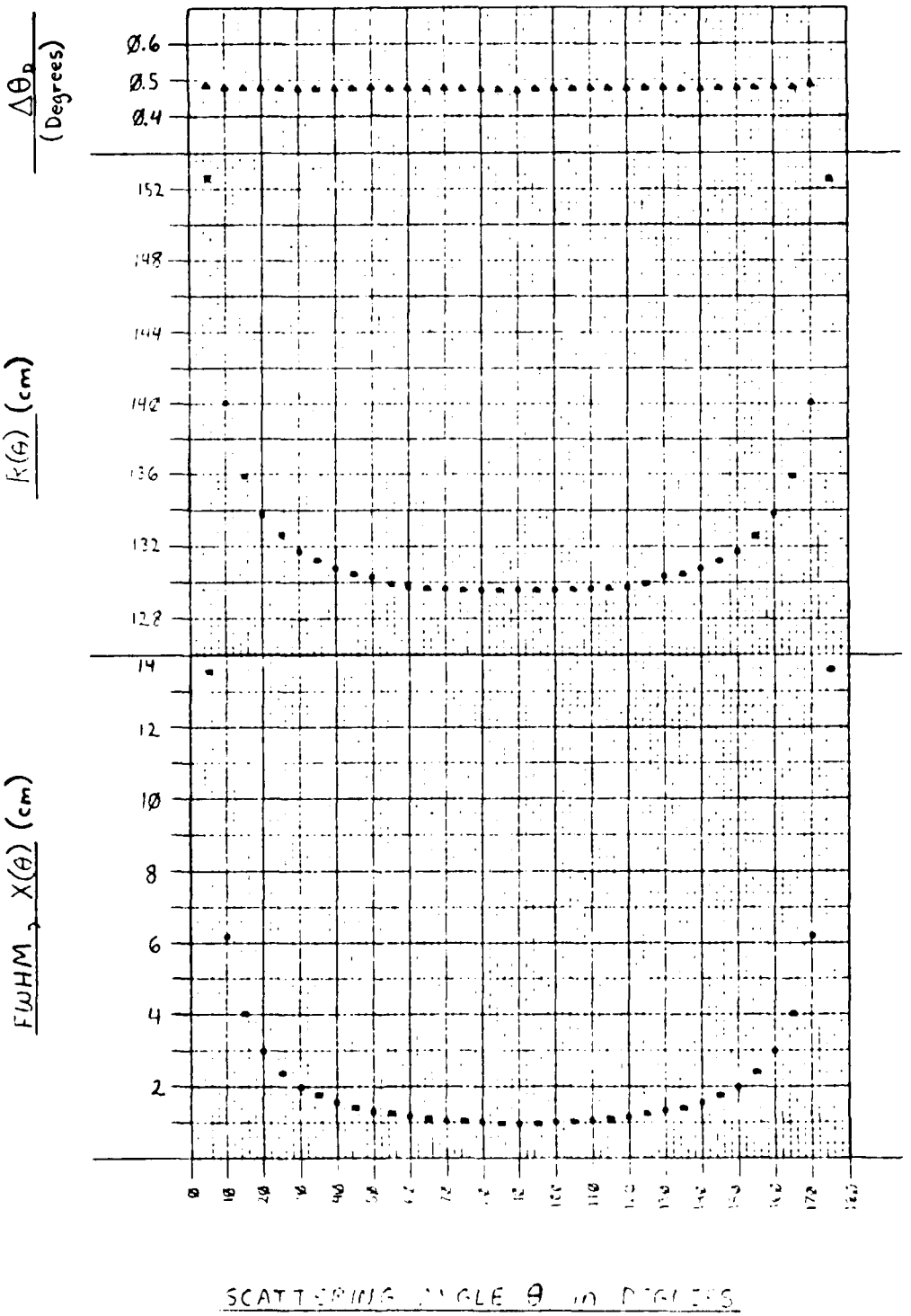
$\Delta\theta_D$ (Degrees)
Ø.6
Ø.5
Ø.4
R(θ) (cm)
152
148
144
140
136
132
128
FWHM, X(θ) (cm)
14
12
10
8
6
4
2
0
10
20
30
40
50
60
70
80
90
100
110
120
130
140
150
160
170
180
SCATTERING ANGLE θ in DEGREES

AEROSOL CIRCULATION/SAMPLING SYSTEM (ACSS)

The Aerosol Circulation/Sampling system is the second of the two major subsystems of our apparatus. It's primary mission is two-fold. First, ACSS establishes a closed system for measuring the properties of an aerosol in a clean atmosphere. This closed system keeps the particles suspended and uniformly distributed throughout the measurement region. Secondly, ACSS provides the necessary equipment needed to introduce to the system, and extract from it, quantities of an aerosol under investigation. ACSS accomplishes its mission via a system of pipes, tubing, valves, pumps, filters, fans, and sampling devices. It's three main functions, categorized as operating modes, are circulation, purging, and sampling.

The circulation mode (CM), as it's name suggests, moves the aerosol around a closed loop consisting of 2" pipe and hose, a 55 gallon drum reservoir and the interior of the chamber itself. See Fig. 20. The "push" that circulates the aerosol comes from a "squirrel cage" fan mounted inside the reservoir. This reservoir sits on shock and vibration insulating floor mounts that keep the small vibrations from the fan from being transmitted to the floor or the chamber via the 2" pipes and hose. As a further insulation of the chamber from fan vibration, we used 2", 'accordian type', hose to connect the loop to the chamber inlets. This 2" hose is even made of opaque black plastic to eliminate any possibility of light getting into the chamber. Rigid, black PVC plastic pipe is used to complete the loop between the reservoir and the return 2" accordian hose.

Three important considerations must be evaluated when dealing with confined aerosols. They are electrostatic deposition and coagulation,

ACSS - CIRCULATION MODE

Fig 20

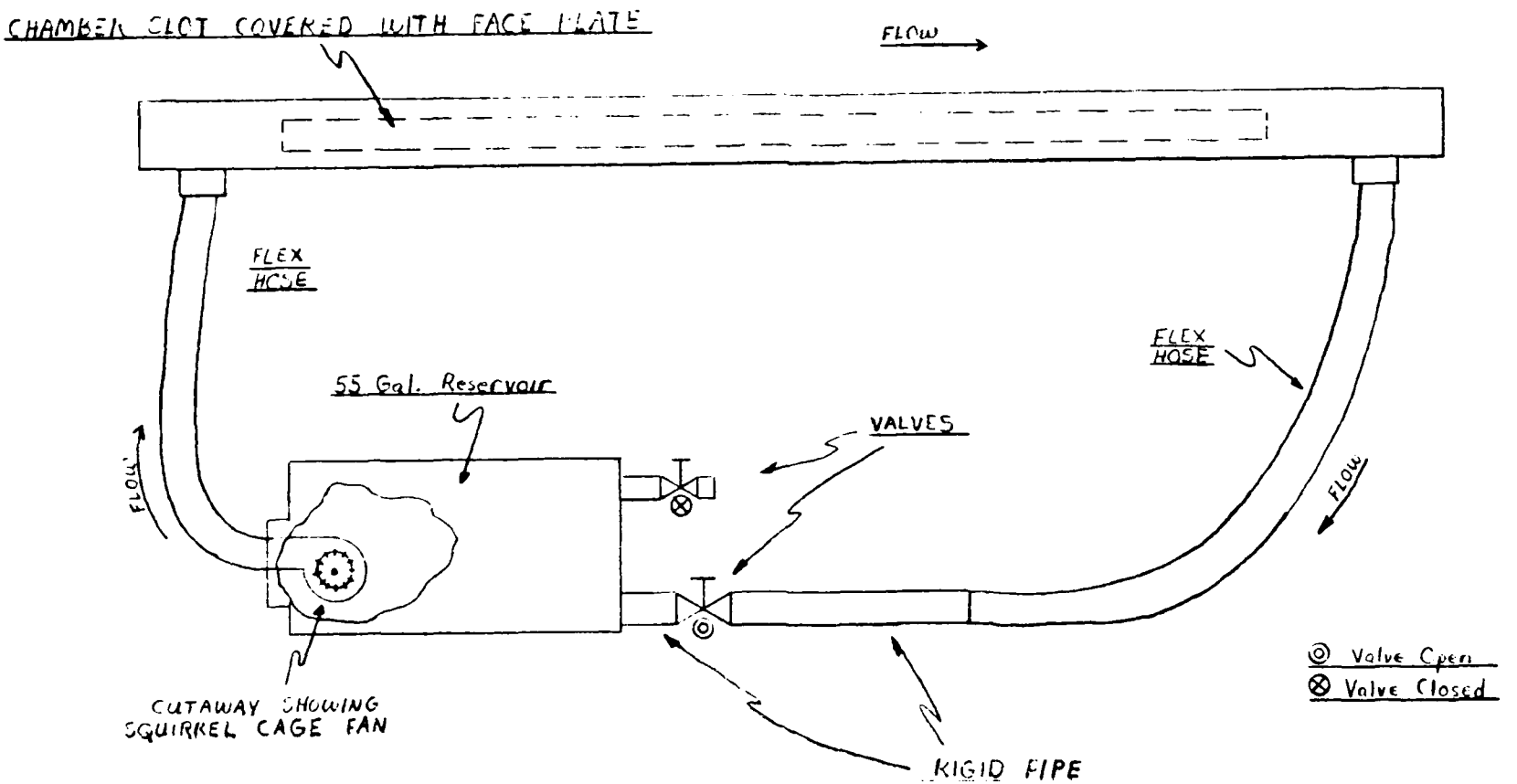

aerodynamic impaction, and Brownian diffusion. First we consider the electrostatic effects on the aerosol. Normal room air is electrically neutral, containing about one thousand ions per cubic centimeter. Statistically, half of these ions are positive and half of them are negative. Excess charge on aerosol particles is neutralized by collisions with these ionized air molecules, to the point where the aerosol obtains a state of charge equilibrium. This charge equilibrium is a Boltzmann equilibrium, and constitutes a state in which the average excess charge (*magnitude only*) per aerosol particle is a minimum. As an example, a sphere one micron in diameter has a minimum average charge of (2.34)e (e is the quantum of electric charge = 1.6×10^{-19} coulombs). A typical particle concentration that ensures single scattering Mie statistics is on the order of $N = 1.5 \times 10^{10}$ particles per cubic meter. This corresponds to an average particle separation of 250 particle diameters. Using these values of charge and particle separation, Coulomb's Law reveals that the average electrostatic force between the particles is on the order of 10^{-21} Newtons. By equating this force to the drag force from the surrounding air molecules, we can solve for the terminal velocity of the particles due to electrostatic attractions or repulsions. The result is $V_{te} = 2.2 \times 10^{-7}$ cm/sec (Hinds, 1982, pp. 42-43). Compare this value to the average thermal velocity (V_{th}) of the particles at STP, i.e., $V_{th} = 0.44$ cm/sec (Hinds p. 136), it is quite clear that electrostatic interactions can be neglected.

Unlike gas molecules, aerosol particles that collide with a surface via diffusion, adhere to it. As a result, the aerosol concentration at this surface is zero, thus establishing a concentration gradient in this region of the surface. This gradient causes a continuous diffusion of

the particles toward the surface, which results in a gradual decay in the aerosol number density (Hinds, 1982, p. 143). Recall that Brownian motion of the particles is the mechanism of this diffusion. It tends to move particles from regions of relatively high concentrations to regions of lower concentrations. Thus there exists this incessant motion of the aerosol towards the walls of the system. This process is characterized by a particle diffusion coefficient D, which is related to the number of particles transiting a unit surface area per unit time (Hinds, 1982, pp. 133-136). An upper limit to the diffusion losses can be gleaned by utilizing the equation:

$$N(t) = 2N_o\sqrt{\frac{Dt}{\pi}} \qquad (27) \qquad \text{(Hinds p. 145)}$$

Here N(t) gives the cumulative number of particles deposited out onto a unit surface area for an infinite volume of stagnant aerosol. (The stagnant condition is important because during actual data taking, the circulation fan is off.) Hence, our diffusion loss should be no greater than this. Using $D = 2.7 \times 10^{-7}$ $(cm)^2/sec$ and $N_o = 1.5 \times 10^4$ $particles/(cm)^3$, we find that after 30 minutes, $N(t) = 3.7 \times 10^2$ $particles/(cm)^2$. This looks like a big loss of particles at first, but consider the percent loss of particles. Let N_v be the actual number of particles in the system, and let N_d be the actual number lost to diffusion.

$N_v=(Vol)N_o=(0.48\ m^3)(1\times10^6\ (cm)^3/m^3)(1.5\times10^4 particles/(cm)^3)$

$N_v = 7.2 \times 10^9$ particles

$N_d = (AREA)N(t)$

$= (3.66\ m^2)(1 \times 10^4\ (cm)^2/m^2)(3.7 \times 10^2\ particles/(cm)^2)$

$= 1.35 \times 10^7$ particles

The actual percent loss is therefore equal to 0.19%, which is quite acceptable for any period during which measurements are taken.

Since the aerosol is moving from time to time, the question of losses due to this dynamic motion should be considered. The moving particles are subjected to inertial accelerations through the cycling fan, collisions with the walls of the system, as well as another type of diffusion called dynamic diffusion. The sum total of these and other effects is difficult to quantify theoretically; however, it can be easily measured. Our original guess was that losses due to these mechanisms would be negligible because of the small size of the particles, the large diameter tubing, as well as what we considered a low flow rate of particles through the system. Measurements of extinction over time, with the fan running at various speeds, or completely off, have shown that there are significant losses of particles due to prolonged circulation. For example, during test runs measuring extinction from rice straw smoke, continuous circulation of the aerosol resulted in losses of as much as 2% per minute. The obvious solution to this problem was to take measurements with the fan off, to render the aerosol effectively stagnant. Further test runs using this procedure have shown that the particle concentration is steady, not varying more than ±1% from the mean over a period of 45 minutes (more than enough time to take a full set of data). So during data taking the circulation fan is only used intermittently to mix up the aerosol as required. On such occasions, the fan is run at 75% of top speed to further minimize dynamic losses.

Although the dynamic loss of particles is a problem during data taking, there are times when this effect works to the researcher's

ACSS - PURGING MODE

Fig 21

◎ VALVE OPEN

⊗ VALVE CLOSED

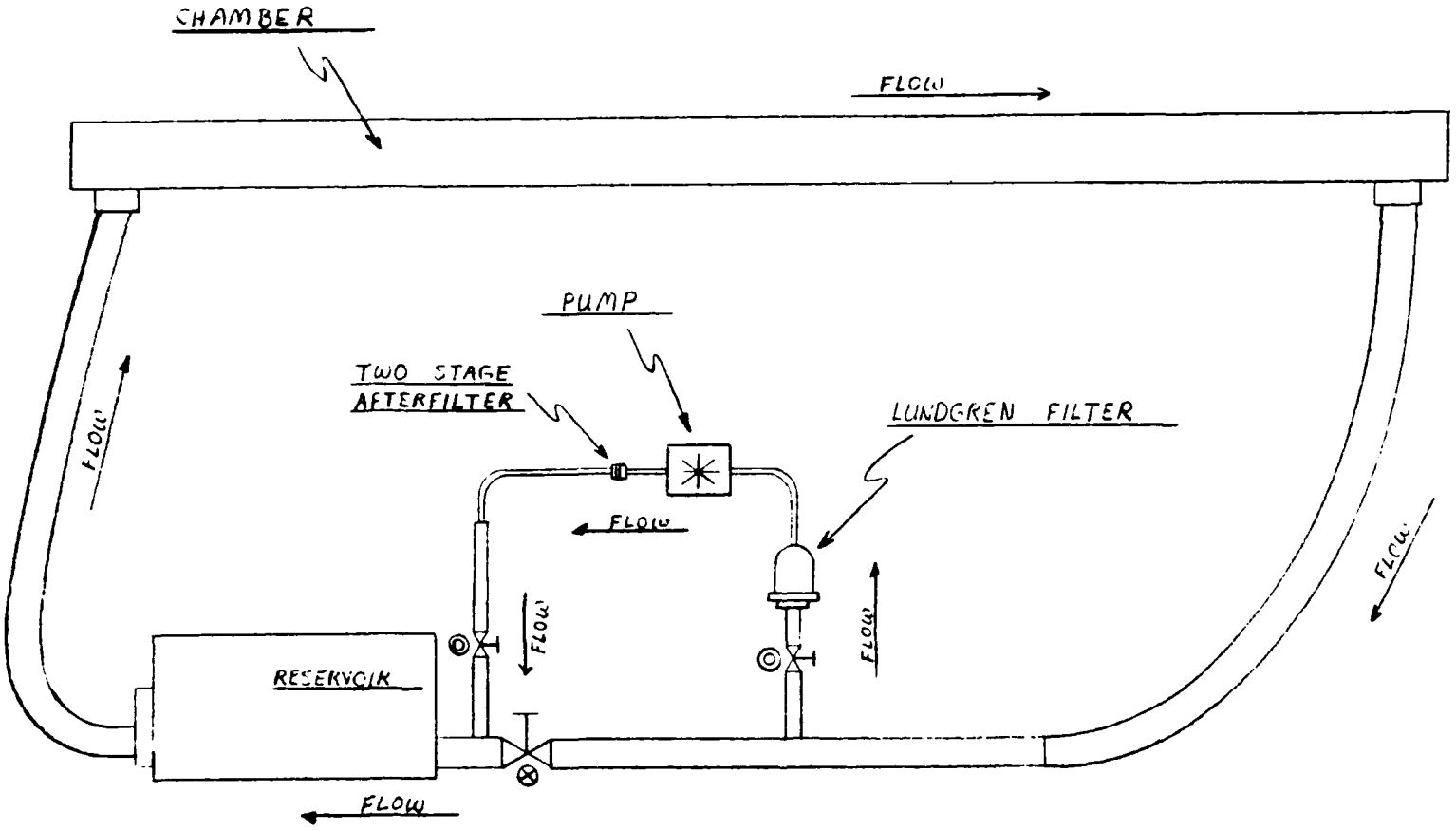

favor. In particular, consider the function of the Purging Mode. Its work is to clean out the air in the circulation system so that no detectable foreign particles remain in it. This is a very important function because even dust particles from ambient laboratory air scatter a detectable amount of light. The Purging mode incorporates all of the "plumbing" of the circulation mode (CM), but adds on a second loop containing a valve, a pump, and two filter units. See Fig. 21. The pump draws air out of the CM plumbing, through a single stage, filter unit. The filter in the unit is a polycarbonate membrane 90mm in diameter, which eliminates all particles larger than 0.8 microns. Upon exiting this filter unit, the air cycles through the pump and then into a second filtering device. This unit houses two filters made of fibrous Teflon and boasts a 98% removal efficiency for all particle sizes. (Cahill, et. al., 1977, p. 675) Once the air is filtered, it completes the loop, re-joining the main flow of the circulation plumbing. During purging, the circulation fan is run at top speed. This not only ensures a steady flow of particles to the purging loop, but also eliminates some particles by the dynamic flow effects mentioned above. A complete purge of the system takes about two hours. Analysis of background scattering in the clean atmosphere reveals the efficacy of the purge. The maximum background to data ratio is about 7%, but typical values of background are 1% or less compared to scattering data.

We now turn our attention to the Sampling Mode (SM) of the ACSS. See Fig. 22. Sampling is basically a drawing of aerosol-laden air out of the circulation system at a calibrated flow rate and into a sampling device. Such aerosol samples may be studied for size, gravimetric, and chemical composition information. Two types of sampling devices are

Fig 22
ACSS - SAMPLING MODE

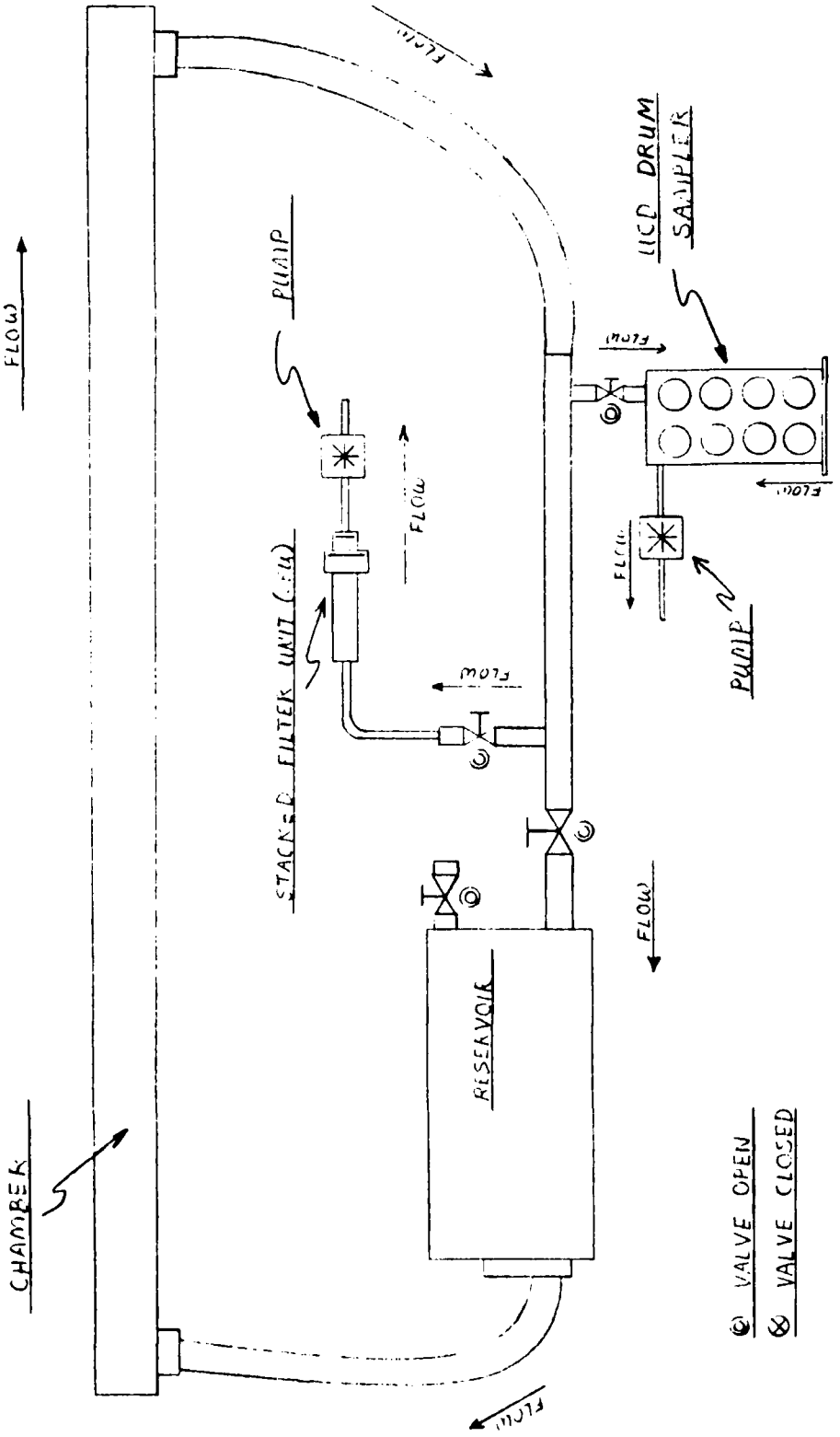

employed, both of which have proven reliability in the UCD Air Quality Group's particulate studies throughout the United States. (Cahill, NPS Report 1984) The samples are known as the Stacked Filter Unit (SFU) and the UCD DRUM.

A Stacked Filter Unit is a sampler that collects aerosol particles via two, in-line filters. See Fig. 23. The first filter is a polycarbonate membrane that collects all particles larger than 8 microns and over 50% of the particles between 2.5 and 8 microns. The second filter is the same Teflon filter used in the post-pump after filter described under the Purging Mode. An SFU is designed to give information on only two aerosol size modes. More importantly, it can be used to determine the mass density of an aerosol. Each filter is pre-weighed and post-weighed with a microgram sensitive electrobalance, to measure the total aerosol mass deposited on the filters. (Feeney, et. al., 1984) Since the flow rate is known and sampling times can be determined, one can calculate the mass density of the aerosol in both coarse and fine size cuts. SFU filters are also used as a substrate for PIXE analysis of the chemical composition of the aerosol.

The second sampling device employed by our system is the Davis, Rotating-drum, Universal-size-cut, Monitoring Sampler; or more succinctly--the DRUM. This device operates on the principle of inertial impaction. An aerosol passes through a jet whose output stream is directed against a flat surface which causes an abrupt 90 degree bend in the streamlines. See Fig. 24. (Hinds, 1982, p. 114). The size of the jet as well as the exit velocity at the jet determine a so-called aerodynamic cutoff size. This cutoff size is not a true geometric size, but is an aerodynamic parameter that contains both mass and size

Fig 23

STACKED FILTER UNIT (SFU)

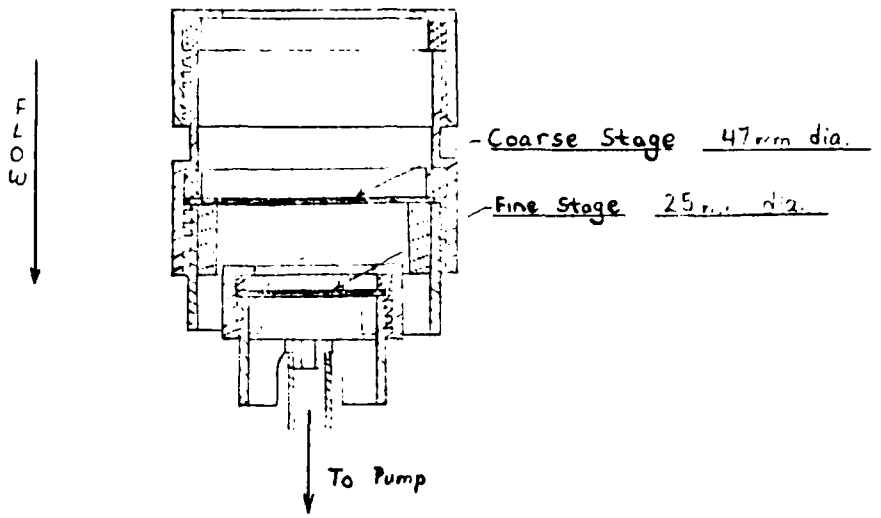

FLOW RATE: VARIABLE, BUT STANDARD RATE IS 10 lpm
COARSE STAGE SIZE CUTOFF : 2.5μm
FINE STAGE SIZE CUTOFF : Ø (98% efficient for all sizes)

Fig 24

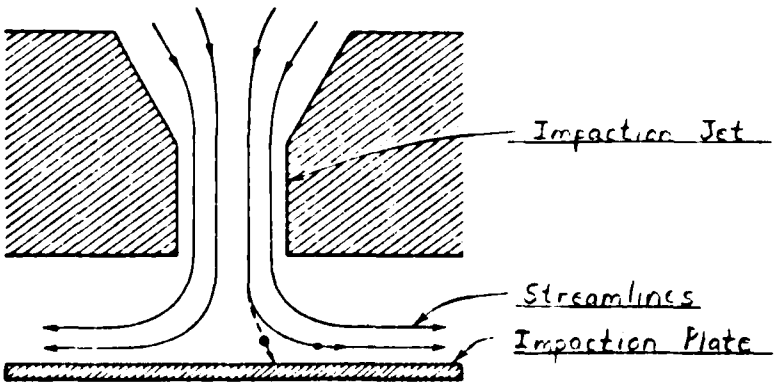

Cross Sectional View of an Impactor

information. (Hinds, 1982, pp. 49-50) Particles larger than the cutoff size have too much inertia to follow the 90 degree bend in the streamlines and therefore impact out on the surface. Particles smaller than a cutoff size follow the stream, remaining in the flow until they impact out at one of the eight different size cut-off stages in the DRUM. In this particular device, the sticky impaction surface is a rotating aluminum drum covered with a Mylar impaction substrate. The drums are electrically rotated to give time resolution on the order of days or weeks. However, the gearing can be modified to make the time resolution work on the order of fractions of an hour or hours. This would be more suitable to our needs and is a refinement that can be easily done in the future. For now though, the DRUM is an excellent vehicle for determining the size distribution of an aerosol, and can be used for comparisons with particle size information extracted from extinction and scattering data. The Mylar substrates containing the aerosol particles can also be analyzed for chemical composition with PIXE and other X-Ray excitation techniques. Fig. 25 is a schematic of the DRUM along with some of the relevant specifications.

At the present time sampling is done immediately after scattering and extinction data are taken. Since the aerosol is contained in a closed system, mass and size information should not vary strongly as a function of time. (Subsequent extinction vs. time measurements have borne this out.) Furthermore, the samplers do significantly reduce the number of particles in the system. For example, with both samplers running, they extract eleven liters per minute from the system. Over a 40 minute data run 440 liters would pass through the samplers, which is more than the volume of the entire system! As a result, it is not now

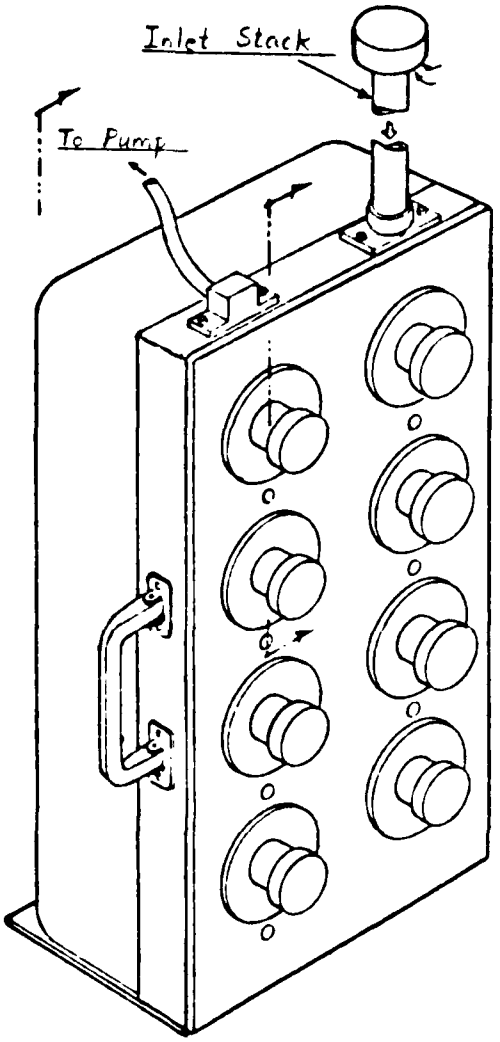

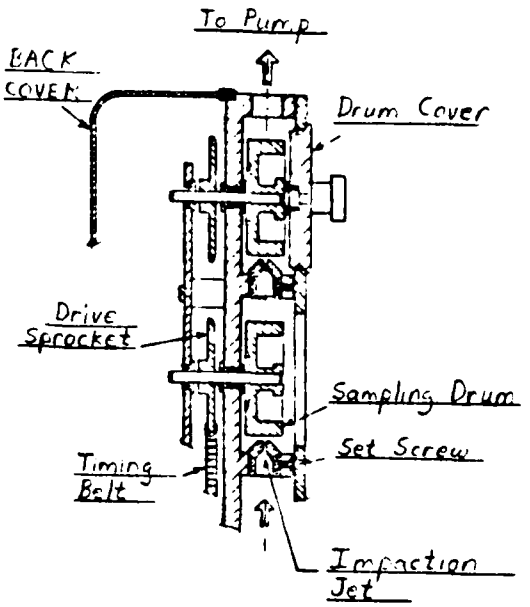

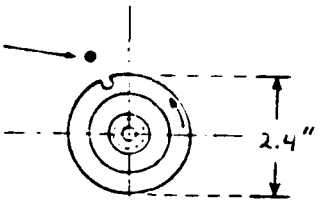

Sampling Drum
Front View

FLOW RATE : 1 lpm

Size Cutoffs in MICRONS

①	8 - 15	⑤	1 - ½
②	4 - 8	⑥	½ - ¼
③	2 - 4	⑦	¼ - ⅛
④	1 - 2	⑧	⅛ - 1/16

Fig 25

Davis Rotating Universal-size-cut Monitoring SAMPLER

DRUM SAMPLER

feasible to sample during data taking. Indications are that this capability can be worked into the system. Computer control of data acquisition would reduce the time required for a set of measurements. In addition, the SFU could be replaced with sampler that draws less than 10 liters per minute. Having a larger reservoir is also a possible fix. Part of the reason for having the 55 gallon reservoir was to provide enough volume so that sampling during data taking would not significantly reduce the particle density in the measurement region. However, its presence alone does not suffice. Subsequent studies are needed to provide this capability for the system.

Reduction of the scattered data was the next step in the analysis process. Background readings were taken for each polarization after the system was completely purged of particles. This background data was taken at different ILP readings than the actual scattered readings. But since ILP was higher on all background readings than on actual scattered readings, we felt we could not go wrong by using more background than was probably present during data taking. This assumption seemed especially appropriate since the background values are so low in comparison to the actual scattered data. For example, at 5 degrees where both scattering and background are a maximum, we find that:

$$\left(\frac{IBK}{ISC}\right) = 0.5\% \qquad \left(\frac{IBK}{ISC}\right) = 0.8\%$$

Also, at 115 degrees where scattering is a minimum, we find that:

$$\left(\frac{IBK}{ISC}\right) = 5.7\% \qquad \left(\frac{IBK}{ISC}\right) = 6.9\%$$

Although these last two values are not that small, most others are less than 1%. Our procedure for reducing the scattering data is as follows:

(1) Both ISC and IBK were first corrected to a reference ILP reading. For IPERP this reference ILP is just the clean system reading, i.e., I_0LP. The laser power reference for IPARA is the mean ILP reading for that set of measurements. These are the same kind of adjustments that were made to IEX previously. The adjusted values are denoted by ISC' and IBK'.

(2) Calculate the "detector reading of scattering", denoted by DSC, as follows: $DSC = ISC' - IBK'$ (33)

(3) Each detector reading DSC has experienced a certain amount of extinction before it departs the chamber through the port above SM1. The amount of extinction is different between the forward and

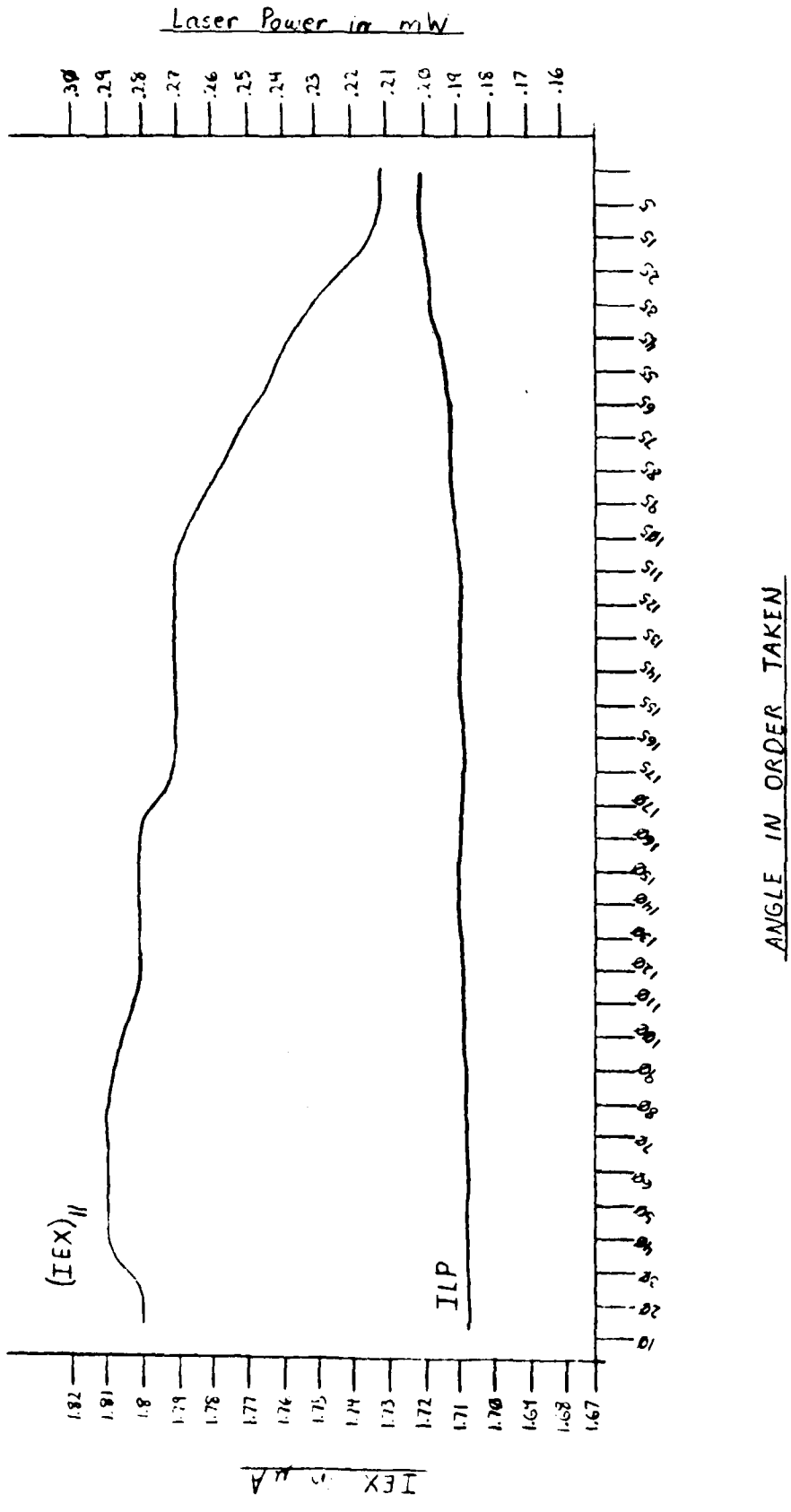
Laser Power in mW
.30
.29
.28
.27
.26
.25
.24
.23
.22
.21
.20
.19
.18
.17
.16
$(IEX)_{II}$
IIP
IEX in μA
1.82
1.81
1.8
1.79
1.78
1.77
1.76
1.75
1.74
1.73
1.72
1.71
1.70
1.69
1.68
1.67
ANGLE IN ORDER TAKEN

Fig 28

have changed when the wave plate was rotated. In addition, at the end of the measurement period, the last eleven data points revealed a curious decrease in IEX, accompanied by an increase in ILP. See Fig. 28. Consider though, that these last two events, observed simultaneously are totally inconsistent. Decreasing IEX values are indicative of increasing numbers of particles; but we were generating no particles during this time. Also, an increase in ILP should invoke an increase in IEX readings. The confusion is lifted by observing that there is some systematic drift downward of the ISC values for these last eleven angles. We took data in the same order as before, beginning with the 10 degree increment angles and ending with the 5 degree increment angles in reverse. So our best assessment is that one of the following two events occurred:

(1) There was actually a loss of particles at the end of this run, resulting in decreased ISC readings. The variations in ILP and IEX were from temperature effects mentioned before.

(2) There was an actual loss in laser power resulting in the decrease in ISC readings. The loss in ILP was masked over by temperature effects on alignment to appear to be an increase in ILP. The change in IEX is alsc a temperature related alignment problem.

The bottom line is that we don't know what happened. Nevertheless, our gut feeling is that the number density of particles remained the same, based on the stability we observed in the first set of measurements. So we felt it appropriate to use the same value of extinction on this second set as was used on the first set. When comparisons of this data with theory are made though, we must be cautious when dealing with the last 1/3 of this data set because of the problems just mentioned.

In this equation Q_{ex} is the so called extinction efficiency. It is defined as:

$$Q_{ex} = \frac{\text{Extinction Cross Section}}{\text{Geometrical Cross Section}}$$

Q_{ex} is a relative measurement of how efficiently the particle removes energy from the incident beam, as compared to simple blocking of the beam by the projected area of the particle. (Hinds, 1982, p. 319) Values of Q_{ex} are tabulated in a variety of sources, or they can be calculated by a computer program. Our Mie scattering program named CALLBH (See Appendix) was used to compute $Q_{ex} = 3.049$ for our 1μm Polystyrene spheres. Also in Eq. 31 above, "r" is the radius of our microsphere. So upon solving for N we calculate:

$$N = \frac{A}{(\pi)[r^2]Q_{ex}} = 4.456 \times 10^3 \text{ particles/cm}^3, \text{ where}$$

$A = 1.067 \times 10^{-4}/\text{cm}$

$r = 0.5 \times 10^{-4}$ cm

$Q_{ex} = 3.049$

Calculations of N based on the data from the SFU sampling is found in Appendix A, along with discussion of this data. The results are very disappointing, being N = 783 particles/cm^3.

Now what about extinction for the parallel orientation? Well, when changing the wave plate from IPERP to IPARA all three data readings, ILP (laser power), IEX (extinction), and ISC (scattering) changed. ISC and ILP decreased, whereas IEX increased. At the outset, a change in ISC does not concern us since we expect to see a difference between the data of the two orientations of polarizations. But the other two should not

IEX' values are the proper values to compare with I_0EX for the purpose of measuring the extinction coefficient. These adjusted EPMT readings are displayed in Fig. 27. Almost every data point lies within one standard deviation of the mean. What variations we do see are some combination of actual fluctuations in the particle number density and systematic effects, e.g., thermal variations in alignment. That these values are as steady as they are is an indication of our success in maintaining a constant room temperature. The average value of IEX' suffices to make our calculations of extinction coefficient and number density of particles. The following steps outline the solution for these two important characteristics of the aerosol.

1. Mean value of IEX'_{av} = 1.4618 μA
2. Initial value of EMPT: I_0EX = 1.51 μA
3. $I/I_0 = IEX'_{av}/I_0EX = 0.968$, which equates to 3.2% extinction
4. Attenuation length, L_x = 304 cm. (Total length of chamber minus 2.5 cm for the recess of the LTA plus 1 cm for the protrusion of the entrance window.)
5. Apply the Bouguer-Lambert Law:

$$I/I_0 = EXP\{-A(L_x)\} \tag{30}$$

Now solve for "A", extinction coefficient.

$$A = -(1/L_x)\ In\{I/I_0\} \tag{31}$$

$$A = 1.067 \times 10^{-4}/cm$$

6. Calculate "N", the number density of particles in the chamber. (Van de Hulst, 1981, pp. 128-129)

$$A = N\{Q_{ex}\}(\pi)[r]^2 \tag{32}$$

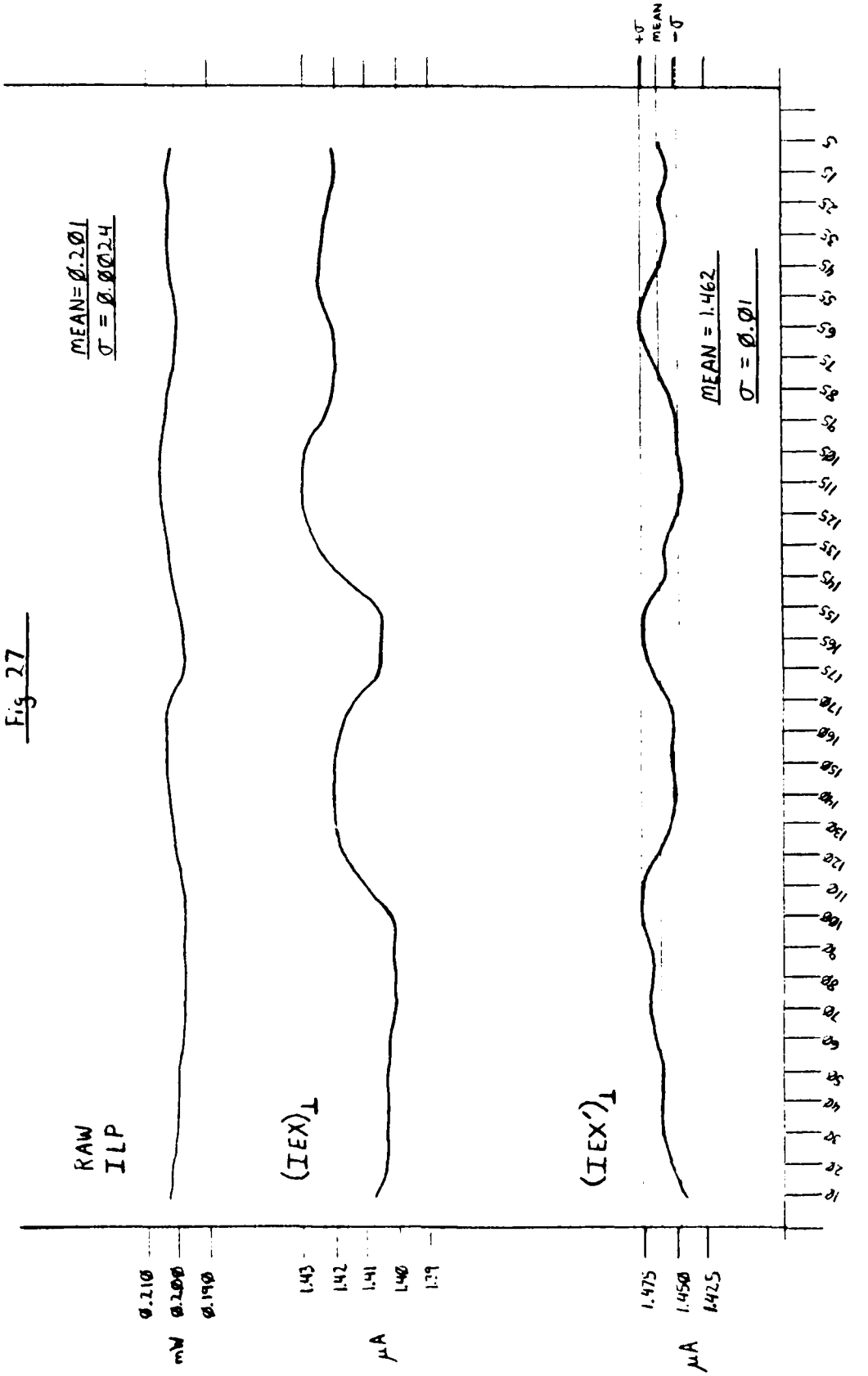
Fig 27
RAW
ILP
MEAN=Ø.2Ø1
σ = Ø.ØØ24
(IEX)⊥
MEAN = 1.462
σ = Ø.Ø1
(IEX')⊥
+σ
MEAN
-σ
mW
Ø.21Ø
Ø.2ØØ
Ø.19Ø
μA
1.43
1.42
1.41
1.4Ø
1.39
μA
1.475
1.45Ø
1.425
ANGLE IN ORDER TAKEN

DATA REDUCTION

With the data in hand, we tackled the problem of interpreting it. Now our task was to apply all necessary adjustments to the data so that it could be properly compared to theoretical data. The first order of business was determining the extinction coefficient and thereby the number density of particles in the system. Fig. 27 shows graphs of raw LPM and IEX readings for the perpendicular laser orientation (PERP). The data is plotted in the order taken as is indicated by the angle labels along the coordinate axis; thus we can see the time evolution of the readings. Note that variations in laser power are accompanied by variations in IEX readings. Consider also that the order that the data is taken gives us a confidence that the variations are due to genuine laser power drift and not due to temperature related changes. By running through the 10 degree angles and then in reverse through the 5 degree angles, we look at each area of the chamber at two different times, and detect no systematic drift in state of the system. Because the LPM readings do drift slightly from the initial (clean system) value, each IEX data point must be adjusted to this initial value in order to compare IEX data with the initial I_0EX value. For example, the initial LPM reading for the clean system is $I_0LP = 0.208$ mW, which corresponds to an initial EPMT reading of $I_0EX = 1.51$ μA. Now suppose that at $\theta = 30$ degrees we measure IEX = 1.404 μA at ILP = 0.200 mW. Since the ILP > I_0LP, then IEX cannot be fairly compared with I_0EX since it is not referenced to the same LPM reading. As a result, we make the following correction to each value of IEX:

$$IEX' = IEX \{I_0LP/ILP\} \tag{29}$$

LPM head and on the face of EPMT, resulting in new readings. The amount of variation observed is inconsistent, at times negligible, but sometimes significant. As a result, data for one polarization is not directly correlated with data from another polarization. Nevertheless, the two sets of data can be compared via an indirect method discussed below under DATA REDUCTION. A third annoyance was slight variations in LPM readings due to pressure surges in the circulation system. We noticed this for example, whenever we cycled the circulation fan on or off, and when we opened or closed the main 2" valve in the circulation loop. The problem is that the beam splitting entrance window for the chamber is not rigidly mounted. Pressure surges move the plate so that the angle of incidence of the laser beam changes, thus changing the position of the beam on the LPM head. The obvious solution is to move the beam splitter from the end of the chamber to the optical bench of the BPS, where it will be unaffected by pressure surges in the circulation loop.

data for every 10 degrees starting at 10 degrees and working through 170 degrees. Next we moved to 175 degrees and worked our way back every 10 degrees, stopping at 5 degrees. Such a procedure allows us to detect any systematic drift in the state of the scattering system. Our first set of measurements was for the perpendicular orientation followed by the data for the parallel polarization.

During data taking, we encountered a few problems that affect the quality of our data. These difficulties must be overcome before full scale calibration test can be undertaken. We discovered, a day before our data run that the performance of the laser, as well as the alignment of the two spatial filters are affected by variations in room temperature. Increases in room temperature tend to reduce the power output of the laser. We had observed these variations in previous weeks but did not make the connection with room temperature until just before the data run. The spatial filters, having only 10 μm pinholes in them, are very sensitive to slight movements in these assemblies due to thermal expansion and contraction of the mounting surfaces. The effect on measurements is inconsistent, and is therefore difficult to account for. However, further study needs to be done on this topic so that a definitive solution can be found. Our interim solution was to control the room temperature, trying to keep it at a constant value over the period of measurements. Another problem noted is that when the wave plate is rotated from one orientation to another, the values of both laser power and extinction change. This effect is probably due to the fact that the wave plate mount is left slightly loose in its housing so that the mount can be easily rotated from one position to another. When the mount is rotated the beam may be slightly shifted in position on the

PARTICLE GENERATION SCHEMATIC

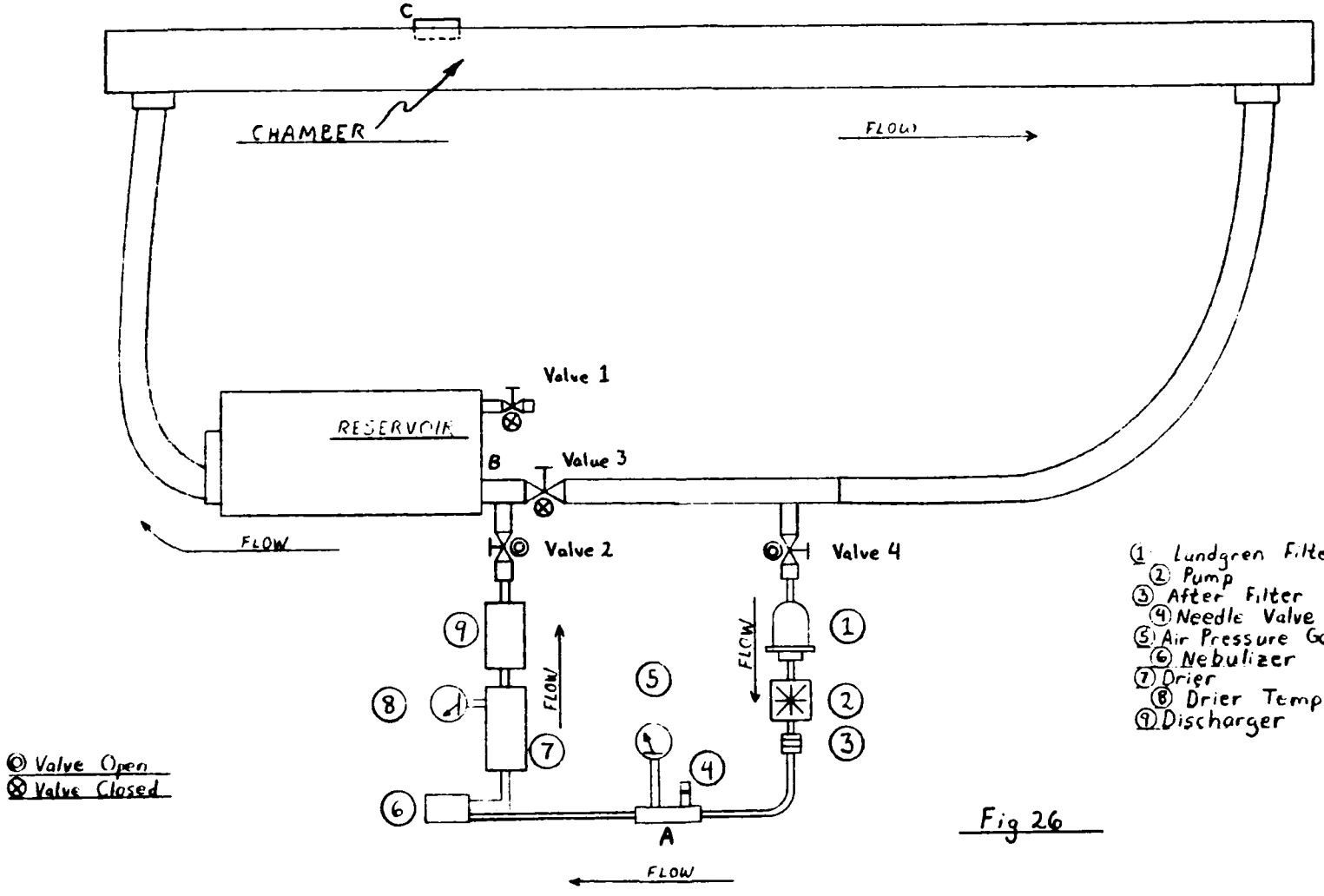

◎ Valve Open
⊗ Valve Closed

① Lundgren Filter
② Pump
③ After Filter
④ Needle Valve
⑤ Air Pressure Gauge
⑥ Nebulizer
⑦ Drier
⑧ Drier Temp Gauge
⑨ Discharger

Fig 26

less, the important features of the scattering spectrum should be unaffected.

Our system for particle generation is shown in Fig. 26. It is nothing more than the entire purge system with the particle generator added to the purge loop. Note that the pressure to run the nebulizer comes from the clean exhaust of the purge pump. Pressure of 30 psi is regulated by the valve and gauge at A. Since the main valve is shut, there exists a negative pressure of 30 psi at B, creating a draw that moves the aerosol into the circulation plumbing. (The circulation fan is off during this entire process.) The idea is that this continuous draw causes the aerosol to fill up the reservoir and then eventually work its way all the way through the system to the purge pump. The progress of the particles can be monitored at the viewing port atop SM1, at C. We ran the aerosol generator for one hour and forty minutes. This provided enough time to completely fill the chamber with particles to the point that we felt sure that aerosol had traveled the entire length of the system. We then shut down the pump, closed valves 2 and 4 to isolate the purge loop, and opened valve 3. A short 20 sec cycle of the circulating fan confirmed our suspicion that the reservoir held the highest density of particles. This mixing the reservoir particles produced a noticeable increase in the brightness of the scattered light viewed from the port.

Having generated our monodisperse aerosol, we proceeded to take extinction scattering, and laser reference readings for a full set of incremental angles between 0 and 180 degrees. We did so for both orientations of the plane of polarization of the incident beam; parallel and perpendicular to the scattering plane. Our method was to record

increases. Raabe (1976) puts forth an equation for calculating F_v given the statistical properties of the microspheres, the nebulizer, and the desired value of R. The equation is (Hinds, 1982, p. 386):

$$F_v = \frac{(1-R)d_p^3 \exp\{-4.5 \ln^2(GSD)\}}{(MMD)^3[1-0.5 \exp\{\ln^2(GSD)\}]} \qquad (28)$$

valid for $R > 0.9$ and $GSD < 2.1$. Nebulizers generate particle sizes that obey a Log-Normal size distribution. MMD stands for Mass Median diameter. In terms of the Log-Normal size distribution, half of the particle mass generated by the nebulizer belongs to particles with diameters larger than the MMD. The other half of the mass belongs to particles having diameters smaller than the MMD. GSD is the Geometric Standard Deviation of the Log-Normal size spectrum. It is defined in a way similar to the standard deviation of the Normal distribution, but takes into account the logarithmic character of the Log-Normal spectrum. Thus, it is a measure of the dispersion of particle sizes about the mean.

Our diluted solution of spheres has an F_v value of 4.52×10^{-4}, which corresponds to a singlet ratio, R = 0.95. These results are based on an MMD of 4.3 μm and a GSD of 1.8; these being the calibrated values for the particular nebulizer we are using. The validity of our calculated singlet ratio was checked on a particle size spectrum analyzer at UCD's Laboratory for Energy Related Health Research (LEHR). The results showed that the nebulizer produces a maximum of 3% doublets along with only trace measurements of triplets. With this number of doublets present, one expects a small amount of "washout" in the structure of the scattering spectrum, especially at minima. Neverthe-

of desiccant granules (Anhydrous $CaSO_4$) that evaporates the water from the droplets, leaving the solid particles suspended in air. The drying chamber is followed by a discharging chamber which contains a weakly radioactive electron source (Beta Particles). During the process of nebulizing the droplets tend to pick up a net positive charge. The electron source neutralizes the charge on the spheres so that electrostatic deposition and agglomeration can be neglected.

One of the inherent problems with nebulizers is producing droplets that contain only one microsphere; such droplets are referred to as singlets. Droplets that contain two (doublets), three (triplets), or more spheres are unwanted because once they are dried out the microspheres remain stuck together. Since good instrument calibration depends on having only single spheres in suspension, the presence of doublets and triplets in suspension must be avoided. The most common cause of doublets and triplets in an aerosol is improper preparation of the dilute water suspension that goes into the nebulizing chamber. Recall that the manufacturers suspension of the spheres is highly concentrated. The suspension must be strongly diluted in order for the nebulizer to operate properly. Diluting water for this purpose must be triple distilled, carbon filtered, and deionized. These properties help prevent the spheres from sticking together in the suspension. The major factor that drives the number of multiplets is the volume fraction of spheres in the diluted solution; this factor is denoted by the symbol F_v. Generally speaking, the more dilute the solution, the higher the ratio R, of singlets to droplets containing particles. On the other hand, the number of empty droplets (those containing no spheres) also

PRELIMINARY MEASUREMENTS

When developing a new instrument for research, it is important to put the device to the test, by using it to measure quantities that are precisely known beforehand. Successful calibration measurements are necessary to interface instrument measurements with the real world, and typically involve the determination of calibration constants. Such constants represent proportionalities between instrument values and actual values and are therefore unique to each instrument. Our instrument was put to such a test, the procedure and results of which now follow.

To test our instrument we measured extinction and scattering properties of an aerosol that is highly monodisperse, highly spherical and easily generated. Polystyrene microspheres (or microbeads) meet these stringent specifications, so much so, that they are sometimes referred to as "the scatterer's friend". Why? Simply because everything about them which is relevant to extinction and scattering is either well known or can be easily calculated. The spheres come suspended in a 15 ml deionized water solution containing 2.5% of the solids. Mass density of the beads is 1.05 g/cc, and the refractive index is 1.600. (Polybead Data Sheet, 1984) We selected spheres with a diameter of 1 micron.

To change our microspheres from hydrosol (particles suspended in water) to an aerosol (particles suspended in air), we employed a device known as a compressed air nebulizer. The nebulizer uses a stream of compressed air (30 psi) to automize a diluted solution of the microspheres into a superfine mist. The mist droplets exit the nebulizer and pass through a drier that consists of a heated chamber containing a tray

back angles. This difference must be corrected out of the data in order to put all angles on an equal footing. Consider Fig. 29 and the following discussion.

For each θ there is a detector reading DSC. If A is the extinction coefficient, the following relations hold at SM1.

(i) DSC_1 has been extinguished by a factor: $EXP[-A(X_1+R_1)]$

(ii) DSC_2 has been extinguished by a factor: $EXP[-A(X_2+R_2)]$

(iii) DSC_3 has been extinguished by a factor: $EXP[-A(X_3+R_3)]$

But note that for all practical purposes (since A is so small and thus extinction is not a strong function of distance)

$$X_1 + R_1 \cong X_2 + R_2 \cong L_0 \qquad (34)$$

In addition, X_3+R_3 is approximately $L_0 + 2(R_3)$. Therefore, all forward angles are on the same basis since they are all extinguished by the same amount. The back angles though are extinguished over an additional distance of $2(R_3)$, where R_3 is a function of angle, θ. So to put the forward and back angles on an equal footing, we make the following adjustments:

For forward angles: $DSC' = DSC$ (35A)

For back angles: $DSC' = DSC \{\exp\{A(2R_3)\}$ (35B)

The size of this correction is small, being a maximum of 3.3% for the most backward angle of 175 degrees. This follows from the fact that the extinction coefficient is rather small. This type of data adjustment could be significant though, for highly absorbing aerosols such as combustion products containing large amounts of carbon soot.

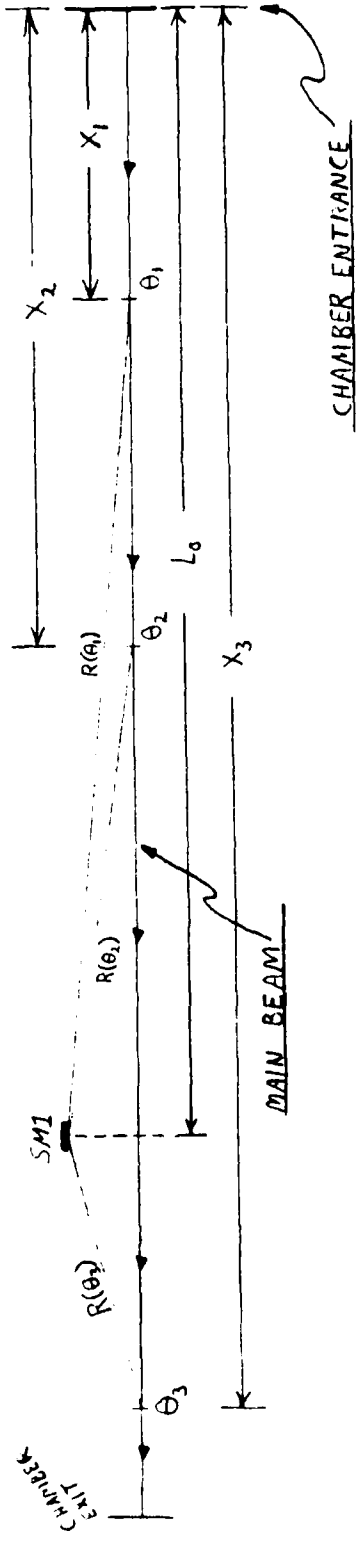

GEOMETRY FOR BACK ANGLE CORRECTIONS

Fig 29

(4) Consider that at each angle θ we have a detector signal DSC'. It follows then that,

$$\frac{DSC'}{(\pi)(R_b)^2 X(\theta)} \tag{36}$$

is the detector signal per unit volume, where R_b is the radius of the beam and where $X(\theta)$ is the FWHM scattering length of the beam. Similarly, if N is the number of particles per unit volume in the system then,

$$\frac{DSC'}{(\pi)(R_b)^2\ X(\theta)\ N} \approx DSC'' \tag{37}$$

is the detector signal per particle. The detector signal is directly related to the differential scattering cross section $\sigma_{sc}(\theta)$ via the relation,

$$DSC'' = \frac{K(\theta)\ I_i}{[R(\theta)]^2}\ \sigma_{sc}(\theta) \tag{38}$$

In this equation, I_i is the incident intensity of the beam in the forward direction. $R(\theta)$ is the distance from the scattering center to the detector, and $K(\theta)$ is a calibration, "dustbin", into which we deposit all our ignorance about instrument calibration factors. Because of the geometry of our system, we were not yet able to measure I_i, but since it is a constant we can take ratios of values of DSC"(θ) to the value of DSC" at some arbitrary reference angle. We choose 5 degrees as our reference angle. We can therefore write,

$$\frac{DSC''(\theta)}{DSC''(5)} = \frac{DSC'(\theta)\ X(5)}{DSC'(5)\ X(\theta)} = \frac{K(\theta)[R(5)]^2\ \sigma_{sc}(\theta)}{K(5)[R(\theta)]^2\ \sigma_{sc}(5)} \tag{39}$$

or

$$\frac{\sigma'_{sc}(\theta)}{\sigma'_{sc}(5)} = \frac{K(\theta)\ \sigma_{sc}(\theta)}{K(5)\ \sigma_{sc}(5)} = \frac{DSC'(\theta)[R(\theta)]^2\ X(5)}{DSC'(5)[R(5)]^2\ X(\theta)} \tag{40}$$

The LHS of equation (40) represents our measurement of the ratio of the differential scattering cross section for angle θ to that at 5 degrees. It is the fundamental measurement of our instrument that will be compared with theoretical data to determine the viability of our device for aerosol research. (Bohren & Huffman, 1983, pp. 391-392)

(5) From McCartney, p. 237, we find that,

$$\sigma_{sc}(\theta)_1 = [\frac{\lambda}{2\pi}]^2 |S_1(\theta)|^2 \qquad (41A)$$

$$\sigma_{sc}(\theta)_2 = [\frac{\lambda}{2\pi}]^2 |S_2(\theta)|^2 \qquad (41B)$$

Reconsider equation 38 and note that since I_i is a constant for all angles we can absorb it into $K(\theta)$ such that

$$K'(\theta) = K(\theta)I_i. \qquad (42)$$

By combining equations 37, 38, 41A&B, and 42 we can derive the important relation for the calibration constants for our system. It is,

$$K'(\theta) = \frac{4(\pi)\ DSC'(\theta)\ [R(\theta)]^2}{(R_b)^2\ X(\theta)\ N\ \lambda^2\ |S_j(\theta)|^2} \qquad (43)$$

where j=1 corresponds to IPERP and j=2 denotes IPARA, and where

R_b = 0.36 cm

N = 4456 particles/cm^3

λ = 632.8 nm

THEORY vs. MEASUREMENTS

We now compare our measured data with what the theory predicts. The most important measured quantities to compare are the ratios $\sigma'_{sc}(\theta)/\sigma'_{sc}(5)$ (measurement) with $\sigma_{sc}(\theta)/\sigma_{sc}(5)$ (theory). To generate the theoretical data we used a program named CALLBH from Bohren and Huffman's book, Absorption and Scattering of Light by Small Particles. The program as published calculates $|S_1(\theta)|^2$, $|S_2(\theta)|^2$, and Q_{ext} (as well as other parameters) for any number of angles between 0 and 180 degrees (inclusive). Input data are the complex refractive index, sphere radius, wavelength of incident light, and the number of angles desired. We modified the program from the published form to tailor it to our specific requirements. In particular, we adjusted the output format so that the first angle presented as data is 5 degrees rather than 0 degrees. In addition, we arranged for the values of $S_1(\theta)^2$ and $S_2(\theta)^2$ to be normalized to their respective values at 5 degrees. In other words, these outputs are the theoretical values of $\sigma_{sc}(\theta)_j/\sigma_{sc}(5)_j$ (referred to as $RATIO_j$) for both the perpendicular (j=1) and parallel (j=2) orientations. All computer calculations were performed on the PDP-1144 at Crocker Nuclear Laboratory (CNL). Computed $RATIO_j$ values from this program are presented in both tabular and graphical form. The tables appear in Appendix whereas the graphs appear here in the text. These plots show both the theoretical and measured values for each $RATIO_j$.

We will first compare the measurements to the theoretical data for the 1.0μm spheres. Consider Figures 30A and 30B. Dotted lines denote theory whereas "o" symbols denote measured values. Fig. 30A applies to perpendicular polarization while Fig. 30B displays parallel polarized

COMPARISON OF MEASUREMENTS TO MIE THEORY FOR 1.0 μm POLYSPHERES

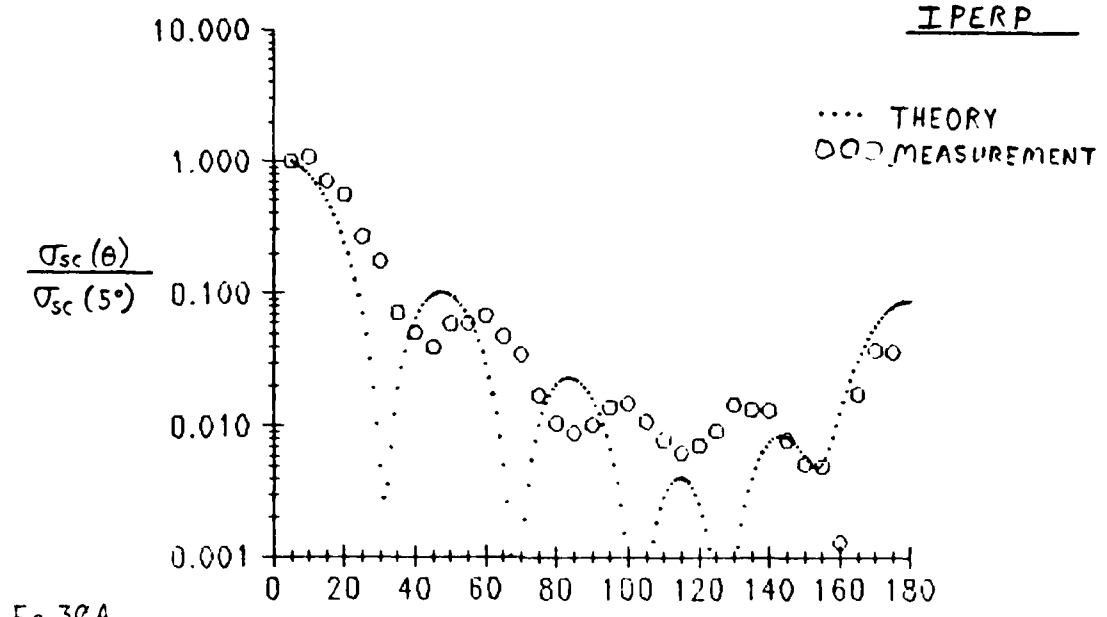

Fig 3PA

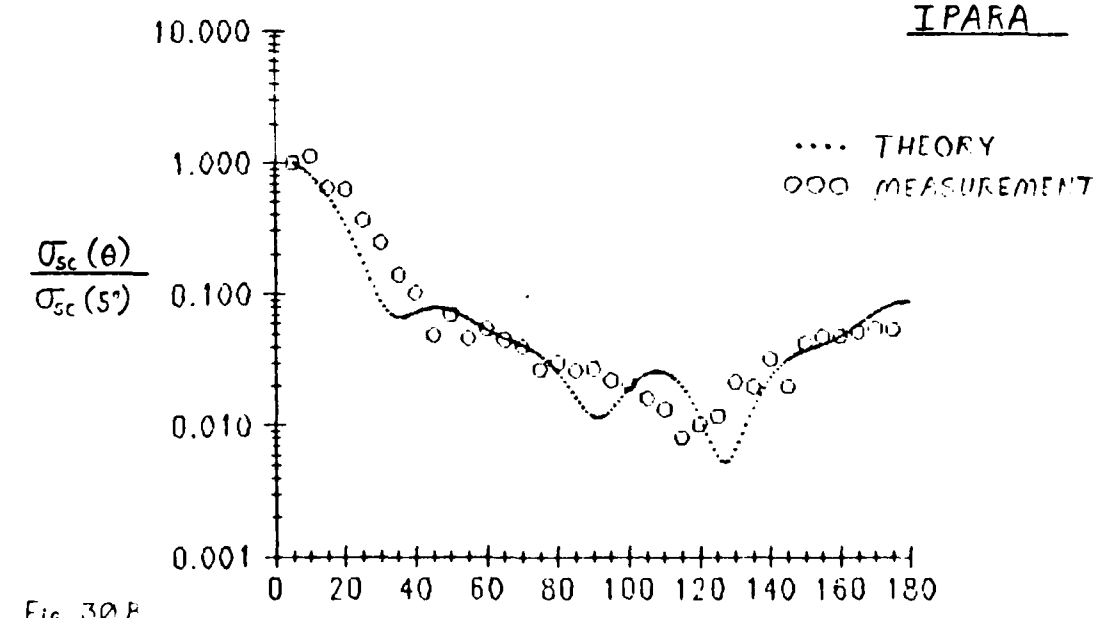

Fig 3PB

data. In both cases the fit of measurements to theory is poor. Major structure of maxima and minima are not reproduced by the measurements, and are at several places actually reversed. For example, at 85 degrees in Fig. 30A theory demands a maximum, but the measurements reveal a minimum. This sad state of affairs, of course, prompts the question, "what went wrong?" The answer to this question appears to be related to the size of the particles. Hinds (1982) cites a 1972 study which calls into question manufacturers claims of microsphere sizes. Several batches of microspheres of various sizes were carefully measured using low intensity electron microscopy. (Normal intensity electron microscopy creates enough heat to swell the polyspheres and thus induce large errors in size measurements.) The study reported sizes that differed from manufacturers claims by -21% to +2%. However, particle size within a batch was very monodisperse; the standard deviation being on average less than 4%. Although the study was ten years old when Hinds' book was published, he treats the study as if its conclusions still had merit. A review of the manufacturers data sheet on the polyspheres turned up the following quote: "The particle diameters and their standard deviations listed may vary with individual batches, but diameter size will be uniform within a batch. Larger particles have greater standard deviations than those found in the smaller particles. We will provide the closest diameter available to that ordered." (Polybead Data Sheet, 1984)

To investigate the possibility of sphere size error, we ran our CALLBH program for sphere sizes from -20% to +20% of 1.0μm, progressing in increments of 2.5%. The results are depicted in Figures 31A and 31B. The fit of data with theory is very good. In Fig. 31A, maxima and

COMPARISON OF MEASUREMENTS TO MIE THEORY FOR 0.85 μm POLYSPHERES

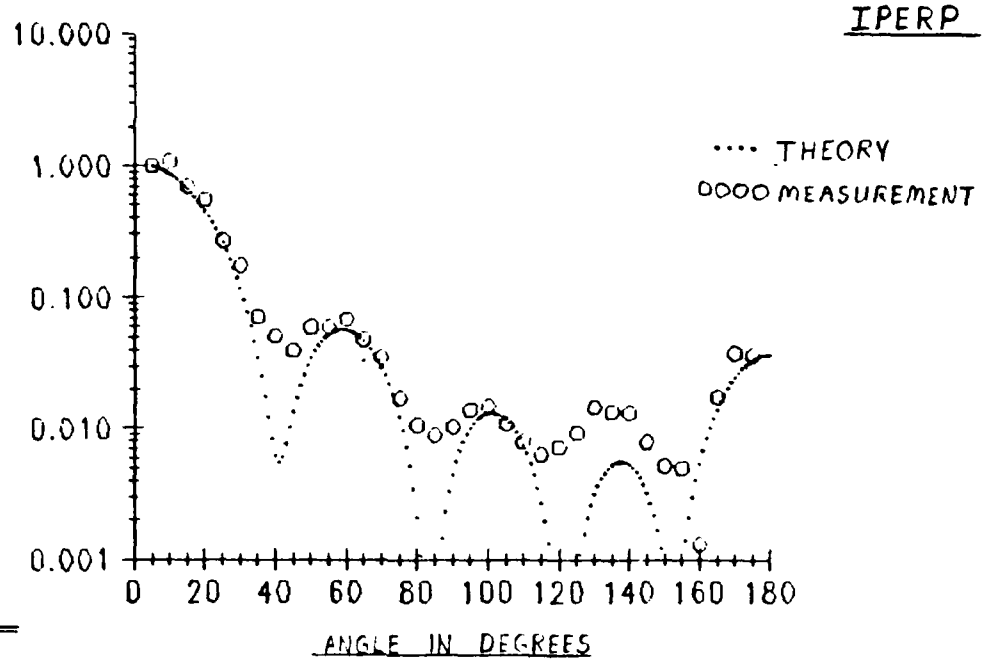

Fig 31A

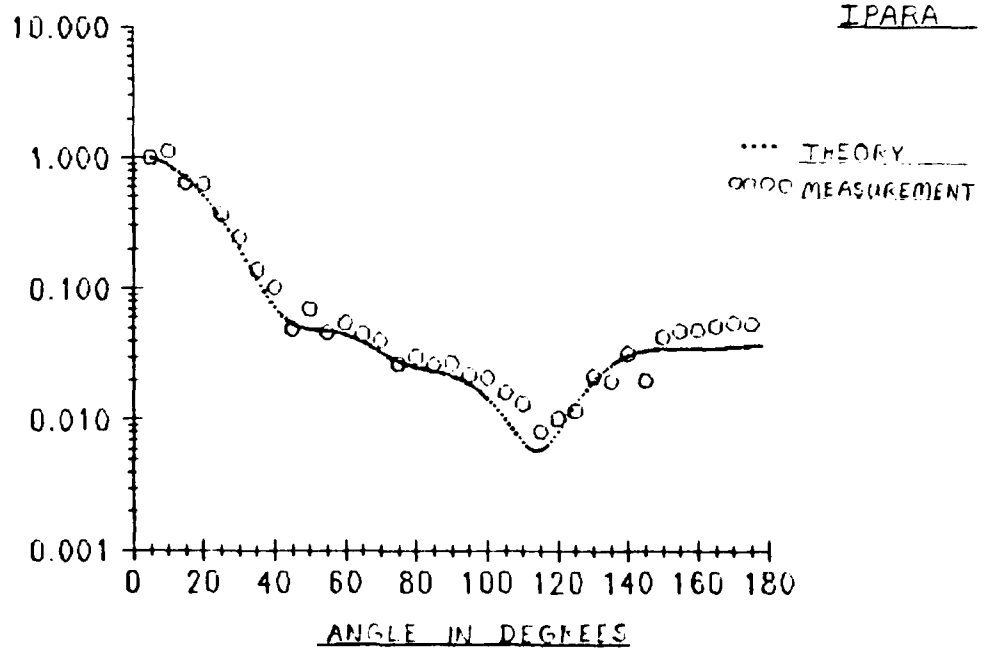

Fig 31B

minima are where they should be. Maxima are the right order of magnitude except for one peak at 140 degrees. The minima are washed out as expected. Any departure from monodispersity results in a washing out of the structure of a scattering diagram. The known presence of doublets in the aerosol contributes to this washout. Consider also the steep slopes between maxima in this graph. Since our system averages over some $\Delta\theta$ (small though it may be), we would expect data points on these slopes to be recorded as higher than the actual values, contributing to the observed washout. Other possible sources of washout are:

(1) Possible departure from monodispersity due to the presence of surfactant particles in the aerosol. Recall that the hydrosol of microbeads contains an anticoagulant or surfactant that inhibits the beads from sticking together in the water solution. When the suspension is nebulized it is possible for surfactant particles to form when the water droplets pass through the drier. (Hinds, 1982. p. 387)

(2) The efficiency of the drier may allow some beads to pass into the system with a coat of water on them. In such a case, these spheres would behave as though they had a different refractive index than the bare polyspheres, thus contributing to the polydispersity of the aerosol.

In Fig. 31B we see an even better fit of theory and data than in the previous figure. The expected washout occurs at the pronounced minimum at 115 degrees. One reason for the close fit here is the lack of steep slopes in the scattering spectrum, such that averaging over $\Delta\theta$ has less effect. The fact that there exists no large bump at 140 degrees helps us to realize that there is no systematic factor causing the enhanced maximum at 140 degrees in Fig. 31A.

It is important to note that the fit of Figures 31A and 31B is approximate in the sense that we varied the size parameter in increments of 2.5% when running the programs. One could further fine tune the fit by running the program at increments of 0.01 in the sphere radius, about 0.425 μm. Our suspicion that the particles are actually this small are based on three things: (1) the size comparison study cited by Hinds, (2) the admission of possible error on the polybead data sheet, and most importantly (3) the fact that we could match two different sets of data, fairly well, by varying one parameter common to both. By using this smaller sphere size we do see more consistency between the particle number densities calculated from extinction and SFU measurements. By using a radius of 0.425 μm and Q_{ext} = 4.07, we calculate N from the extinction coefficient to be $N_{ext} \approx 4620$ particles/cc. This is only slightly higher than what we had before. The revised SFU result for the number density is N_{sfu} = 1275 particles/cc. So at least this gets SFU measurements within the correct order of magnitude of N_{ext}.

The calculation of K'(θ) values, the constants of calibration, may be performed using equation 43 in the previous section. We forego that step in this study because of the unresolved uncertainties in the number density of particles N and the size of the polyspheres. Both parameters require an independent check, in order for calculations of K'(θ) to be a fruitful venture. An important point to observe is that if the sphere size agrees with our results here then we have at our disposal an excellent system for particle sizing measurements. The CALLBH program could be modified to automatically compare and fit the theory to scattering data by varying particle size as a parameter.

CONCLUSIONS

This project, which now comes to a conclusion for one researcher, has brought with it a breadth of experience that transcends the textbook. The construction of this device, (which took eight of the twelve months involved) was a long series of trial designs and prototype units which eventually coalesced into the system presented here. So many things were learned that are not presented in this paper. For example, the delicate job of aligning the beam production and detection optics could be presented as a thesis by itself. Also, the frustrating task of troubleshooting a variety of photodetectors can only be hinted at. Many other unreported topics could be mentioned. Nevertheless, the fundamental prerequisites for full scale testing and calibration have been met. The device as it stands requires no major design changes. The geometric relationships are known as well as the important equations needed for data reduction.

Our study has shown that the instrument developed has potential as an in-situ aerosol research instrument. Extinction and differential scattering measurements were taken for a test aerosol of polystyrene latex spheres which are claimed by the manufacturer to be 1.0 μm in diameter. Test measurements strongly indicate that the spheres are actually about 0.85 μm in diameter; an indication supported by previous size comparison studies on such microspheres. There is room for improvement. Several design and operational changes mentioned in the text will greatly enhance the potential of the device for studies of real aerosols. Those that stand out are:

(1) Solution of the temperature related alignment problem.

(2) Addition of an analyzing polarizer for polarization studies of scattered light.

(3) Addition of a computer interfaced stepping motor for SM1, as well as computer linked data acquisition.

(4) Solution of the SFU number density problem. Data analysis needs an accurate independent measurement of the number density of the aerosol.

(5) Modifications to the DRUM Sampler for time resolved sampling measurements simultaneous with extinction and scattering measurements.

(6) An independent check of sphere size so that the merits of our preliminary measurements can be weighed.

With these improvements, the door is open to full scale testing and calibration, as well as a wide array of aerosol research projects. The measurement of the total scattering matrix of an aerosol in terms of the Stokes parameters has been done only once or twice and is a real possibility with this instrument. Such information would completely determine the behavior of an aerosol under any known conditions of illumination. In fact, the future holds the promise of a total aerosol analysis system. Extinction, scattering, and absorption data could be measured along with polarization studies. Compound with these, information on size and mass distributions as well as accurate elemental analysis via PIXE and FAST at CNL. Throw in the possibilities of gravimetric settling studies, research on static and dynamic diffusion, or the untouched domain of inverting Mie theory for first principles calculations of the complex refractive index of aerosols. Properly exploited, this system could be a cornerstone of a wide ranging program in aerosol physics at UCD.

BIBLIOGRAPHY

Bohren, C.T. and Huffman, D.R. Absorption and Scattering of Light by Small Particles. New York: Wiley-Interscience, 1983.

Cahill, T.A., Annual Report to the National Park Service for Particulate Monitoring and Data Analysis, (1984). NPS Contract No. USDICX-0001-3-0056.

Cahill, T.A., Ashbaugh, L.L., Barone, J.B., Eldred, R.A., Feeney, P.J., Flocchini, R.G., Goodard, C., Shadoan, D.J. and Wolfe, G.W. (1977). Analysis of Respirable Fractions in Atmospheric Particulates Via Sequential Filtration. J. Air Poll. Control Assoc., Vol. 27:675-678.

Cahill, T.A., Kusko, B.H., Ashbaugh, L.L., Barone, J.B., Eldred, R.A., Walther, F.G. (1981). Regional and Local Determinations of Particulate Matter and Visibility in the Southwestern United States. During June and July, 1979, Atmospheric Environment, Vol. 15, No. 10/11:2011-2016.

Complete Catalog of Optical Systems and Components. Stamford, Conn.: Oriel Corporation, 1979.

Feeney, P.J., Cahill, T.A., Olivera, J. and Guidara, R. Gravimetric Determination of Mass on Lightly-Loaded Membrane Filters, (1984). J. Air. Poll. Control Assoc., Vol. 34, No. 4:376-378.

Flocchini, R.G., Cahill, T.A., Pitchford, M.L., Eldred, R.A., Feeney, P.J., Ashbaugh, L.L. (1981). Characterization of Particles in the Arid West. Atmospheric Environment 15:2017-2030.

Hecht, E., Zajac, A. Optics. Reading, Mass: Addison-Wesley, 1975.

Hinds, W.C. Aerosol Technology. New York: Wiley-Interscience, 1982.

Jenkins, F.A. and White, H.E., Fundamentals of Optics, New York: McGraw-Hill, 1976.

Malm, W., Private communication with Dr. T.A. Cahill, 1984.

Malm, W.C., Walther, E.G., O'Dell, K., Kleine, M. Visibility in the Southwestern United States From Summer 1978 to Spring 1979, (1981). Atmospheric Environment; Vol. 15, No. 10/11:2031-2042.

Melles Griot Optics Guide 2. Irvine, California: Melles Griot Optical Components Division, 1982.

Polybead Microparticles Data Sheet No. 238. Warrington, PA: Polysciences, Inc., 1984.

Reitz, J.R., Milford, T.J., Christy, R.W. Foundations of Electromagnetic Theory. Reading, Mass.: Addison-Wesley, 1980.

Van de Hulst, H.C. Light Scattering by Small Particles. New York: Dover, 1981.

AD-A158 044 DIFFERENTIAL SCATTERING CROSS SECTION AND TOTAL EXTINCTION MEASUREMENTS O.. (U) AIR FORCE INST OF TECH WRIGHT-PATTERSON AFB OH J M DORMAN 1985 2/2

UNCLASSIFIED AFIT/CI/NR-85-69T F/G 7/4 NL

END

FILMED

DTIC

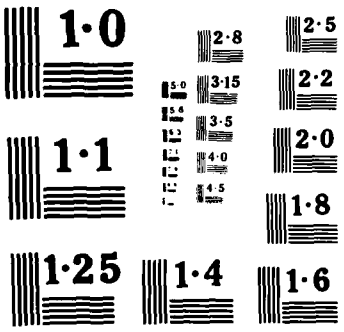

NATIONAL BUREAU OF STANDARDS
MICROCOPY RESOLUTION TEST CHART

APPENDIX A

CALCULATION OF THE NUMBER DENSITY OF PARTICLES BASED ON SFU SAMPLING DATA.

Definition of Parameters

(1) $M_{SFU} \equiv$ Total mass deposited on SFU filters during sampling period

(2) $V \equiv$ Total volume of ACSS system

(3) $\rho \equiv$ Mass density of microsphere

(4) $\upsilon_p \equiv$ Volume of each microsphere

(5) $Q \equiv$ Flow rate of air through the SFU

(6) $\tau \equiv$ Timed duration of sampling

(7) $N_o \equiv$ Initial number density of particles prior to sampling

(8) $N(t) \equiv$ Number density of particles remaining after a sampling time t.

This preliminary test of the SFU sampler was performed as a precursor to a system purge. We allowed the sampler to run for several hours, in the hopes that a larger amount of mass collected would yield more accurate data. The flow rate was reduced below the standard SFU rate of 10 liters per minute, because the standard rate caused excessive leakage (into the system) at the seals on the chamber slot face plate. Consider now the following analysis.

Prior to sampling there exists some number density of particles, N_o dispersed throughout the fixed volume of the system V, i.e.

$$N_o = \frac{\text{Total Number of Particles in the System}}{V} \qquad (1)$$

As we sample we extract a certain volume of air at a rate Q. For every ΔV ($\Delta V << V$) containing aerosol that departs the system, it is replaced by a ΔV containing no aerosol (i.e. clean air). So before removing ΔV we have,

$$N(t = 0) = N_o \tag{2}$$

The number of particles removed when ΔV is extracted is then $N_o(\Delta V)$. So the change in the number density of particles is given by

$$\Delta N = \{\frac{N_o V - N_o(\Delta V)}{V}\} - N_o = -N_o(\frac{\Delta V}{V}) \tag{3}$$

Consider now that in a time Δt, the volume of air removed from the system is

$$\Delta V = Q(\Delta t) \tag{4}$$

Combine equations (3) and (4) to get ...

$$\Delta N = -N_o(\frac{\Delta V}{V})$$

$$\Rightarrow \quad \frac{\Delta N}{\Delta t} = -\frac{N_o}{V}\frac{\Delta V}{\Delta t} \tag{5}$$

Now take the infinitesimal limit to get ...

$$\frac{dN}{dt} = -\frac{N_o}{V}\frac{dV}{dt} = -\frac{N_o}{V}Q \tag{6}$$

Solving for N(t) we find ...

$$N(t) = N_o \exp\{-Qt/V\} \tag{7}$$

But if we are given N(t), V, the mass density of the particles, ρ, as well as the particle size, we can determine the mass present in the system as a function of time. Specifically it is evident that,

$$M(t) = N(t)V\rho\upsilon_p \tag{8}$$

where υ_p is the volume of each microsphere. Plugging in for N(t) from equation (7), we find,

$$M(t) = \{N_o V\rho\upsilon_p\} \exp[-Qt/V] \tag{9}$$

$$\text{or} \quad dM(t) = \{N_o V\rho\upsilon_p\}\{-\frac{Q}{V}\} \exp[-Qt/V]dt \tag{10}$$

So how much mass is extracted from the system in some sampling period τ? Well,

$$\int_0^{\tau} dM(t) = \{-\frac{Q}{V}\}\{N_o V \rho \upsilon_p\} \int_0^{\tau} e^{-Qt/V}\, dt \tag{11}$$

$$\Rightarrow \quad M(\tau) - M(0) = \{-\frac{Q}{V}\}\{N_o V \rho \upsilon_p\}\{-\frac{V}{Q}\, e^{-Qt/V}\}\Big|_0^{\tau} \tag{12}$$

Note that $M(\tau) - M(0)$ is the negative of the amount of mass deposited on the SFU during a sampling period τ.

$$-M_{SFU} = \{N_o V \rho \upsilon_p\}[e^{-Q\tau/V} - 1] \tag{13}$$

Upon solving for N_o, we find ...

$$N_o = \frac{(M_{SFU})}{V \rho \upsilon_p \{1 - e^{-Q\tau/V}\}} \tag{14}$$

which has the proper units of inverse volume. The following is a list of the parameters for solving for N_o based on the assumption that the spheres are 1.0 μm in diameter.

(1) $M_{SFU} = 0.206 \times 10^{-3}$ gm (Total difference between the pre- and post-weights of the SFU filters).

(2) $V = 480$ liters $= 4.8 \times 10^5$ cm^3

(3) $\rho = 1.05$ gm/cm^3

(4) $\upsilon_p = \frac{4}{3}\pi(r_p)^3 = 5.236 \times 10^{-13}$ cm^3

(5) $Q = 5.63 \times 10^3$ cm^3/min

(6) $\tau = 498.4$ min

The calculation reveals $(N_o)_{SFU} = 783$ particles/cm^3, which is quite distant from the value determined from extinction of $(N_o)_{ext} = 4456$ particles/cm^3. If we assume the spheres to be 0.85 μm in diameter, only υ_p changes from the value above; $\upsilon_p' = 3.22 \times 10^{-13}$ cm^3. The result is that we calculate $(N_o')_{SFU} = 1275$ particles/cm^3. A revised value of

$(N_o)_{ext}$ *based on the new sphere size is* $(N_o')_{ext} \approx 4620$ *particles/cm*^{3}. The correct order of magnitude is there but the results are still disappointing. The problem may lie in the sampling time. Solving for τ in equation (14) we find,

$$\tau = -(\frac{V}{Q})\ln[1 - \frac{M_{SFU}}{V\rho\upsilon_p N_o}] \qquad (15)$$

Plugging in for υ_p' and $(N_o')_{ext}$ we find that the sampling time for the mass collected should be $\tau = 27.4$ minutes. So perhaps after a long enough time some of the assumptions in the derivation given here break down. Regardless, this is a good starting point for further investigations on this matter. A variety of tests using various sampling times, flow rates as well as different sampling points will hopefully solve this important problem.

APPENDIX B

ADJUSTED PERPENDICULAR DATA

This table lists the scattering (ISC') and background (IBK') values in units of microvolts. ISC' and IBK' are normalized to the average value of the laser power meter readings over the period of the measurements. DSC' is ISC' minus IBK' with the back angles corrected for extra extinction. $\sigma_{sc}'(\theta)/\sigma_{sc}'(5)$ is the unitless ratio of the differential scattering cross section at the given angle (θ) to the value of the same quantity at 5 degrees.

θ	ISC'	IBK'	DSC'	$\frac{\sigma_{sc}'(\theta)}{\sigma_{sc}'(5)}$
5	97820	528	97560	1.0000
10	57380	122.8	57260	1.0830
15	25620	66.49	25550	0.7010
20	15520	32.61	15490	0.5540
25	6180	21.562	6158	0.2690
30	3430	16.367	3414	0.1760
35	1230	12.688	1217	0.0715
40	790	15.561	774	0.0509
45	560	13.568	546	0.0394
50	770	12.599	757	0.0591
55	720	8.722	711	0.0593
60	780	6.832	773	0.0680
65	520	4.915	515	0.0474
70	370	5.856	364	0.0347
75	181	6.832	174.3	0.0171
80	110	3.932	106	0.0106
85	92.2	3.932	88.29	0.0089
90	105	3.932	101.2	0.0103
95	137.7	3.960	137.57	0.0139
100	147.8	3.946	147.94	0.0148
105	111.6	2.981	111.7	0.0109
110	84.0	2.981	83.34	0.0079
115	70.68	4.003	68.55	0.0063
120	91.06	3.002	90.54	0.0072
125	111.6	3.013	111.7	0.0093
130	184.4	3.046	186.5	0.0146
135	184.4	3.046	186.5	0.0135
140	198.8	3.046	201.3	0.0132
145	133.9	3.046	134.5	0.0079
150	102.5	4.077	101.2	0.0052
155	115.6	4.107	114.7	0.0050
160	310	4.077	314.9	0.0113
165	630	5.134	643.4	0.0176
170	1960	5.115	2014	0.0381
175	3470	9.207	3576	0.0366

APPENDIX C

ADJUSTED PARALLEL DATA

This table lists the scattering (ISC') and background (IBK') values in units of microvolts. Each of these values is adjusted to the average value of the laser power over the period of the measurements. DSC' is ISC' minus IBK' with the back angles corrected for extra extinction. $\sigma'_{sc}(\theta)/\sigma'_{sc}(5)$ is the differential scattering cross section at the given angle, normalized to the value of the same quantity at 5 degrees.

θ	ISC'	IBK'	DSC'	$\frac{\sigma'_{sc}(\theta)}{\sigma'_{sc}(5)}$
5	76260	652.5	75610	1.000
10	46000	142.1	45860	1.1196
15	18250	78.33	18170	0.6430
20	13720	41.46	13680	0.6312
25	6468	25.62	6442	0.3636
30	3742	21.366	3721	0.2477
35	1853	17.853	1835	0.1391
40	1220	18.382	1202	0.1019
45	536	15.205	520.8	0.0485
50	705	12.164	693	0.0698
55	446	13.178	432.8	0.0465
60	491	12.164	478.8	0.0543
65	338	10.137	378	0.0449
70	337	10.1	327	0.0402
75	220	9.123	211	0.0267
80	245	9.06	236	0.0304
85	210	8.021	202	0.0263
90	214	5.994	208	0.0272
95	171	5.972	169.6	0.0221
100	163	5.951	161.4	0.0208
105	131	5.930	128.5	0.0162
110	112	5.930	109	0.0134
115	71	4.906	68.0	0.0081
120	92	4.906	89.5	0.0102
125	111	4.924	109.1	0.0117
130	212	5.887	211.9	0.0213
135	214	5.8664	213.9	0.0199
140	374	4.924	379.4	0.0322
145	263	5.887	264.3	0.0200
150	627	5.887	638.8	0.0425
155	824	5.866	841.5	0.0475
160	1017	5.866	1040	0.0480
165	1423	6.893	1458	0.0516
170	2177	6.869	2236	0.0546
175	3965	10.793	4085	0.0540

APPENDIX D

Geometric Quantities:

(1) $X(\theta)$ = FWHM beam segment viewed by the scattering detector
(2) $R(\theta)$ = Distance from scattering detector to midpoint of $X(\theta)$
(3) $\Delta\theta_D$ = Angular size of the beam segment viewed by the scattering detector

θ	$X(\theta)$ (cm)	$R(\theta)$ (cm)	$\Delta\theta_D$ (degrees)
5	13.57	152.642	0.4424
10	6.190	140.069	0.4396
15	4.020	135.900	0.4387
20	2.990	133.832	0.4383
25	2.400	132.605	0.4380
30	2.010	131.800	0.4378
35	1.750	131.235	0.4377
40	1.555	130.823	0.4376
45	1.409	130.511	0.4375
50	1.298	130.272	0.4374
55	1.212	130.086	0.4373
60	1.146	129.940	0.4375
65	1.094	129.827	0.4375
70	1.054	127.741	0.4374
75	1.025	129.677	0.4375
80	1.005	129.634	0.4374
85	0.993	129.608	0.4374
90	0.989	129.600	0.4372
95	0.993	129.608	0.4374
100	1.005	129.634	0.4374
105	1.025	129.677	0.4375
110	1.054	129.741	0.4374
115	1.094	129.827	0.4375
120	1.146	129.940	0.4375
125	1.212	130.086	0.4373
130	1.298	130.272	0.4374
135	1.409	130.511	0.4375
140	1.555	130.823	0.4376
145	1.750	131.235	0.4377
150	2.010	131.800	0.4378
155	2.400	132.605	0.4380
160	2.990	133.832	0.4383
165	4.020	135.900	0.4387
170	6.190	140.069	0.4396
175	13.57	152.642	0.4424

APPENDIX E

SPHERE SCATTERING PROGRAM FOR 1 MICRON SPHERES

REFMED= 1.0000 REFRE= 0.160000E+01 REFIM= 0.000000E+00
SPHERE RADIUS = 0.500 WAVELENGTH = 0.6328
SIZE PARAMETER = 4.965

QSCA= 0.304892E+01 QEXT= 0.304892E+01 QBACK= 0.558997E+01

ANGLE	|S1|**2	|S2|**2
05.00	0.100000E+01	0.100000E+01
10.00	0.780828E+00	0.808891E+00
15.00	0.499148E+00	0.562717E+00
20.00	0.241311E+00	0.333685E+00
25.00	0.704698E-01	0.171773E+00
30.00	0.493253E-02	0.895049E-01
35.00	0.193232E-01	0.673342E-01
40.00	0.651352E-01	0.725926E-01
45.00	0.978967E-01	0.788397E-01
50.00	0.965281E-01	0.753287E-01
55.00	0.666619E-01	0.645925E-01
60.00	0.294675E-01	0.536024E-01
65.00	0.504534E-02	0.461351E-01
70.00	0.778600E-03	0.408356E-01
75.00	0.101983E-01	0.343235E-01
80.00	0.206312E-01	0.253765E-01
85.00	0.228860E-01	0.164603E-01
90.00	0.162932E-01	0.116898E-01
95.00	0.677586E-02	0.132430E-01
100.00	0.804660E-03	0.192443E-01
105.00	0.435130E-03	0.247871E-01
110.00	0.288575E-02	0.253059E-01
115.00	0.408439E-02	0.197926E-01
120.00	0.258518E-02	0.115274E-01
125.00	0.460928E-03	0.584013E-02
130.00	0.738206E-03	0.653937E-02
135.00	0.403522E-02	0.135480E-01
140.00	0.769322E-02	0.233497E-01
145.00	0.839569E-02	0.318048E-01
150.00	0.603845E-02	0.372047E-01
155.00	0.523205E-02	0.413158E-01
160.00	0.125530E-01	0.476702E-01
165.00	0.311921E-01	0.583994E-01
170.00	0.571012E-01	0.719870E-01
175.00	0.800109E-01	0.836703E-01
180.00	0.891668E-01	0.882987E-01

APPENDIX F

SPHERE SCATTERING PROGRAM FOR 0.85 MICRON SPHERES

REFMED= 1.0000 REFRE= 0.160000E+01 REFIM= 0.000000E+00
SPHERE RADIUS = 0.425 WAVELENGTH = 0.6328
SIZE PARAMETER = 4.220

QSCA= 0.406789E+01 QEXT= 0.406789E+01 QBACK= 0.271912E+01

ANGLE	|S1|**2	|S2|**2
5.00	0.100000E+01	0.100000E+01
10.00	0.861708E+00	0.876234E+00
15.00	0.665421E+00	0.701156E+00
20.00	0.451706E+00	0.510677E+00
25.00	0.259758E+00	0.337942E+00
30.00	0.117283E+00	0.204744E+00
35.00	0.348759E-01	0.118060E+00
40.00	0.623807E-02	0.720563E-01
45.00	0.134343E-01	0.536738E-01
50.00	0.347654E-01	0.489280E-01
55.00	0.522618E-01	0.474705E-01
60.00	0.563549E-01	0.442819E-01
65.00	0.466442E-01	0.388132E-01
70.00	0.292409E-01	0.327876E-01
75.00	0.123441E-01	0.280188E-01
80.00	0.208888E-02	0.251401E-01
85.00	0.260205E-03	0.234707E-01
90.00	0.444334E-02	0.216945E-01
95.00	0.100691E-01	0.187791E-01
100.00	0.130745E-01	0.146157E-01
105.00	0.118185E-01	0.101095E-01
110.00	0.743884E-02	0.674731E-02
115.00	0.270494E-02	0.589534E-02
120.00	0.169227E-03	0.816975E-02
125.00	0.695533E-03	0.131570E-01
130.00	0.314049E-02	0.195875E-01
135.00	0.527388E-02	0.258600E-01
140.00	0.532914E-02	0.306678E-01
145.00	0.324443E-02	0.334446E-01
150.00	0.853158E-03	0.344517E-01
155.00	0.890924E-03	0.344986E-01
160.00	0.536251E-02	0.344656E-01
165.00	0.141874E-01	0.348733E-01
170.00	0.249086E-01	0.357041E-01
175.00	0.336816E-01	0.365356E-01
180.00	0.370633E-01	0.368822E-01

APPENDIX G

The following is a modified version of the program CALLBH as published in Bohren and Huffman's book, Absorption and Scattering of Light by Small Particles,New York: Wiley-Interscience, 1983.

```
      PROGRAM CALLBH-UCD1985
C     ************************************************************
C     CALLBH-UCD1985 CALCULATES THE SIZE PARAMETER (X) AND RELATIVE
C     REFRACTIVE INDEX (REFREL) FOR A GIVEN SPHERE REFRACTIVE
C     INDEX, MEDIUM REFRACTIVE INDEX, RADIUS, AND FREE SPACE
C     WAVELENGTH.  IT THEN CALLS BHMIE, THE SUBROUTINE THAT COMPUTES
C     AMPLITUDE SCATTERING MATRIX ELEMENTS AND EFFICIENCIES.
C     ************************************************************
      COMPLEX REFREL,S1(360),S2(360)
      OPEN (UNIT=2, FILE='MIE.DAT', TYPE='NEW')
      WRITE(2,11)
      WRITE(5,11)
C     ************************************************************
C     REFMED=(REAL) REFRACTIVE INDEX OF SURROUNDING MEDIUM
C     ************************************************************
C
C     TYPE *, 'WHAT IS THE REFRACTIVE INDEX OF THE MEDIUM ?'
C     ACCEPT *, REFMED
      REFMED=1.0
C     ************************************************************
C     REFRACTIVE INDEX OF SPHERE = REFRE + I*REFIM
C     ************************************************************
C
      TYPE *, 'WHAT IS THE REAL REFRACTIVE INDEX OF THE SPHERE ?'
      ACCEPT *, REFRE
      TYPE *, 'WHAT IS THE IMAGINARY REFRACTIVE INDEX OF THE SPHERE ?'
      ACCEPT *, REFIM
C     REFRE=1.55
C     REFIM=0.0
      REFREL=CMPLX(REFRE,REFIM)/REFMED
      WRITE(2,12)REFMED,REFRE,REFIM
      WRITE(5,12)REFMED,REFRE,REFIM
C     ************************************************************
C     RADIUS (RAD) AND WAVELENGTH (WAVEL) SAME UNITS
C     ************************************************************
C
      TYPE *, 'WHAT IS THE RADIUS OF THE SPHERE ?'
      ACCEPT *, RAD
C     TYPE *, 'WHAT IS THE WAVELENGTH ?'
C     ACCEPT *, WAVEL
C     RAD=.525
      WAVEL=.6328
      X=2.*3.14159265*RAD*REFMED/WAVEL
      WRITE(2,13)RAD,WAVEL
      WRITE(5,13)RAD,WAVEL
      WRITE(2,14)X
      WRITE(5,14)X
C     ************************************************************
C     NANG = NUMBER OF ANGLES BETWEEN 0 AND 90 DEGREES
C     MATRIX ELEMENTS CALCULATED AT 2*NANG-1 ANGLES
```

```
C       INCLUDING 0, 90, AND 180 DEGREES
C       *********************************************************
C
        TYPE *, 'HOW MANY ANGLES BETWEEN 0 AND 90 DEGREES (INCLUSIVE) ?'
        ACCEPT *, NANG
C       NANG=11
        DANG=1.570796327/FLOAT(NANG-1)
C       *********************************************************
C       CALL SUBROUTINE TO COMPUTE AMPLITUDE SCATTERING
C       MATRIX ELEMENTS AND EFFICIENCIES
C       *********************************************************
C
        CALL BHMIE(X,REFREL,NANG,S1,S2,QEXT,QSCA,QBACK)
        WRITE(2,65)QSCA,QEXT,QBACK
        WRITE(5,65)QSCA,QEXT,QBACK
        WRITE(2,17)
        WRITE(5,17)
C       *********************************************************
C       S33 AND S34 MATRIX ELEMENTS NORMALIZED BY S11.
C       S11 IS NORMALIZED TO 1.0 IN THE FORWARD DIRECTION
C       POL=DEGREE OF POLARIZATION (INCIDENT UNPOLARIZED LIGHT)
C       *********************************************************
C
C       S11NOR=0.5*(CABS(S2(1))**2+CABS(S1(1))**2)
        NAN=2*NANG-1
        IF (NANG .EQ. 19) L=2                    ! STARTING POINT
        IF (NANG .EQ. 37) L=3
        IF (NANG .EQ. 91) L=6
C       S11NOR=0.5*CABS(S1(L))*CABS(S1(L))
C       S12NOR=0.5*CABS(S2(L))*CABS(S2(L))
        S1MNOR=CABS(S1(L))**2
        S2MNOR=CABS(S2(L))**2
        DO 355 J=L,NAN
        AJ=J
        S11=0.5*CABS(S2(J))*CABS(S2(J))
        S11=S11+0.5*CABS(S1(J))*CABS(S1(J))
        S12=0.5*CABS(S2(J))*CABS(S2(J))
        S12=S12-0.5*CABS(S1(J))*CABS(S1(J))
        POL=-S12/S11
        S33=REAL(S2(J)*CONJG(S1(J)))
        S33=S33/S11
        S34=AIMAG(S2(J)*CONJG(S1(J)))
        S34=S34/S11
C       S11=S11/S11NOR
C       S12=S12/S12NOR
        ANG=DANG*(AJ-1.)*57.2958
        S1MAG=CABS(S1(J))**2 / S1MNOR
        S2MAG=CABS(S2(J))**2 / S2MNOR
        WRITE(2,75)ANG,S11,S12,S1MAG,S2MAG
355     WRITE(5,75)ANG,S11,S12,S1MAG,S2MAG
65      FORMAT (';'/';'/,';','QSCA= ',E13.6,3X,'QEXT= ',E13.6,3X,
     2'QBACK= ',E13.6)
75      FORMAT ('RD',F6.2,2X,E13.6,2X,E13.6,2X,E13.6,2X,E13.6)
11      FORMAT (';  SPHERE SCATTERING PROGRAM'/,';')
12      FORMAT (';',4X,'REFMED= ',F8.4,3X,'REFRE= ',E14.6,3X,
     2'REFIM= ',E14.6)
13      FORMAT(';',4X,'SPHERE RADIUS = ',F7.3,3X,'WAVELENGTH = ',F7.4)
14      FORMAT (';',4X,'SIZE PARAMETER = ',F8.3)
17      FORMAT(';'/';'/,';','ANGLE',7X,'S11',13X,'S12',
     *12X,'|S1|**2',10X,'|S2|**2'/';'/';')
        STOP
        END
```

APPENDIX H

The following is the exact subroutine BHMIE as published in Bohren and Huffman's book, Absorption and Scattering of Light by Small Particles, New York, Wiley-Interscience, 1983.

```
C       ****************************************************
C       SUBROUTINE BHMIE CALCULATES AMPLITUDE SCATTERING MATRIX
C       ELEMENTS AND EFFICIENCIES FOR EXTINCTION, TOTAL SCATTERING
C       AND BACKSCATTERING FOR A GIVEN SIZE PARAMETER AND
C       RELATIVE REFRACTIVE INDEX
C       ****************************************************
C
        SUBROUTINE BHMIE (X,REFREL,NANG,S1,S2,QEXT,QSCA,QBACK)
        DIMENSION AMU(100),THETA(100),PI(100),TAU(100),PI0(100),
     1PI1(100)
        COMPLEX D(3000),Y,REFREL,XI,XI0,XI1,AN,BN,S1(360),S2(360)
        DOUBLE PRECISION PSI0,PSI1,PSI,DN,DX
        DX=X
        Y=X*REFREL
C       *****************************************
C       SERIES TERMINATED AFTER NSTOP TERMS
C       *****************************************
        XSTOP=X+4.*X**.3333+2.0
        NSTOP=XSTOP
        YMOD=CABS(Y)
        NMX=AMAX1(XSTOP,YMOD)+15
        DANG=1.570796327/FLOAT(NANG-1)
        DO 555 J=1,NANG
        THETA(J)=(FLOAT(J)-1.)*DANG
555     AMU(J)=COS(THETA(J))
C       ***************************************************************
C       LOGARITHMIC DERIVATIVE D(J) CALCULATED BY DOWNWARD
C       RECURRENCE BEGINNING WITH INITIAL VALUE 0.0 +I*0.0
C       AT J = NMX
C       ***************************************************************
        D(NMX)=CMPLX(0.0,0.0)
        NN=NMX-1
        DO 120 N=1,NN
        RN=NMX-N+1
120     D(NMX-N)=(RN/Y)-(1./(D(NMX-N+1)+RN/Y))
        DO 666 J=1,NANG
        PI0(J)=0.0
666     PI1(J)=1.0
        NN=2*NANG-1
        DO 777 J=1,NN
        S1(J)=CMPLX(0.0,0.0)
777     S2(J)=CMPLX(0.0,0.0)
C       ************************************************************
C       RICCATI-BESSEL FUNCTIONS WITH REAL ARGUMENT X
C       CALCULATED BY UPWARD RECURRENCE
C       ************************************************************
C
        PSI0=DCOS(DX)
        PSI1=DSIN(DX)
        CHI0=-SIN(X)
        CHI1=COS(X)
```

```
      APSI0=PSI0
      APSI1=PSI1
      XI0=CMPLX(APSI0,-CHI0)
      XI1=CMPLX(APSI1,-CHI1)
      QSCA=0.0
      N=1
200   DN=N
      RN=N
      FN=(2.*RN+1.)/(RN*(RN+1.))
      PSI=(2.*DN-1.)*PSI1/DX-PSI0
      APSI=PSI
      CHI=(2.*RN-1.)*CHI1/X-CHI0
      XI=CMPLX(APSI,-CHI)
      AN=(D(N)/REFREL+RN/X)*APSI-APSI1
      AN=AN/((D(N)/REFREL+RN/X)*XI-XI1)
      BN=(REFREL*D(N)+RN/X)*APSI-APSI1
      BN=BN/((REFREL*D(N)+RN/X)*XI-XI1)
      QSCA=QSCA+(2.*RN+1.)*(CABS(AN)*CABS(AN)+CABS(BN)*CABS(BN))
      DO 789 J=1,NANG
      JJ=2*NANG-J
      PI(J)=PI1(J)
      TAU(J)=RN*AMU(J)*PI(J)-(RN+1.)*PI0(J)
      P=(-1.)**(N-1)
      S1(J)=S1(J)+FN*(AN*PI(J)+BN*TAU(J))
      T=(-1.)**N
      S2(J)=S2(J)+FN*(AN*TAU(J)+BN*PI(J))
      IF(J.EQ.JJ) GO TO 789
      S1(JJ)=S1(JJ)+FN*(AN*PI(J)*P+BN*TAU(J)*T)
      S2(JJ)=S2(JJ)+FN*(AN*TAU(J)*T+BN*PI(J)*P)
789   CONTINUE
      PSI0=PSI1
      PSI1=PSI
      APSI1=PSI1
      CHI0=CHI1
      CHI1=CHI
      XI1=CMPLX(APSI1,-CHI1)
      N=N+1
      RN=N
      DO 999 J=1,NANG
      PI1(J)=((2.*RN-1.)/(RN-1.))*AMU(J)*PI(J)
      PI1(J)=PI1(J)-RN*PI0(J)/(RN-1.)
999   PI0(J)=PI(J)
      IF(N-1-NSTOP)200,300,300
300   QSCA=(2./(X*X))*QSCA
      QEXT=(4./(X*X))*REAL(S1(1))
      QBACK=(4./(X*X))*CABS(S1(2*NANG-1))*CABS(S1(2*NANG-1))
      RETURN
      END
```

END

FILMED

10-85

DTIC